CONTENTS


| SECTION | | PAGE |
|---|---|---|
| 1 | SUMMARY | 1 |
| 2 | THE MECHANICS OF MACHINING | 2 |
| | 2.1 The Models of Merchant | 2 |
| | 2.2 The Model of Spaans | 5 |
| 3 | THE ROLE OF INCLUSIONS | 7 |
| | 3.1 Inclusions in Ductile Fracture | 7 |
| | 3.2 Inclusions and Wear | 8 |
| | 3.2.1 Tool Technology | 9 |
| | 3.3 Inclusions and Lubrication | 10 |
| 4 | MODERN DEVELOPMENTS | 12 |
| | 4.1 Reduction or Elimination of Pb | 12 |
| | 4.2 Inclusion Engineering | 12 |
| | 4.2.1 The Elimination of Alumina | 12 |
| | 4.2.2 Optimization of Machinability and Transverse Ductility | 13 |
| | 4.3 Steelmaking Control | 13 |
| 5 | FUTURE RESEARCH AND DEVELOPMENT IN CANADA | 15 |
| APPENDIX I | VELOCITY, FORCE AND WORK RELATIONSHIPS IN ORTHOGONAL CUTTING | 17 |
| | AI.1 The Merchant Models | 17 |
| | AI.2 Deviations from the Plane Strain Model | 22 |
| APPENDIX II | SHEAR ZONE STREAMLINE ANALYSIS | 24 |
| | AII.1 The Model of Spaans | 24 |
| | AII.1.1 Effect of Normal Stress on the Shear Stress. | 28 |
| APPENDIX III | THE INITIATION AND PROPAGATION OF DUCTILE FRACTURE | 31 |
| | AIII.1 The Model of Knott and Co-workers | 31 |
| | AIII.1.1 Strain Localisation | 39 |
| APPENDIX IV | INCLUSIONS AND MACHINABILITY | 42 |
| | AIV.1 Inclusions and Ductile Fracture | 42 |
| | AIV.2 Sulphide Modification | 43 |
| | AIV.3 Oxide Modification | 44 |
| | AIV.4 Modification Methods | 44 |
| | AIV.5 The Effect of Sulphur | 46 |
| | AIV.5.1 Chip Formation | 48 |
| | AIV.6 The Effect of Lead | 51 |
| APPENDIX V | EMPIRICAL STRUCTURE-DUCTILITY RELATIONSHIPS IN STEEL. | 54 |

| SECTION | | PAGE |
|---|---|---|
| APPENDIX VI | CUTTING TEMPERATURES | 57 |
| | AVI.1 Temperature Distributions | 57 |
| | AVI.2 Temperature and the Role of Inclusions | 60 |
| APPENDIX VII | THE BUILT UP EDGE (BUE) | 61 |
| APPENDIX VIII | TOOL WEAR, FRICTION AND SURFACE FINISH | 63 |
| | AVIII.1 Types of Tool Wear | 63 |
| | AVIII.2 The Taylor Relationship | 64 |
| | AVIII.3 Friction | 67 |
| | AVIII.4 Wear | 67 |
| | AVIII.5 Surface Finish | 70 |
| APPENDIX IX | CUTTING FLUIDS | 72 |
| REFERENCES | | 73 |

## LIST OF FIGURES


| FIGURE | | PAGE |
|---|---|---|
| 2.1 | Temperature, Strain and Strain Rate Profiles after Spaans (7). | 6 |
| AI.1 | The Composite Force Diagram of Merchant (1) | 18 |
| AII.1 | Model of Deformation in the Shear Zone (7) | 25 |
| AII.2 | Temperature, Strain and Strain Rate Profiles in the Shear Zone. $V_C$ = 200 m/min. | 29 |
| AIII.1 | The Model for Ductile Fracture (9) | 32 |
| AIII.2 | $\delta_i/X_o$ as a function of $X_o/R_o$ (9) | 33 |
| AIII.3 | Slip Line Fields for a) a Sharp Crack Tip and b) a Blunted Crack Tip (9) | 33 |
| AIII.4 | The Process and Plastic Strain Zones (9) | 35 |
| AIII.5 | Schematic Plastic Zones for Low and High Work-hardening Rate Materials (9) | 35 |
| AIV.1 | The $CaO-Al_2O_3-SiO_2$ Phase Diagram (15) | 45 |
| AIV.2 | Cuttting Forces $F_C$ and $F_T$ as a function of Cutting Speed, $V_C$, for Resulphurised Steels (22,23) | 49 |
| AIV.3 | Cutting Forces $F_C$ and $F_T$ as a function of Cutting Speed, $V_C$, for Non-leaded (NL) and Leaded (L) Steels (13). | 52 |
| AV.1 | a) The Effect of Volume Fraction of Second Phase Particles on Total Ductility, $\epsilon_T$(46) | 55 |
| | b) The Effect of Volume Fraction of Sulfides on Longitudinal and Transverse Total Ductiliy, $\epsilon_T$(46) | 55 |
| AVI.1 | Temperature Distribution in the Cutting Zone for HSS Machining (47) | 58 |
| AVI.2 | Tool-Chip Interface Temperature Distribution in Carbide Cutting (48) | 59 |
| AVI.3 | Tool Flank Temperature Distribution in Carbide Cutting (48) | 59 |

AVIII.1 Taylor Tool Life Relationships for Resulphurised Hot-rolled Steels (22) 65

## LIST OF TABLES


| TABLE | | PAGE |
|---|---|---|
| 2.1 | Cutting Forces and Related Quantities in Machining NE 9445 Steel. Sintered Carbide. Width of cut: 0.25 in. | 3 |
| AIII.1 | Effect of Work-hardening Capacity on Notch Tip Ductility | 36 |
| AIII.2 | The Effect of Inclusion Spacing, $X_o$, on $\delta_i$ | 37 |
| AIII.3 | The Effect of Sulphur Content on $\delta_i/X_o$ | 38 |
| AIII.4 | The Effect of Sulphur Content on Crack Propagation | 39 |
| AIV.1 | Composition of Resulphurised Steels (22,23) | 47 |
| AIV.2 | Tensile Properties of Hot-Rolled Steels (22,23) | 47 |
| AVIII.1 | Taylor Tool Life Equations (0.03 in.wear land) Feed:0.0046 ipr. Depth of cut 0.10 in. | 66 |
| AVIII.2 | Taylor Tool Life Equations (0.03 in.wear land) Feed: 0.0046 ipr. Depth of cut 0.10 in. | 66 |

## SUMMARY

This report is not intended to be an exhaustive review of all the literature on machining and machinability. It is a summary of that portion of the literature which the authors have found to be helpful in their attempt to understand the basic principles of the machining process, and to lay a rational foundation for research and development aimed at the industrial production of lead-free machining steels in Canada.

Areas for research and development include:

1. The control of sulphide volume fraction, distribution and morphology in all free-machining grades.
2. The elimination of oxide inclusions in resulphurized grades, with and without Pb, for HSS tool machining.
3. The reduction of the Pb content of Pb-bearing steels.
4. The development of a screwstock steel, containing Bi as a substitute for Pb.
5. Oxide inclusion modification in low carbon, quality carbon and low alloy steels by Ca-Si deoxidation.
6. The optimization of machinability with transverse ductility properties in quality carbon and low alloy steels by Zr or Ti.
7. Development of a continuous casting technology.

Each of these areas involve steelmaking control and inclusion engineering which require the direct involvement of the steel industry. Stage II of the current research program can only initiate research and development and should be structured so as to conform with the technological capabilities and economic priorities of the industry itself.

# 2. THE MECHANICS OF MACHINING

## 2.1 THE MODELS OF MERCHANT (1,3)

A review of the literature on the mechanics of metal cutting reveals that the plane strain model developed independently by Merchant (1) and Piispanen (2), has been extensively used in metal cutting research to calculate force and work relationships from measured cutting forces and chip geometry in orthogonal cutting. The basis of the Merchant models is given in Appendix I and the results of one of his analyses, obtained from machining an NE 9445 steel under a variety of cutting conditions, are reproduced in Table 2.1.

Some of the more important points to be noted from the data in Table 2.1 are:

(i) the magnitude of the shear strain in the shear plane, $\varepsilon$,

(ii) the magnitude of the normal stress on the shear plane, $S_N$, which is the origin of hydrostatic stresses in machining.

(iii) the work doen in shear, $W_S$, is 70–80% of the total work of cutting, $W_C$,

(iv) the work done in overcoming friction, $W_F$, is only 20% of the total work of cutting,

(v) the coefficient of friction, $\mu$, is a poor indicator of the work done against friction.

Reduction of the work done against friction, $W_F$, through the use of lubricating cutting fluids and free machining additives, can reduce the specific cutting energy, $W_C$, improve surface finish and improve tool life by a reduction in the tool/chip interface temperature and tool/chip contact area. The specific cutting energy can be reduced to a much

Table 2.1 Cutting Forces and Related Quantities in Machining NE.9445 Steel. Sintered Carbide. Width of Cut: 0.25 in.

| Observed | | | | | | | Calculated | | | | | | | | |
|---|---|---|---|---|---|---|---|---|---|---|---|---|---|---|---|
| $t_1$ | $V_C$ (mean) | | | | $F_C$ | $F_T$ | | | $F$ | $F_S$ | $S_S$ | $S_N$ | | | $W_C$ |
| in./1000 | ft./min | $\alpha$ | $\phi^\circ$ | $r_c$ | lbs. | lbs. | $\epsilon$ | $\mu$ | lbs. | lbs. | psi. | psi. | $W_F/W_C$ | $W_S/W_C$ | in.-lb./in.$^3$ |
| 3.70 | 197 | +10° | 17.0 | 0.29 | 370 | 273 | 3.4 | 1.05 | 335 | 270 | 85,000 | 115,000 | 0.27 | 0.73 | 400,000 |
| | 400 | | 19.0 | .33 | 360 | 283 | 3.1 | 1.11 | 345 | 250 | 88,000 | 137,000 | .32 | .68 | 390,000 |
| | 642 | | 21.5 | .37 | 329 | 217 | 2.7 | .95 | 270 | 230 | 90,000 | 129,000 | .30 | .70 | 355,000 |
| | 1186 | | 25.0 | .44 | 303 | 168 | 2.4 | .81 | 220 | 205 | 93,000 | 130,000 | .32 | .68 | 330,000 |
| 3.70 | 400 | -10° | 16.5 | .32 | 416 | 385 | 3.9 | .64 | 310 | 290 | 89,000 | 153,000 | .24 | .76 | 450,000 |
| | 637 | | 19.0 | .37 | 384 | 326 | 3.5 | .58 | 255 | 255 | 90,000 | 152,000 | .25 | .75 | 415,000 |
| | 1160 | | 22.0 | .44 | 356 | 263 | 3.1 | .51 | 200 | 230 | 94,000 | 154,000 | .25 | .75 | 385,000 |
| 1.09 | 542 | +10° | 19.0 | .33 | 127 | 101 | 3.1 | 1.12 | 120 | 85 | 103,000 | 164,000 | .33 | .67 | 460,000 |
| 2.34 | | | 18.5 | .32 | 242 | 186 | 3.1 | 1.08 | 225 | 170 | 92,500 | 140,000 | .30 | .70 | 410,000 |
| 3.70 | | | 21.5 | .37 | 336 | 226 | 2.7 | .96 | 280 | 230 | 91,000 | 131,000 | .31 | .69 | 360,000 |
| 7.88 | | | 25.0 | .44 | 605 | 315 | 2.4 | .76 | 420 | 415 | 89,000 | 116,000 | .31 | .69 | 310,000 |
| 1.09 | 542 | -10° | 10.5 | .23 | 181 | 198 | 5.0 | .78 | 165 | 130 | 103,000 | 179,000 | .22 | .78 | 670,000 |
| 2.34 | | | 16.0 | .30 | 295 | 291 | 4.0 | .70 | 230 | 205 | 96,000 | 172,000 | .23 | .77 | 500,000 |
| 3.70 | | | 19.0 | .37 | 401 | 350 | 3.5 | .60 | 275 | 265 | 94,000 | 164,000 | .29 | .71 | 430,000 |
| 7.88 | | | 22.5 | .46 | 698 | 472 | 3.1 | .46 | 345 | 465 | 90,000 | 138,000 | .23 | .77 | 350,000 |

greater extent through a decrease in the work done in shear, $W_S$. This is one of the other functions of free-machining additives, i.e. to decrease the strain to fracture through the presence of inclusions and other second phase particles.

As far as tool crater-wear is concerned, see Appendix VIII, the value of the normal force, N, is of much greater significance than the value of the coefficient of friction, $\mu$.

In later models, Merchant (3) attempted to analyse the force systems from a knowledge of chip geometry alone through the introduction of certain plasticity assumptions. A model based on the assumption that the flow stress in the shear plane, equivalent to the shear strength of the workpiece, resulted in the condition:

$$2\phi + \tau - \alpha = 90^{o} \qquad (1)$$

which clearly did not agree with practice.*

A second model, based on the assumption that the flow stress in the shear plane is a linear function of hydrostatic stress resulted in the condition:

$$2\phi + \tau - \alpha = C \qquad (2)$$

where C is a constant dependent on cutting conditions, gave only limited agreement with practice. The work of Kobayashi and Thomsen (6) indicates that flow stress is independent of hydrostatic pressure, and the relationship derived from machining tests could be erroneous since flow stress is a function of temperature, strain rate and strain.

---

* $\phi$ is the shear angle, $\tau$ is the friction angle and $\alpha$ is the rake angle – see Appendix I.

The fact that the measured shear plane flow stress is approximately equal to that which may be predicted, using distortion energy criteria, from iniaxial tensile data at equivalent strains, might suggest that cutting forces can be predicted from conventional mechanical testing data. This possibility can be ruled out, however, since neither the shear angle, $\phi$, are the friction angle, $\tau$ ($\tan \tau = F/N$), can be predicted.

## 2.2 THE MODEL OF SPAANS (7)

Spaans (7) has modelled the shape of the streamlines in the shear zone assuming that the shear zone flow stress was a function of temperature, strain and strain rate but nevertheless constant. It was assumed that the flow stress was not affected significantly by hydrostatic pressure. Details of the treatment are given in Appendix II. An example of the model's predictions are given in Fig. 2.1 which shows temperature, strain and strain rate profiles in the shear zone for given flow stresses, cutting speeds and cutting ratios. Clearly, the machining process is characterised by shearing processes in the shear zone taking place under conditions of high strain, high strain rate and high temperatures .

Spaans' treatment can only be regarded as approximate, however, since the functions relating flow stress to temperature, strain rate and strain were estimated from the Ferrovac 'E' data of Muller (8). There is a critical gap in knowledge relating to the ductile rupture of steel at high strain rates, in the presence of second phase particles exhibiting wide ranges of size and distribution.

| CUTTING SPEED | 40 M/min. | 200 M/min. | 400 M/min. |
|---|---|---|---|
| FLOW STRESS | 500 N/mm$^2$ | 540 N/mm$^2$ | 560 N/mm$^2$ |
| CUTTING RATIO | 2.5 | 1.85 | 1.75 |

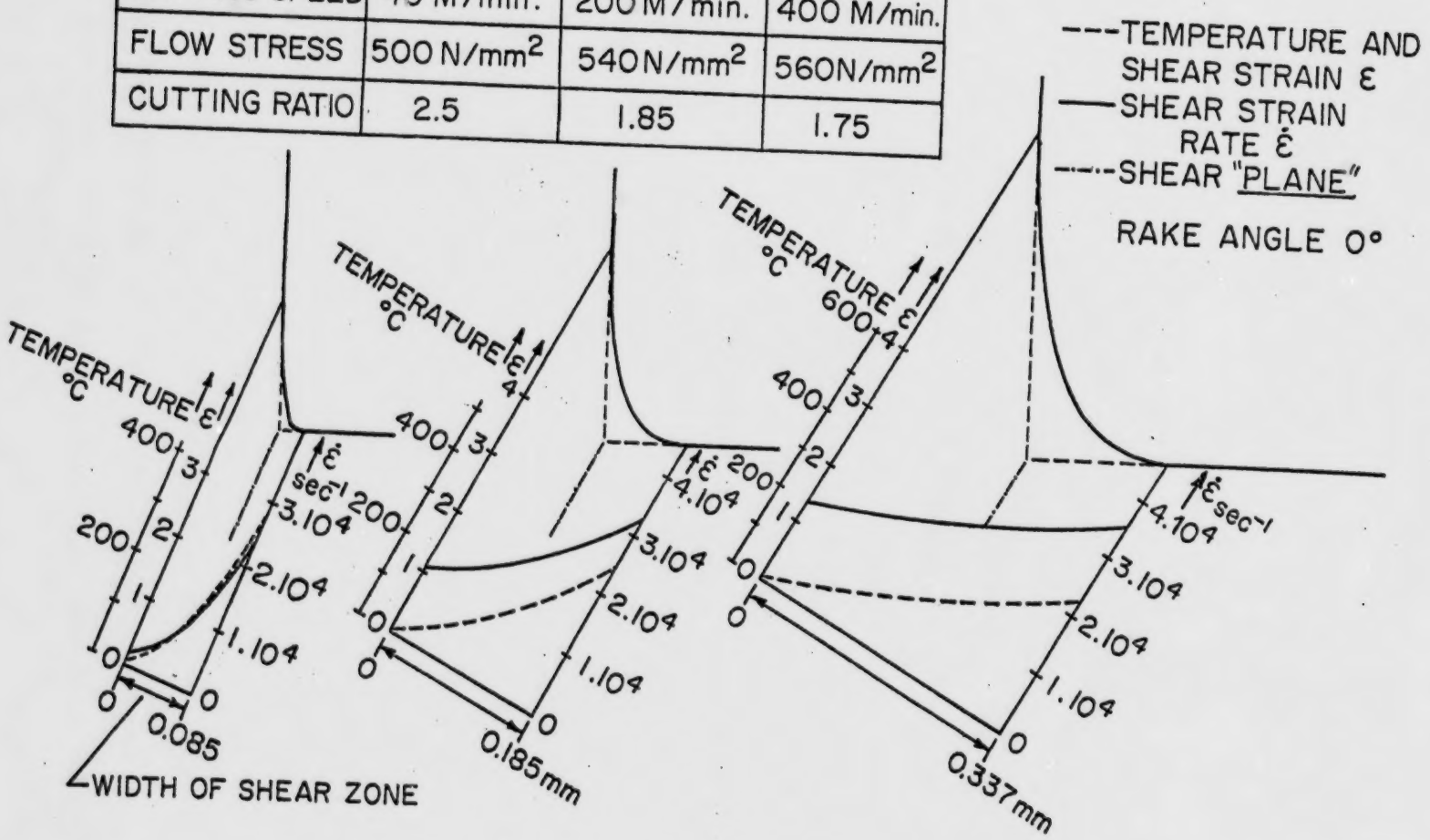


Fig. 2.1 - Temperature, Strain and Strain Rate Profiles after Spaans (7).

## 3. THE ROLE OF INCLUSIONS

### 3.1 INCLUSIONS IN DUCTILE FRACTURE

Some insight into the mechanical behaviour of materials at high strain rates can be derived from the concepts of fracture mechanics, in particular the concept of crack opening displacement, COD. The treatment of Knott and his co-workers (9,11,13) is summarised in Appendix III, from which it is apparent that non-metallic inclusions and other second phase particles play a critical role in ductile fracture by void nucleation, growth and ultimate friction. In the case of non-metallic inclusions in steel, matrix decohesion occurs at very small strains and the role of large inclusions (nominally > 5 μm) is to determine the gauge lengths over which the total strain to fracture takes place, and the role of smaller inclusions is to decrease the strain to fracture, i.e. in the case of machining, to decrease the cutting energy. These conclusions are in accordance with the early work of Van Vlack (30) and the later work of Fröhlke (31) which emphasise the inportance of inclusion volume fraction, distribution and morphology in machinability. Any microstructural feature, e.g., banding, or property which leads to strain localisation can decrease the total strain to fracture. Green and Knott (9) emphasize the effects of work-hardening capacity, which are consistant with the observed affects of cold working on machinability (32), as outlined schematically on the following page.

In a material of low work-hardening capacity, shear fracture with negligible crack blunting occurs when voids nucleate round inclusions at low strains. Shear bands become localised in the directions of the nearest voids ahead of the crack tip and it is possible for decohesion

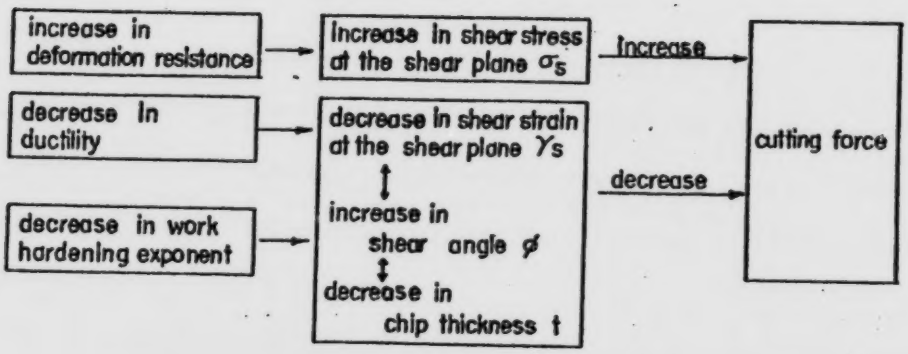
increase in deformation resistance
decrease in ductility
decrease in work hardening exponent
increase in shear stress at the shear plane $\sigma_s$
decrease in shear strain at the shear plane $\gamma_s$
increase in shear angle $\phi$
decrease in chip thickness t
increase
decrease
cutting force

to occur along those bands before the crack tip has blunted substantially. The final fracture will be crack-like and zig-zag from inclusion to inclusion. This type of mechanism is graphically illustrated in a micrograph of Fröhlke (31), showing shear zone shear bands.

In the production of free machining steels it is important that methods designed to decrease the total strain to fracture do not adversely affect tool wear.

## 3.2 INCLUSIONS AND WEAR

In principle, non-metallic inclusions of any composition can influence the total strain to fracture, but inclusions which are substantially harder than the tool promote flank wear and have an adverse effect on tool life. The relative hardness of the tool and workpiece is a function of temperature, and therefore cutting speed. While all oxides have been generally found to be harmful at the low cutting temperatures of HSS tools (33), oxides in the $CaO-Al_2O_3-SiO_2$ systems have been found to be beneficial at the high cutting

temperatures of carbide tools containing tianium. In this particular case crater wear is reduced through the formation of a diffusion behaviour between chip and tool.

The development of the Cal-De-Ox steels by Republic Steel Corporation has been summarised by Tipnis (34). This development was designed to improve the life of HSS tools through the elimination of hard abrasive alumina inclusions by Ca deoxidation (35). Alumina inclusions were replaced by softer calcium aluminates (36), the abrasive nature of which was further reduced by their envelopment in an even softer CaMn(S) phase. The tool life of HSS gear cutters used to make gears from these steels was improved by as much as 70-100% (35). This type of deoxidation control has been the subject of more recent development (16, 17, 18).

Although the improvement in HSS tool life reported by Fujiwara et al. (18) was attributed to the presence of plastic anorthitic ($CaO.Al_2O_3.2SiO_2$) inclusions, the development of steels containing inclusions in the $CaO-Al_2O_3-SiO_2$ system originated through their ability to form a thermal diffusion barrier at the chip/tool interface, thus greatly reducing crater wear when using a carbide tool containing titanium (37,38). This development was actively pursued in Germany and Japan and more recently by Randak et al. (17) and Brunet et al. (19).

### 3.2.1 Tool Technology

Recent developments in carbide tool technology (39, 40,41) have also involved the use of titanium, usually in the form of:

(i) TiC + TaC additions to the WC-Co base,

(ii) a TiC-Ni base with other complex carbides

and (iii) TiC coatings on WC-Co bases with an without other complex carbides.

TiC has a high hardness, excellent chemical stability and imparts an excellent resistance to crater wear at speeds in the range 700-1000 sfm (39). TaC is reported to decrease flank wear (39). The exact mechanisms by which TiC and TaC reduce wear has not yet been determined conclusively.

These improvements in tool technology decrease the susceptibility of carbide tools to wear by oxide inclusions and have to be taken into consideration in the development of free-maching grades.

## 3.3 INCLUSIONS AND LUBRICATION

Although MnS inclusions in steel are known to deposit on the tool during HSS machining (42) it is not clear that they can act as lubricants or retard tool wear. It may be that their function is to decrease the total strain to fracture in the primary shear zone and to facilitate chip cracking (43), thereby decreasing the tool/chip contact area. Again it is uncertain whether the silicate thermal diffussion barriers referred to in the previous section have a lubricating function.

However, since it is now considered that frictional interfaces at high cutting speeds consist of flow zones (44) of low shear stress, analogous to boundary layers in fluid mechanics, any 'insoluble' inclusion material which is sufficiently plastic at machining temepratures to forma a boundary film, must to some extent act as a thermal diffusion barrier and have some lubricating effect. Thus Pb acts as a lubricant at the low speeds (temperatures) of HSS machining

and one would expect MnS and then $CaO-Al_2O_3-SiO_2$ inclusions to become active in turn as the cutting speed (temperature) increases.

The role of lead as a lubricant in HSS screw stock machining can only be filled by other low melting point/high boiling point, "insoluble" metallics such as Bi. Here the development of the LaSalle/Inland (45) free-machining steel containing Bi is of particular interest.

## 4. MODERN DEVELOPMENTS

### 4.1 REDUCTION OR ELIMINATION OF Pb

Ito et al. (28) report a good correlation between tool life and 'Pb + S' contents in SAE 1050 steels and have achieved satisfactory tool life performance with lead contents as low as 0.03 - 0.08%, compared to the 0.2% levels formerly used. This approach, in conjunction with pollution control techniques such as grinding instead of scarfing, may help to alleviate some of the problems associated with lead free-matching additives.

The replacement of Pb by Bi (45) in screw stock HSS machining appears to be the only development in which Pb is actually replaced by another additive which functions in exactly the same way. In this particular application there appears to be no alternative other than the use of Bi and other low melting metallics. The steel developed by the LaSalle, and Inland Steel Companies is of the following composition by weight:

| C | Mn | P | S | Bi |
|---|---|---|---|---|
| 0.09 max | 0.85-1.15 | 0.04-0.09 | 0.26-0.35 | 0.40 max |

Whether, in the long term, Bi will prove to be less hazardous than Pb, is a matter for conjecture but the development is certainly of short term interest.

### 4.2 INCLUSION ENGINEERING

#### 4.2.1 The Elimination of Alumina

The emphasis of recent research has been the elimination of the

harmful effects of alumina on the wear of both HSS and carbide tools. This has been made possible either by:

i) deoxidation with Ca or Ca-Si alloys with the replacement of alumina by calcium aluminates envloped in (Ca,Mn) S (35,17)

or

ii) controlled deoxidation with Ca-Si to produce inclusions of compositions close to that of calcium metasilicate ($CaO.SiO_2$), (16), or anorthite ($CaO.Al_2O_3.2SiO_2$), (18,19).

Independent developments (37,38) led to the production of steels containing these types of inclusions in order to decrease crater wear in carbide tools containing Ti.

### 4.2.2 Optimization of Machinability and Transverse Ductility

One of the key roles of free machining additives is to decrease the total strain to fracture. When this is achieved through the addition of sulphur to killed grades of steel, the Type II manganese sulphides deform plastically during hot working and there is a marked decrease in transverse ductility. In the case of high quality carbon and low alloy steels this decrease in transverse ductility is unacceptable and optimization of machinability and transverse ductility is achieved through control of inclusion morphology. Thevellier et al. (20) report Type II MnS inclusion modification by S-Se-Mg and S-Se-Ca, while Yamaguchi et al. (21) have used Zr modification techniques.

## 4.3 STEELMAKING CONTROL

The developments in inclusion engineering have been made possible by advances in ladle metallurgy. The CaB process has been used in Ca-Si

deoxidation and the Finkl-Mohr unit for Pb additions (27). Steelmaking techniques have been designed not only for controlled deoxidation and the production of inclusions of specific composition but also to control inclusion volume fraction and distribution. Backer (27) also reports the results of an investigation on the effect of continuous casting on high quality leaded steels.

It is clear that if the developments outlined above are to be taken up in Canada, the steel industry itself must play a major role in process development.

## 5. FUTURE RESEARCH AND DEVELOPMENT IN CANADA

The areas of research and development outlined below require the direct involvement of the steel industry. Stage II of the current research program can only initiate that research and development, and should be structured so as to conform with the technological capabilities and the economic priorities of the industry itself.

### 5.1 DEVELOPMENT OF FREE MACHINING STEELS

Based on the analysis in the preceding sections, possible areas of research and development in the production of free-machining steels are outlined below.

I. The incorporation of methods in steelmaking practice designed to:
   a) control sulphide inclusion volume fraction, distribution and morphology in all free-machining grades,
   b) eliminate oxide inclusions in resulphurised grades, with and without Pb, for HSS tool machining,
   c) reduce the Pb content of Pb-bearing grades. This development, in conjunction with other techniques, such as grinding instead of scarfing, could aid environmental control.

II. The development of a screwstock steel, similar to the LaSalle/Inland 83-420 product, containing Bi or other low melting point additives as a substitute for Pb.

III. The development of Ca-Si deoxidation practice to produce machining grades in low carbon, quality carbon and low alloy steels containing modified oxide inclusions of controlled volume fraction, distribution and morphology, with specified compositions in the

$CaO-Al_2O_3-SiO_2$ system.

IV. The optimization of machinability with transverse ductility properties in quality carbon and low alloy steels by sulphide inclusion modification techniques involving Zr or Ti for example.

V. The development of continuous casting techniques where changes in inclusion volume fraction, distribution and morphology can cause significant variations in machinability.

## APPENDIX I

## VELOCITY, FORCE AND WORK RELATIONSHIPS IN ORTHOGONAL CUTTING

### AI.1 THE MERCHANT MODELS

Force diagrams showing the relationships between working forces were developed independently by Merchant (1) and Piispanen (2). The composite force diagram of Merchant, reproduced in Figure AI.1, shows the components of a single force vector, R, which represents two equal and opposite forces, R' and R, holding the chip in equilibrium.

The following velocity, force, stress and work relationships are derived from the geometry of Figure AI.1:

$$V_S = V_C \cos\alpha/\cos(\phi-\alpha) \qquad \text{AI.1}$$

$$V_F = V_C \sin\phi/\cos(\phi-\alpha) \qquad \text{AI.2}$$

$$\mu = F/N = (F_T + F_C \tan\alpha)/(F_C - F_T/\tan\alpha) \qquad \text{AI.3}$$

$$F = F_T \cos\alpha + F_C \sin\alpha \qquad \text{AI.4}$$

$$F_S = F_C \cos\phi - F_T \sin\phi \qquad \text{AI.5}$$

$$S_S = F_S/A_s = (F_C \sin\phi \cos\phi - F_T \sin^2\phi)/A_o \qquad \text{AI.6}$$

$$S_N = F_N/A_s = S_S \tan(\phi + \gamma - \alpha) \qquad \text{AI.7}$$

$$W_F = Fr_C/A_o = F/A_c \qquad \text{AI.8}$$

$$W_S = S_S \cdot \varepsilon \qquad \text{AI.9}$$

$$W_C = S_S \cdot \varepsilon + F/A_c = W_S + W_F \qquad \text{AI.10}$$

where

$\alpha$ is the true rake angle of the cutting tool,

$\phi$ is the shear angle,, i.e. the angle which the shear plane makes with the surface generated,

$V_C$ is the cutting velocity,

$V_S$ is the velocity of shear in the shear plane,

$V_F$ is the chip velocity on the rake face of the tool,

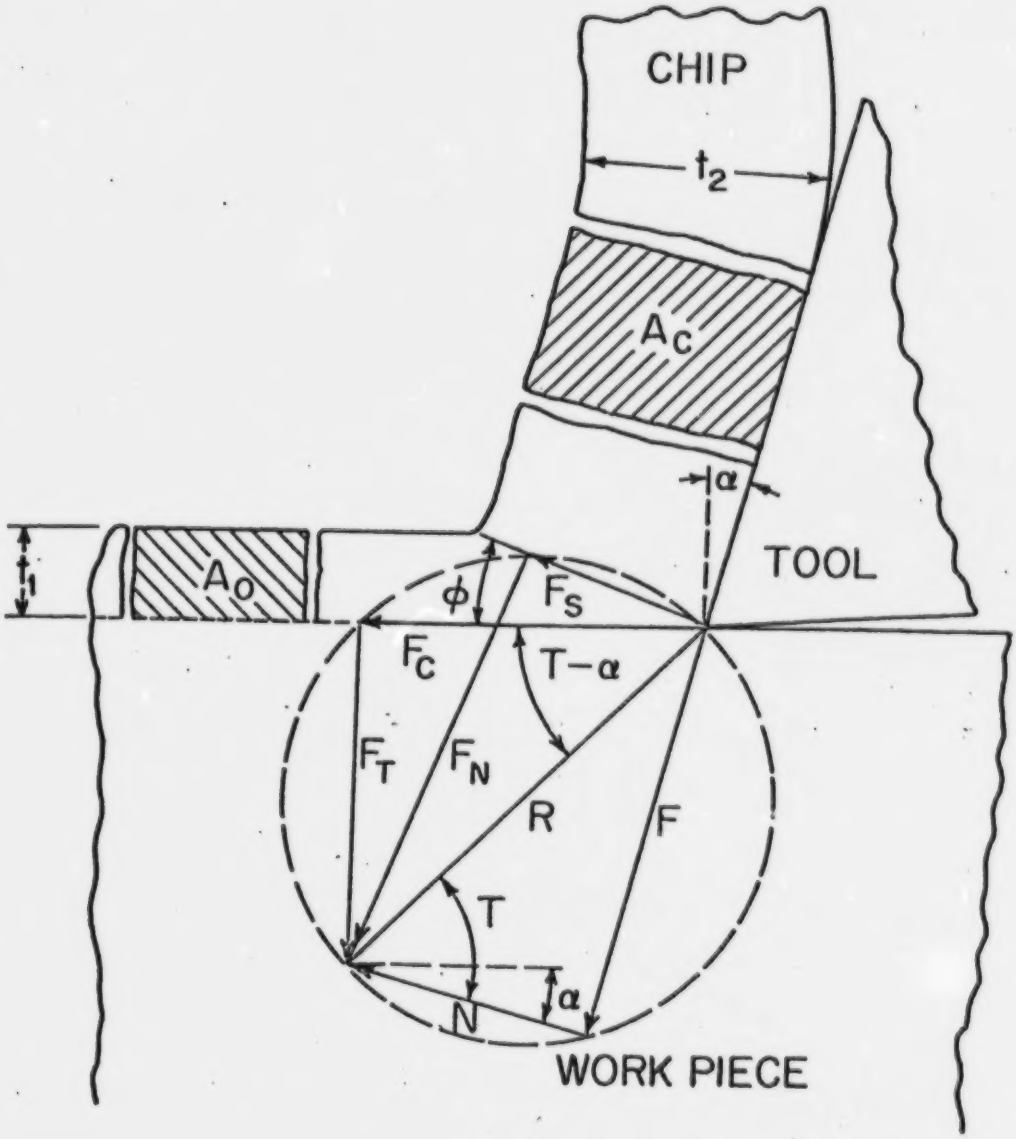


Fig. AI.1 - The Composite Force Diagram of Merchant (1).

$F$ and $N$ are, respectively, the friction force along the rake face the force normal to the rake face which result from the resolution of the force R', exerted by the tool on the chip, relative to the rake face,

$\mu$ is the coefficient of friction,

$\tau$ is the friction angle between N and R',

$F_S$ and $F_N$ are, respectively, the shearing force on the shear plane and the compressive force normal to the shear plane resulting from the resolution of the force R, exerted by the workpiece on the chip, relative to the shear plane,

$F_C$ and $F_T$ are, respectively, the cutting force and the thrust force, resulting from the resolution of the force R along the direction of motion of the tool relative to the workpiece,

$S_S$ is the mean shear stress on the shear plane and is equal to the mean shear strength of the workpiece,

$A_s$ is the area of the shear plane,

$A_o$ is the cross-sectional area of the "chip" before removal,

$S_N$ is the mean compressive stress on the shear plane,

$W_F$ is the work expended in friction between the chip and tool per unit volume of metal removed,

$r_c$ is the cutting ratio, which is the ratio of the length of the chip before removal to its length after removal (equivalent to $t_1/t_2$ in Fig. AI.1),

$A_c$ is the cross-sectional area of the chip after removal ($A_c = A_o/r_c$)

$W_S$ is the work expended in shearing the metal per unit volume of metal removed,

and, $W_C$ is the total work expended in cutting per unit volume of metal removed.

The shear strain, $\varepsilon$, may be derived from the relationship:

$$\varepsilon = \cot\psi = \cot\phi + \tan(\phi - \alpha) \qquad \text{AI.11}$$

where $\psi$ is the angle the direction of crystal elongation makes with the shear plane.

In a subsequent development of this treatment, Merchant (3) assumed that the shear strength of the workpiece would establish the value of the shear angle, $\phi$, for any given value of the angle $(\tau-\alpha)$ in Fig. AI.1 such that the total work done in cutting was a minimum, i.e., the angle $\phi$ must satisfy the condition $dF_c/d\phi = 0$.

From the geometry of Fig. AI.1:

$$F_C = R\cos(\tau-\alpha) = F_C\cos(\tau-\alpha)/\cos(\phi+\tau-\alpha) \qquad \text{AI.12}$$

and since

$$F_S = S_S A_o/\sin\phi$$

$$F_C = S_S A_o\cos(\tau-\alpha)/\sin\phi\cos(\phi+\tau-\alpha) \qquad \text{AI.13}$$

During cutting,

$$S_S = S_S' \qquad \text{AI.14}$$

where $S_S'$ is the sleve strength of the workpiece. $S_S'$ is not a constant during cutting but is a function of strain, strain rate, temperature and the compressive stress acting on the shear plane, $S_N$. As a first approximation, Merchant assumed that $S_S'$ was a linear function of $S_N$:

$$S_S' = S_o + k\,S_N \qquad \text{AI.15}$$

where $S_o$ is the shear strength of the workpiece under zero compressive stress and k is a constant. The formulation of this type of

relationship was based on the data of Bridgeman (4). Substitution of Eqs. AI.7 and AI.14 into Eq. AI.15 yields:

$$S_S' = S_o/[1 - k \tan(\phi+\tau-\alpha)] \qquad \text{AI.16}$$

Substitution of Eq. AI.14 and AI.16 into Eq. AI.13 leads to the following expession for the cutting force, $F_C$:

$$F_C = S_o A_o \cos(\tau-\alpha)/[\sin\phi \cos(\phi+\tau-\alpha) - k\sin\phi \sin(\phi+\tau-\alpha)] \qquad \text{AI.17}$$

Application of the minimum energy principle, $dF_C/d\phi = 0$, gives the following condition:

$$\cot(2\phi+\tau-\alpha) = k \qquad \text{AI.18}$$

or

$$2\phi + \tau - \alpha = C \qquad \text{AI.19}$$

where C = arc cot k.

Substitution of Eqs. AI.14 and AI.19 in Eqs. AI.3 through AI.10 give force, stress and work relationships free of force components:

$$\mu = \tan(C-2\phi+\alpha) \qquad \text{AI.20}$$

$$F = A_o S_S' \sin(C-2\phi+\alpha)/\sin\phi \cos(C-\phi) \qquad \text{AI.21}$$

$$F = A_o S_S'/\sin\phi \qquad \text{AI.22}$$

$$S_S' = S_o/[1 - k \tan(C-\phi)] \qquad \text{AI.23}$$

$$S_N = S_S' \tan(C-\phi) \qquad \text{AI.24}$$

$$W_F = S_S' [\tan(C-\phi) - \tan(\phi-\alpha)] \qquad \text{AI.25}$$

$$W_F = S_S' \cdot \varepsilon \qquad \text{AI.26}$$

$$W_C = S_S' [\tan(C-\phi) + \cot\phi] \qquad \text{AI.27}$$

The cutting and thrust forces are given by the relationships:

$$F_C = A_o S_S' [\tan(C-\phi) + \cot\phi] \qquad \text{AI.28}$$

and

$$F_T = A_o S_S' [\tan(C-\phi) \cot\phi - 1] \qquad \text{AI.29}$$

respectively.

Using this analysis, values of the constants $S_o$ and k can be obtained from cutting tests in which both forces and chip geometry are measured. A prior knowledge of $S_o$ and k would enable the analysis of the force system from chip formation geometry and no force measurements would be required.

The assumption that the flow stress is independent of the normal stress, i.e., k=o, leads to the expression:

$$2\phi = 90^o + \alpha - \tau \qquad \text{AI.30}$$

Merchant found that experimental data did not meet the conditions given by Eq. AI.30, better agreement being obtained with Eq. AI.19. A variety of expressions for $\phi$ have been formulated based on more complicated models, even invoking the principles of irreversible thermodynamics, but none of these is in good agreement with experimental data.

## AI.2 DEVIATIONS FROM THE PLANE STRAIN MODEL

Models of the machining process assume that plane strain conditions are satisfied. Factors leading to deviations from plane strain conditions are outlined below.

1) Deformation of material takes place in a shear zone and not instantaneously in a shear plane. This zone may or may not be straight (5) and its thickness may not be constant along its length. Hence, the strain and the strain rate that a small element undergoes depends on its position in the zone, (see Appendix II).

2) There is further deformation on the tool side of the chip as it is subjected to friction forces on the face of the tool. The grain deformation lines bend downwards as they approach the tool face.

3) Under certain circumstances some of the workpiece material adheres to the tool. This gives rise to the formation of a built-up-edge, (BUE), which profoundly changes the geometry of cutting.

4) The assumption of continuous chip, (Type II), formation is made and in practice the chip can curl away from the tool.

5) In ideal models, the tool is assumed to be infinitely sharp. In fracture a radius is soon established and the lower portion of the nose is constantly rubbing against the freshly machined surface.

## APPENDIX II

## SHEAR ZONE STREAMLINE ANALYSIS

### AII.1 THE MODEL OF SPAANS

Spaans (7) has studied streamline shape in the shear zone, by carrying out quick-stop tests on a workpiece consisting of two discs of a 0.45% C steel bolted together. A grid cut into the inside of one of the discs was pressed into the other one during cutting by the local hydrostatic pressure. Spaans found that streamline shape could be best predicted by a model in which it was assumed that the shear zone flow stress is constant. This means that the shape of the streamlines must satisfy the requirements of a constant flow stress under conditions of changing hydrostatic pressure, temperature, strain and strain rate. The model, which assumes that:

a) the normal stress does not affect the flow stress significantly, and

b) the shear zone boundaries are parallel

is summarized below.

The material in the shear zone is considered as a number of slices of thickness $\Delta x$, as shown in Fig. AII.1. The distance any particular slice slides over its neighbour, if that slice has moved a distance $\Delta x$ in the X-direction, is given by the corresponding increment $\Delta y$. The local shear strain increment for unit time for the limit $\Delta x \to 0$ is then given by:

$$\dot{\varepsilon} = d(dy/dx)/dt \qquad \text{AII.1}$$

The velocity of the material perpendicular to the shear zone, $V_N$, can be found from the shear velocity, $V_S$ and the shear angle, $\phi$:

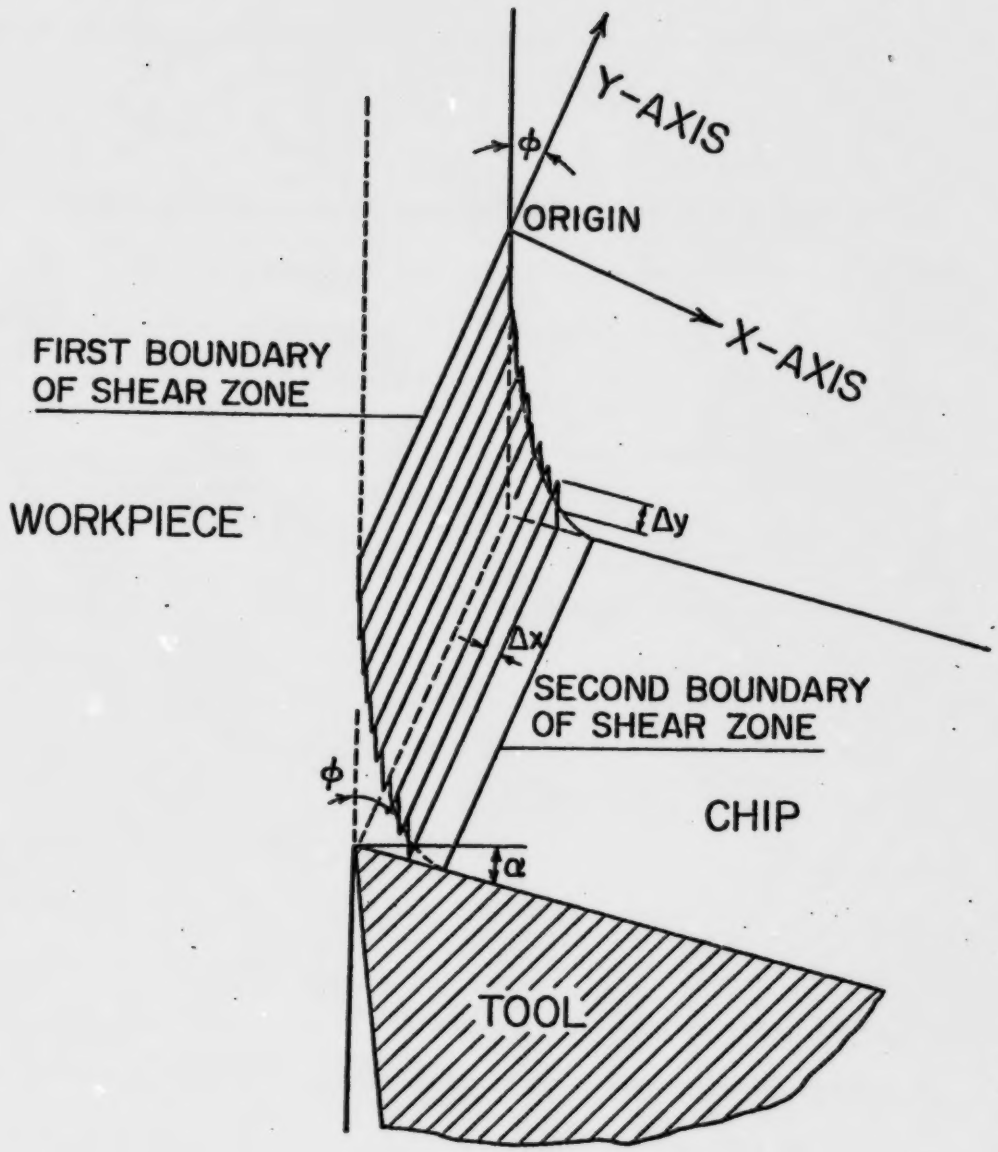


Fig. AII.1 - Model of Deformation in the Shear Zone (7).

$$V_N = V_S \sin\phi \qquad \text{AII.2}$$

and therefore

$$\dot{\varepsilon} = V_N(d^2y/dx^2) \qquad \text{AII.3}$$

The relationship expressing the flow stress $S'_S$ as a linear function of strain rate and temperature:

$$S'_S = S'_o + A(\dot{\varepsilon} - \dot{\varepsilon}_o) - B\, S'_S \varepsilon \qquad \text{AII.4}$$

where $S'_o$ is the flow stress at the origin, see Fig. AII.2, at room temperature and a strain rate $\dot{\varepsilon}_o$, and A and B are constants, is based qualitatively on the work of Muller (8) who examined the stress-strain behaviour of Ferrovac-E as a function of strain rate and temperature. Muller found a linear dependence between flow stress and strain rate at strain rates > 1500 $sec^{-1}$ and temperatures between 20 and 500°C. The "constant", A, is a function of temperature and Spaans chose a value based on the mean temperature of the shear zone. The local temperature is assumed to result adiabatically from the dissipation of the work done in shear, $W_S = S'_S \cdot \varepsilon$. From Muller's results it appears that there is an almost linear relationship between flow stress and temperature between 20 and 250°C at strain rates of ~ 6000 $sec^{-1}$.

The shear strain, $\varepsilon$, is given by the relationship:

$$\varepsilon = \int_o^x \frac{d^2y}{dx^2} \cdot dx = \frac{dy}{dx} + C_1 \qquad \text{AII.5}$$

and since $\varepsilon = 0$ and $dy/dx = -\cot\phi$ at the origin,

$$\varepsilon = dy/dx + \cot\phi \qquad \text{AII.6}$$

For constant $S'_s$ throughout the shear zone the differential equation:

$$AV_N(d^2y/dx^2) - BS'_S(dy/dx) = A\dot{\varepsilon}_o + BS'_S \cot\phi \qquad \text{AII.7}$$

can be obtained from Eqs. AII.3, AII.4 and AII.6. The solution of this equation is:

$$y = C_2\, e^{ax} - x((A\dot{\varepsilon}_o/BS_S') + \cot\phi) + C_3 \qquad \text{AII.8}$$

where

$$a = BS_S'/AV_N.$$

Making use of the relationship for the strain rate at the origin:

$$\dot{\varepsilon}_o = V_N \left(\frac{d^2y}{dx^2}\right)_{x=o} = V_N\, C_2\, a^2 \qquad \text{AII.9}$$

and with the boundary conditions that the streamline should pass through the origin of the coordinate system, $dy/dx = \tan(\phi-\alpha)$ and $x = d_s$, the thickness of the shear zone, Eq. AII.8 transforms to:

$$y = C_2(e^{ax} - 1) - x(C_2 a + \cot\phi) \qquad \text{AII.10}$$

where

$$C_2 = (\tan(\phi-\alpha) + \cot\phi)/a(e^{ad_s} - 1) \qquad \text{AII.11}$$

Eliminating $C_2$ from Eqs. AII.9 and AII.10, the following expression is obtained for $d_s$:

$$d_s = \frac{1}{a}\, \ell n\left\{\frac{a\, V_N}{\dot{\varepsilon}_o}\, (\tan(\phi-\alpha) + \cot\phi) + 1\right\} \qquad \text{AII.12}$$

The expression developed by Muller (8):

$$\sigma_h - \sigma_B = 0.35\, \ell n\, (1 + 10^5\, \dot{\varepsilon}_n) + 1.6\, \ell n\, (1 + 2\dot{\varepsilon}_n) + 1.7 \times 10^{-3}\, \dot{\varepsilon}_n \qquad \text{AII.13}$$

where $\sigma_n$ and $\varepsilon_n$ are the true stress and strain, respectively, and $\sigma_B$ is obtained from a low strain tensile test at room temperature, enables $\dot{\varepsilon}_o$ to be determined from the flow stress determined during cutting.

The values of the constants A and B in eq. AII.4 can be determined approximately from the data of Muller (8). The increase in the true stress, $\Delta\sigma_n$, with strain rate, $\dot{\varepsilon}_n$, at strain rates of about $10^3$ $sec^{-1}$ can be taken from Eq. AII.13:

$$\Delta\sigma_n = 1.7 \times 10^{-3} \dot{\varepsilon}_n \qquad \text{AII.14}$$

Applying the distortion energy criteria for plane strain conditions (29), $S_S' = \sigma_n/\sqrt{3}$ and $\dot{\varepsilon} = \dot{\varepsilon}_n \sqrt{3}$:

$$\Delta S_S' = (1.7 \times 10^{-3} \dot{\varepsilon})/3 \qquad \text{AII.15}$$

The coefficient A is then given by the relationship:

$$A = 1.7 \times 10^3/3 = 0.57 \text{ Kgf/mm}^2/\text{sec}^{-1} \qquad \text{AII.16}$$

Again from the data of Muller, $\partial\sigma_n/\partial T$ is constant and can be taken as 0.116 Kgf/mm$^2$/$^o$C at strain rates of between $1.5 \times 10^3$ sec$^{-1}$ and $5.5 \times 10^3$ sec$^{-1}$, and thus $\partial S_S'/\partial T = 0.116/\sqrt{3}$ Kgf/mm$^2$/$^o$C. The increase in temperature in the shear zone is given by the relationship:

$$\Delta T = \varepsilon S_S'/JpC_\omega \qquad \text{AII.17}$$

where J is the mechanical equivalent of heat, p the density and $C_\omega$ the specific heat of the workpiece. For a 0.45% steel, the value of $1/JpC_\omega$ is about 0.55$^o$C/KgF/mm$^2$ in the temperature range under consideration giving a value of the coefficient B of 0.17. The thickness of the shear zone and the shape of the streamlines can then be determined from Eqs. AII.12 and AII.10, respectively.

The calculated shape of the streamlines, together with profiles of temperature, stress and strain rate in the shear zone, is shown in Fig. AII.2, for a 0.45%C steel at a cutting speed of 200 m/min.

### AII.1.1 Effect of Normal Stress on the Shear Stress

In contrast to Merchant (1,3) who assumed that the flow stress was a linear function of the normal stress acting on the shear plane (Eq. AI.15), Spaans assumed that the normal stress does not affect the flow stress significantly. Supporting evidence for this assumption is provided by the work of Kobayashi and Thomsen (4) who studied the

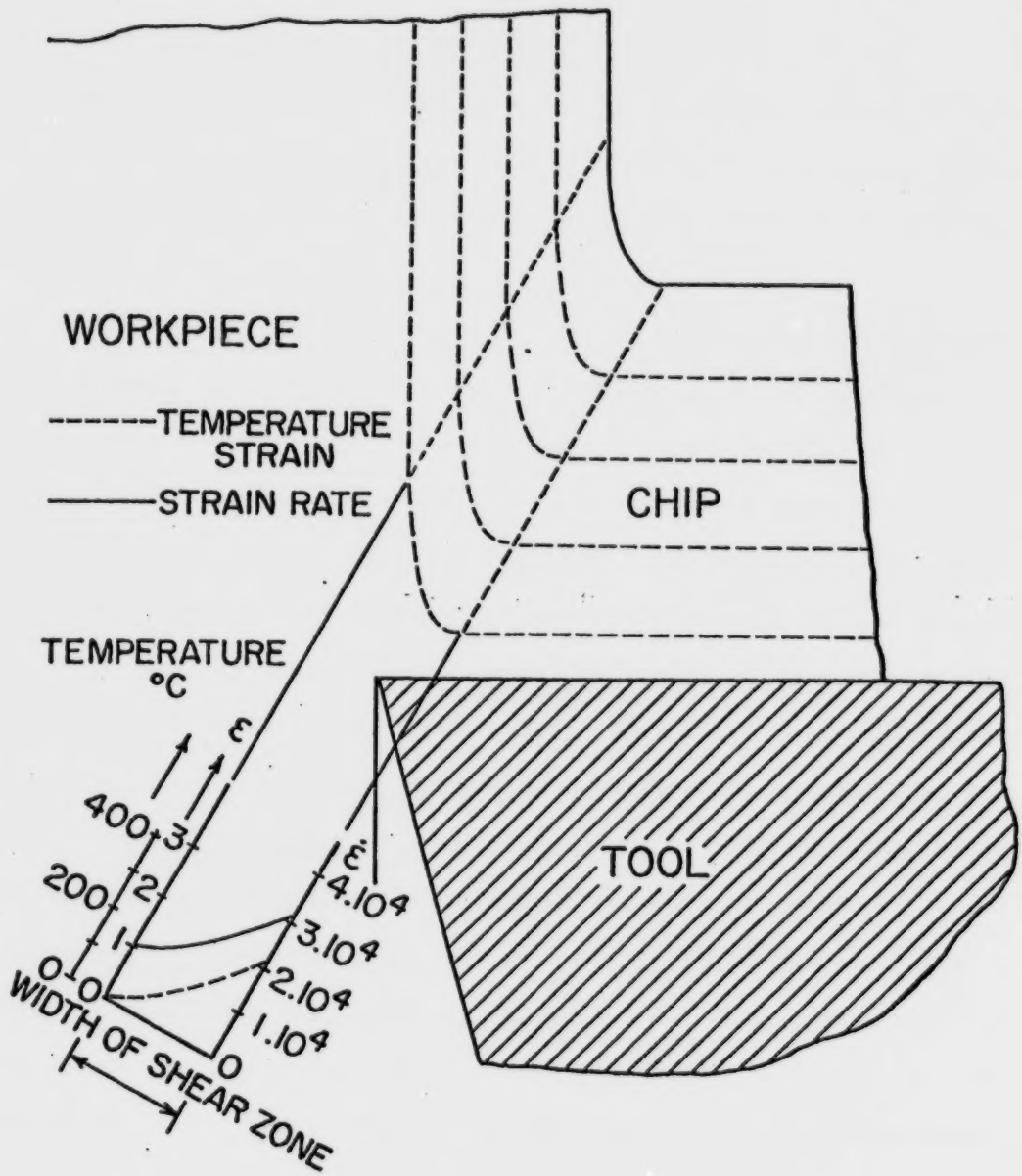


Fig. AII.2 - Temperature, Strain and Strain Rate Profiles in the Shear Zone. $V_C$ = 200 m/min. (7).

variation of the shear and normal stresses when cutting an 85/15 brass with varying rake angles and depth of cut. While the shear stress is independent of rake angles between 20 and 40°, larger normal stresses are associated with smaller rake angles. The implication is that the normal stress has no effect on the magnitude of the shear stress. This observation requires verification from independent mechanical tests at high strain rates.

# APPENDIX III

# THE INITIATION AND PROPAGATION OF DUCTILE FRACTURE

## AIII.1 THE MODEL OF KNOTT AND CO-WORKERS

The effects of work-hardening rates and inclusion content on the initiation and propagation of ductile fracture in low strength steels during chip formation can be treated using the concepts of fracture mechanics.

Green and Knott (9) have used the fracture mechanics crack opening displacement, COD, concept to relate fracture processes to measurable microstructural parameters. The COD concept considers that there is a critical displacement at the tip of a stress concentrator, such as a crack, at which fibrous fracture initiates. The basis for the model, Fig. AIII.1, is that the ligament between the crack tip and the nearest inclusion must be strained sufficiently for a void to be nucleated, to grow and to coalesce with the crack tip. This model has been treated mathematically by Rice and Johnson (10), and their predictions for variation of $\delta_i/X_o$ with $X_o/R_o$ are shown in Fig. III.2, where $\delta_i$ is the COD required for the initiation of fibrous fracture, $X_o$ is the inclusion spacing and $R_o$ is the inclusion radius. The experimental results for a number of steels are also shown in Fig. AIII.2 and since both normalised C/Mn steel and resulphurised free cutting steel lie close to the theoretical curve, it is possible to calculate a value of K, the stress intensity factor, at the initiation of fracture, from the microstructural parameter, $X_o$. The essential features of the Green & Knott paper are summarised below.

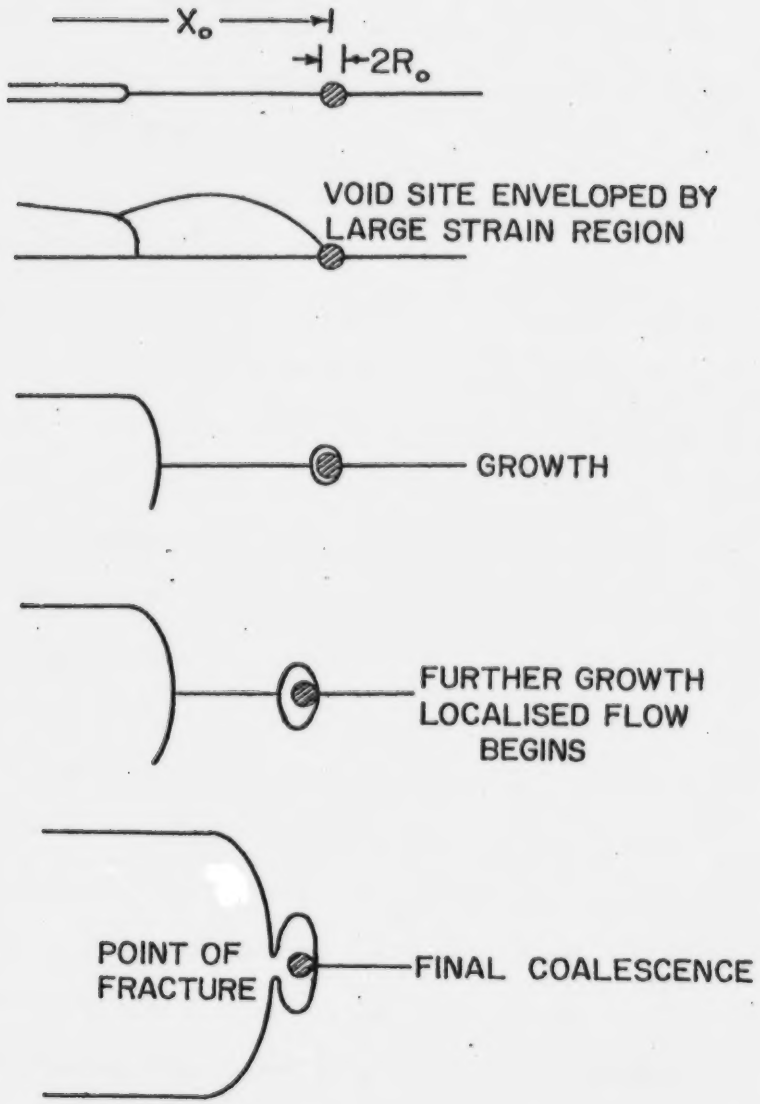


Fig. AIII.1 - The Model for Ductile Fracture (9).

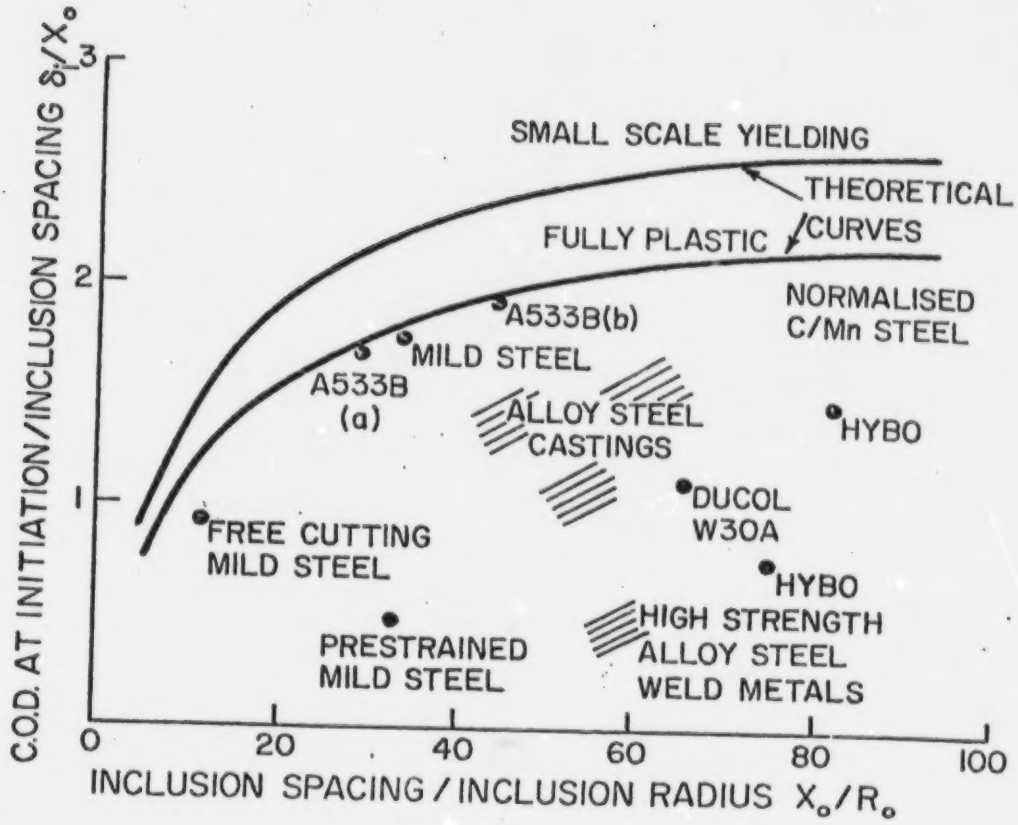


Fig. AIII.2 - $\delta_i/X_o$ as a function of $X_o/R_o$ (9).

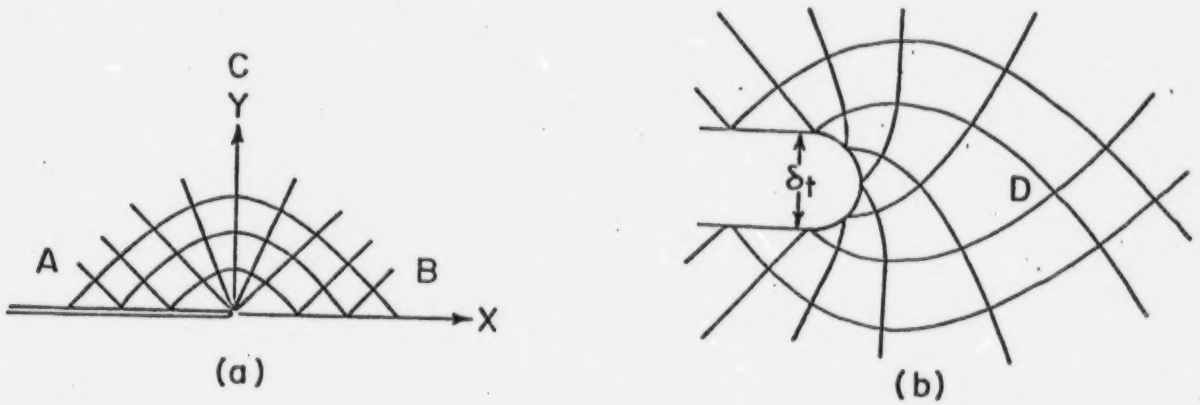


Fig. AIII.3 - Slip Line Fields for a) a Sharp Crack Tip and b) a Blunted Crack Tip (9).

Slip line fields for a sharp and blunted crack tip are shown in Figs. AIII.3. The point D in Fig. AIII.3(b) is the focus of the logarithmic spiral of shear lines, and intense strain concentrations are found there. For oxide and sulphide inclusions in steel, no void formation is necessary, and when the point D is coincident with the centre of the inclusion, localised linkage occurs in non-hardening materials, with final shear along the logarithmic spirals at values of $\delta_i \simeq 0.5X_o$. When work hardening can occur, the local strain distribution ahead of the crack tip is more widespread, since each successive increment of strain causes the next strain increment to occur in a different position. More local uniform strain occurs before the conditions for final necking between the expanding void and the blunting tip are attained. Predicted values of $\delta_i$ are now between 0.5 $X_o$ and 2.5 $X_o$, depending on the initial void radius.

Fibrous fracture initiation is characterised by two strain zones, see Fig. AIII.4. The first of these is the 'process zone' in which the strains are large and approximately equal to the fracture strain. The second is the 'plastic zone', where the strains are smaller but the area is very much larger. The development of the process zone requires the development of a plastic zone of sufficient size to accomodate the displacements involved through strain gradients which vary according to the work-hardening capacity of the matrix. Schematic plastic zones in low and high work-hardening materials are shown in Fig. AIII.5. For a given notch tip ductibility the plastic zone size is smaller in materials of low work-hardening capacity.

The notch tip ductibility is also influenced by the work-hardening capacity of the material (11) as is shown in Table AIII.1, which

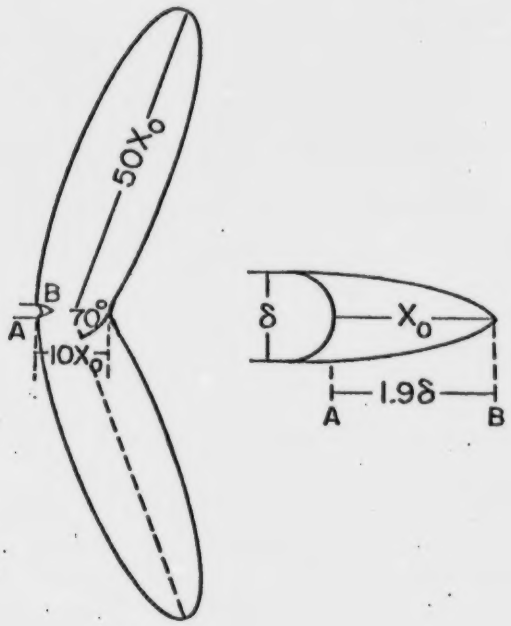


AIII.4 - The Process and Plastic Strain Zones (9).

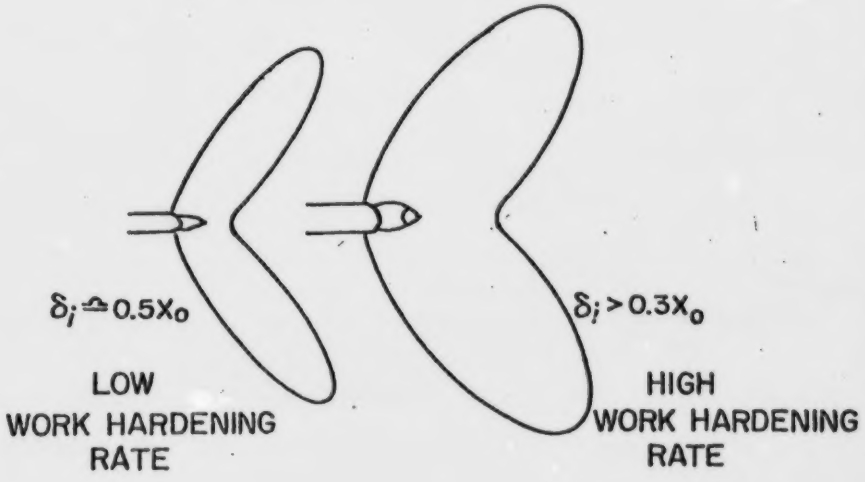


AIII.5 - Schematic Plastic Zones for Low and High Work-hardening Materials (9).

illustrates the effect of prestraining a free machining mild steel on $\delta_i/X_o$ values.

Table AIII.1 The Effect of Work-Hardening Capacity on Notch Tip Ductility

| Material condition | $\delta_i$ μm | $\delta_i/X_o$ ($X_o$=120 μm) |
|---|---|---|
| Normalised free machining mild steel | 220 | 1.83 |
| 20% prestrain | 68 | 0.56 |
| 40% prestrain | 59 | 0.49 |

In the prestrained material, the ligament between the void and the crack tip is work-hardened sufficiently to become unstable once the process zone has enveloped a favourable inclusion and the ratio $\delta_i/X_o$ approaches 0.5, in accordance with theory.

Inclusions affect the initiation of ductile fracture in two ways. They influence the strain required to initiate fracture and they determine the gauge lengths over which the fracture strain is attained. A marked decrease in ductility is observed with increasing volume fraction of inclusions. The ductility is influenced by the inclusion shape and the degree of triaxiality since both these affect the rates of void growth. Theoretical models concentrate on void growth and predict instability when the void spacing approaches a critical value. Local deformation sets in at this stage and fracture occurs with little further elongation.

The theoretical models predict a variation of fracture strain, $\varepsilon_f$, with volume fraction of inclusions, $V_f$, of the type:

$$\varepsilon_f = \beta \ln (1/V_f) \qquad \text{AIII.1}$$

where $\beta$ is a constant.

Smith and Knott (11) have shown that $\delta_i$ can be expressed as the product of an apparent fracture strain and a microstructurally determined gauge length:

$$\delta_i = \varepsilon_f X_o \qquad \text{AIII.2}$$

To a first approximation, the fracture strain can be estimated from the effect of inclusion content on tensile ductibility, Eq. AIII.1, and hence:

$$\delta_i = \beta X_o \ln (1/V_f) \qquad \text{AIII.3}$$

Since $1/\sqrt{V_f}$ is proportional to $X_o$:

$$\delta_i = \beta' X_o \ln X_o \qquad \text{AIII.4}$$

Green & Knott (9) showed that, for two steels of differing $X_o$, the observed and predicted $\delta_i$ ratios were in good agreement, see Table III.2.

Table III.2 The Effect of Inclusion Spacing, $X_o$ on $\delta_i$.

| | $X_o$ μm | $\delta_i$ μm | Observed $\delta_i$ ratio | Calculated $\delta_i$ ratio |
|---|---|---|---|---|
| Steel 1 | 210 | 320 | 2.2 | 1.95 |
| Steel 2 | 120 | 145 | | |

Where there is a range of inclusion sizes, it is the large inclusions (>4μm) which determine the gauge length over which the fracture process takes place and the small inclusions determine the fracture strain required on that gauge length. (The choice of inclusion

size appears to be arbitrary in Green & Knott's paper, but it may be based on phenomenonological observations). Green & Knott compared two mild steels of differing sulphur content, Table AIII.3. The low sulphur mild steel (0.032%S) contained a number of large (>6μm) manganese sulphide stringers and many more smaller manganese sulphide inclusions. The high sulphur mild steel (0.24%S) contained mostly large sulphide inclusions.

Table AIII.3 The Effect of Sulphur Content on $\delta_i/X_o$.

| | $\delta_i$ μm | $X_o$ μm | $\delta_i/X_o$ |
|---|---|---|---|
| 0.24%S steel | 40 | 46 | 0.88 |
| 0.032%S steel | 220 | 104 | 2.11 |

It is the spacing of the large inclusions which determine the gauge length in the 0.32%S mild steel. In materials of high work-hardening capacity where the small inclusions are closely spaced, a reduction in ductility is observed.

The greatest effect of inclusions on the energy needed for ductile fracture initiation is in fixing the characteristic distance over which the fracture strain is reached. This dictates the process zone size which in itself determines the plastic zone size for given work hardening properties. A small decrease in inclusion content can therefore produce a large increase in ductility. Thus the values of $\delta_i$ can be related to the inclusions distribution and to the matrix work-hardening capacity.

The work expended in the process zone for the <u>initiation</u> of

fracture in a medium strength low carbon alloy steel has been estimated by Green & Knott to be 1GJ $m^{-3}$, whereas the work absorbed in the plastic zone is 144 GJ $m^{-3}$. In comparison, the work required for crack propagation is estimated to be 1GJ $m^{-3}$ for the process zone and 2.5 GJ $m^{-3}$ for the plastic zone. For materials with similar flow properties the relative resistance to crack propagation should be proportional to the initiation resistance. Higher values of plane strain crack growth resistance ($d\delta/da$) are observed in materials with higher values of $\delta_i$, see Table AIII.4, where values of $d\delta/da$ are obtained from curves of COD vs fibrous crack length (a), and values of $\delta_i$ are obtained by extrapolating these curves back to zero fibrous crack length.

Table AIII.4 The Effect of Sulphur Content on Crack Propagation

| Material | $\delta_i$-mm | $d\delta/da$ |
|---|---|---|
| 0.032%S | 0.15 | $12.5 \times 10^{-2}$ |
| 0.24%S | 0.273 | $7.4 \times 10^{-2}$ |

It is important to note that the plastic zone is reduced in size to a greater extent in materials of low work-hardening capacity. Intense local strains can develop in the process zone without the need for accommodation by strain gradients in the plastic zone. The plastic work term and the value of $\delta_i$ for such materials is drastically reduced.

AIII.1.1 Strain Localization

As shown in Fig. AIII.2, the $\delta_i$ values of a number of steels are well below the prediction of Rice & Johnson. In a material of low

work-hardening capacity, e.g., a cold worked steel, shear fracture with negligible crack blunting occurs when voids nucleate round inclusions at low strains. Shear bands become localised in the directions of the nearest voids ahead of the crack tip and it is possible for decohesion to occur by shear along these bands before the crack tip has blunted substantially. The final fracture will be crack-like and zig-zag from inclusion to inclusion. A similar effect can occur in a precipitation hardened matrix containing widely spaced non-melattic inclusions. As the matrix is strained, dislocations loop around the carbides until such high local stress levels are reached that the interfaces decohere. At this point the resistance to flow drops catastrophically and a fast shear fracture results. It has been found that carbide/matrix interfaces can be embrittled by inpurity element segregation, possibly phosphorous, resulting in a 50% decrease in value of $\delta_i$ for ductile separation and a corresponding decrease in the value of $d\delta/da$.

The effect of work-hardening capacity and its influence upon flow localisation is the basis of a simple model due to Hahn and Rosenfield (12) which attempts to relate the fracture toughness parameter to unidirectional tensile properties and microstructional parameters. A material having a high strain-hardening capacity (a high value for the constant, n, where the form of the tensile stress-strain curve is given by $p = p_o \varepsilon_p^n$) will effectively have a lower strain concentration at the crack tip for a given stress level. Work-hardening essentially causes lateral spreading of the zone of plasticity into a more diffuse region thereby causing crack tip displacements. Assuming ductile fracture will occur when a given critical strain is reached, higher stress levels can be supported before failure occurs, i.e., the material has a greater

toughness. Hahn and Rosenfield express the critical crack opening displacement, $\delta_c$, in terms of a critical fracture strain, $\epsilon_c^*$ and the plastic zone width, $\ell^*$, at the onset of fracture:

$$\delta_c = 2\ \epsilon_c^*\ \ell^* \qquad \text{AIII.5}$$

Experimentally, they observed that the width of the plastic zone is proportional to $n^2$, and development of the model gives:

$$K_{Ic} \propto n(p_y \epsilon_c^*)^{1/2} \qquad \text{AIII.6}$$

$\epsilon_c^*$ is dependent on the volume fraction of void-nucleating particles and Garrett and Knott (13) have found Eq. AIII.6 to give reasonable agreement with measured values of $K_{Ic}$ in a range of commercial and pure aluminum alloys.

## APPENDIX IV

## INCLUSIONS AND MACHINABILITY

### AIV.1 INCLUSIONS AND DUCTILE FRACTURE

The theory of ductile fracture involving void nucleation, growth and coalescence in the final catastrophic stage of fracture, to give the characteristic 'dimple and cusp' appearance of the fracture surface, has been summarized by Gladman et al. (14). The treatment of Green and Knott (9) relating to the mirostructural changes taking place during the initiation and propagation of ductile fracture, is given in Appendix III.

In the case of non-metallic inclusions in steel, cavitation occurs by decohesion of the matrix/inclusion interface at negligible strain. The total strain to fracture, $\varepsilon_T$, can then be represented by the relationship:

$$\varepsilon_T = \text{ln}[(\phi^2/f_o^2 + k(r^2)/1 + k\,r^2)]/2 \qquad \text{AIV.1}$$

where $\phi$ is the critical volume fraction of voids ($\simeq 0.05$) required for coalescence,

$f_o$ is the original volume fraction of inclusions

$k$ is a strain intensification constant of about 2

and $r$ is the length to width ratio of the inclusion where straining is in the length direction.

The equation indicates that increasing the volume fraction of inclusions reduces the strain to fracture, (one of the major effects of MnS inclusions during machining). The shape factor, r, exerts a major effect on the denominator of the logarithmic term when $\phi >> f_o$. An increase in the length to width ratio improves ductility in the

longitudinal direction. A decrease in the length-to-width ratio to a value less than unity will reduce the longitudinal ductility.

## AIV.2 SULPHIDE MODIFICATION

The oxygen content of steel has a pronounced effect on the plasticity of sulphides during hot working and hence on their final morphology. The high oxygen content of rimmed or semi-killed steels give rise to the so-called globular Type I manganese sulphide inclusions which contain dissolved oxygen. These Mn(S,O) oxysulphides do not deform readily at hot-working temperatures and they remain fairly globular even in wrought bars and plates. In killed steels, where low levels of soluble oxygen are attained through the use of strong deoxidisers such as aluminum, Type II inclusions elongate parallel to the principal working direction during hot rolling or forging and lead to a decrease in transverse ductility. Improvements in transverse ductility can be achieved by modificatiton of the Type II 'pure' MnS inclusion to form complex Type III sulphide inclusions which do not readily deform at hot-working temperatures. In the manufacture of machining grades, sulphide inclusion modification has been reported using additions such as Ca, Ca-Si, Zr, Ti, Se and/or Te, and Pb. This has been particularly popular in the production of quality carbon, low alloy and alloy machining grades, where good machinability must be consistent with the maintenance of adequate transverse ductility. In this respect, it should be noted that sulphide inclusion modification leading to improved ductility is not consistent with improvements in machinability associated with decreases in the total strain to fracture, $\varepsilon_T$.

## AIV.3 OXIDE MODIFICATION

The modification of oxide inclusions in the production of machining grades has been carried out primarily to achieve improvements in tool wear. The modification of hard abrasive alumina particles is reported to have a beneficial effect on both HSS and carbide tool wear. The formation of $CaO-Al_2O_3-SiO_2$ inclusions, which become 'plastic' at the high cutting temperatures achieved using carbide tools, and form an oxide diffusion barrier on the rake face of the tool, has a beneficial effect on carbide tool wear. In this respect the $CaO-Al_2O_3-SiO_2$ phase diagram (15), reproduced in Fig. AIV.1 has been used extensively in controlled deoxidation studies.

## AIV.3 MODIFICATION METHODS

Iodkovsky et al. (16) have studied the effect of controlled deoxidation using Ca-Si and Ca-Al-Si treatments. Deoxidation with Ca-Si alone produced duplex inclusions containing phases with compositions close to $CaO-SiO_2$ and $3CaO.Al_2O_3.3SiO_2$. The elimination of $Al_2O_3$ inclusions greatly increased HSS tool life and even small additions of aluminum deoxidant were found to be harmful. Randak et al. (17) emphasized the reduction of oxide inclusion content in the production of special constructional steels, containing 0.06-0.09%S, for HSS machining. The advantages of Ca-Si deoxidation were attributed to the envelopment of the harmful $Al_2O_3$ inclusions by soft CaS. Radnal et al. also attributed reduced carbide tool wear to the formation of a lubricating/diffusion barrier film of $CaO-Al_2O_3-SiO_2$ inclusions. Fujiwara et al. (18) also report improved HSS tool life in the machining of Ca-deoxidised steels and attributed the improvement to the presence

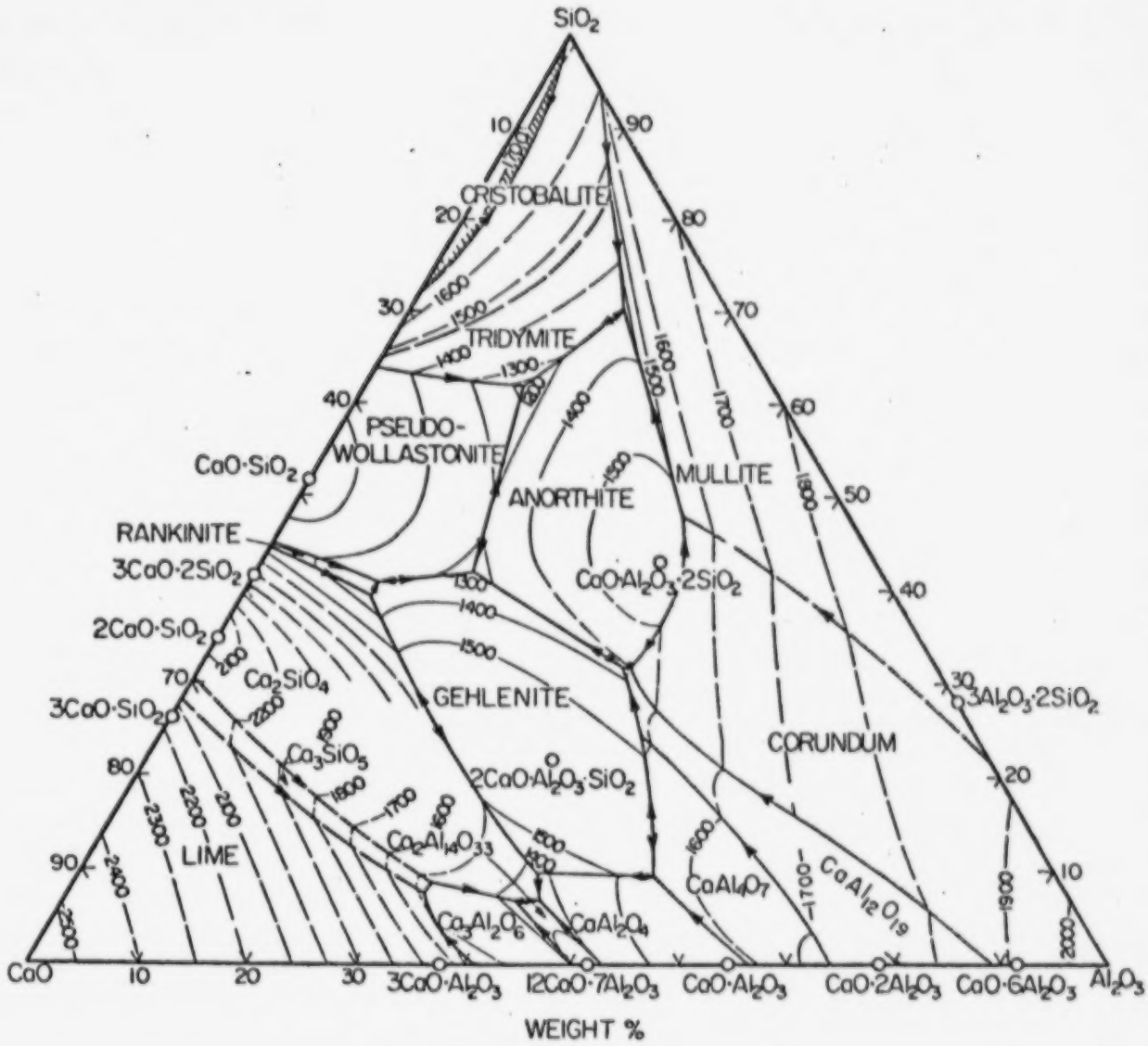


Fig. AIV.1 - The $CaO-Al_2O_3$ - $SiO_2$ Phase Diagram (15).

of anorthitic inclusions. Steels containing gehlenitic inclusions gave about the same tool life as conventional Al-killed steels containing alumina inclusions. The effect of different $CaO-Al_2O_3-SiO_2$ phases on machinability is related to their melting point, the lower the melting point the better the machinability. The observation was also made that anorthitic inclusions deform plastically along with the matrix, while gehlenitic inclusions act as stress concentrators and are nucleation sites for microcracks. They also reported that the lubricating effect of anorthitic inclusions was better than that of gehlenitic inclusions at high normal force levels. Brunet et al. (19) report the use of controlled deoxidation to produce anorthitic inclusions in the improvement of the tool life of carbide tools containing titanium.

Thivellier et al. (20) compared the benefits of Type I Mn(S,O) inclusions, and reported the modification of low oxygen Type II MnS inclusions by S-Se-Ca or S-Se-Mg treatments in order to increase transverse ductility. Yamaguchi et al. (21) have studied the effect of zirconium additions on the machinability, cold forgeability and mechanical properties of resulphurised medium-carbon steels. The modification of sulphide morphology through the formation of non-deformable $MnS-Zr_3S_4$ eutectic inclusions gave improved HSS tool life and good transverse ductibity. The increase in carbide tool wear was attributed to the formation of a $ZrO_2$ diffusion barrier.

## AIV.5 THE EFFECT OF SULPHUR

The effect of sulphur additions on machinability has been studied extensively by Boulger et al. (22) and Shaw and his co-workers (22, 23, 24).

The composition of the hot-rolled steels studied (22,23) are given in Table AIV.1 and the corresponding tensile properties are reproduced in Table AIV.2.

Table AIV.1 Composition of Resulphurised Steels (22,23)

| Ingot No. | Per cent by weight C | Mn | P | S | Si | N |
|---|---|---|---|---|---|---|
| 1 | 0.08 | 0.99 | 0.08 | 0.033 | 0.004 | 0.002 |
| 2 | 0.08 | 0.99 | 0.09 | 0.11 | 0.006 | 0.003 |
| 3 | 0.08 | 0.99 | 0.09 | 0.18 | 0.005 | 0.002 |
| 4 | 0.07 | 0.99 | 0.09 | 0.26 | 0.005 | 0.002 |
| 5 | 0.09 | 1.04 | 0.09 | 0.37 | 0.006 | 0.002 |

Table AIV.2 Tensile Properties of Hot-Rolled Steels (22,23)

| Steel No. | Sulfur content, per cent | Upper yield point, psi | Lower yield point, psi | Tensile strength psi | Elongation in 2-inches, per cent | Reduction in area, per cent | Hardness Rb |
|---|---|---|---|---|---|---|---|
| 1 | 0.033 | 36,700 | 32,600 | 55,700 | 41.0 | 71.8 | 56.6 |
| 2 | 0.11 | 36,500 | 32,900 | 54,700 | 40.5 | 68.1 | 59.3 |
| 3 | 0.18 | 34,600 | 32,000 | 54,500 | 38.5 | 66.4 | 56.5 |
| 4 | 0.26 | 31,900 | 29,500 | 53,300 | 38.5 | 65.1 | 56.2 |
| 5 | 0.37 | 33,400 | 29,800 | 54,700 | 34.00 | 57.4 | 58.4 |

The ductility of these steels is seen to decrease uniformly with sulphur content and there is a general tendency for sulphur to reduce the tensile strength and the upper and lower yield points. The impact properties of these steels were not determined but the presence of manganese sulphide inclusions leads to a marked reduction in shelf energy and ductility, see Appendix V. The results of force measurements

made during the machining of these steels are shown in Fig. AIV.2, where the cutting forces $F_C$ and $F_T$ (see Appendix I), are shown as a function of cutting speed, $V_C$. The addition of sulphur reduces the forces acting on the tool for equivalent feeds and the minima, B, and maxima A, are attributed (15) respectively, to the formation and reduction or elimination of the BUE, see Appendix VII.

Using distortion energy criteria, $\bar{\sigma} = \sqrt{3}\tau_S$ and $\bar{\varepsilon} = \gamma_S/\sqrt{3}$, Thomsen et al. (24) compared the shear stress-strain ($\tau_S$-$\gamma_S$) data with static effective stress-strain ($\bar{\sigma}$-$\bar{\varepsilon}$) data using the relationships:

$$\bar{\sigma} = \sqrt{3}[(F_S - F_{So})/A_S] \qquad \text{AIV.2}$$

and $$\bar{\varepsilon} = [\cot\phi + \tan(\phi-\alpha)]/\sqrt{3} \qquad \text{AIV.3}$$

where $F_{So}$ is the ordinate intercept when $F_S$ is expressed as a linear function of the shear plane area, $A_S$. The effective stresses in metal cutting were found to be in approximate agreement with the static properties at the same strain. This would seem to imply that the combined effect of hydrostatic pressure, temperature and strain rate on flow stress during machining is slight, under those particular cutting conditions. Thomsen et al. (24) concluded that the effect of sulphur was to reduce the energy required for cutting which can be interpreted in terms of Green and Knotts' model (9) of ductile fracture, Appendix III, as a reduction in the total strain to fracture, $\varepsilon_T$. This is now recognized as one of the main functions of MnS inclusions in machining grades and the role of MnS as a lubricant is of marginal importance at low cutting speeds (temperatures).

### AIV.5.1 Chip Formation

Shaw et al. (23) made the following observations on the effect of

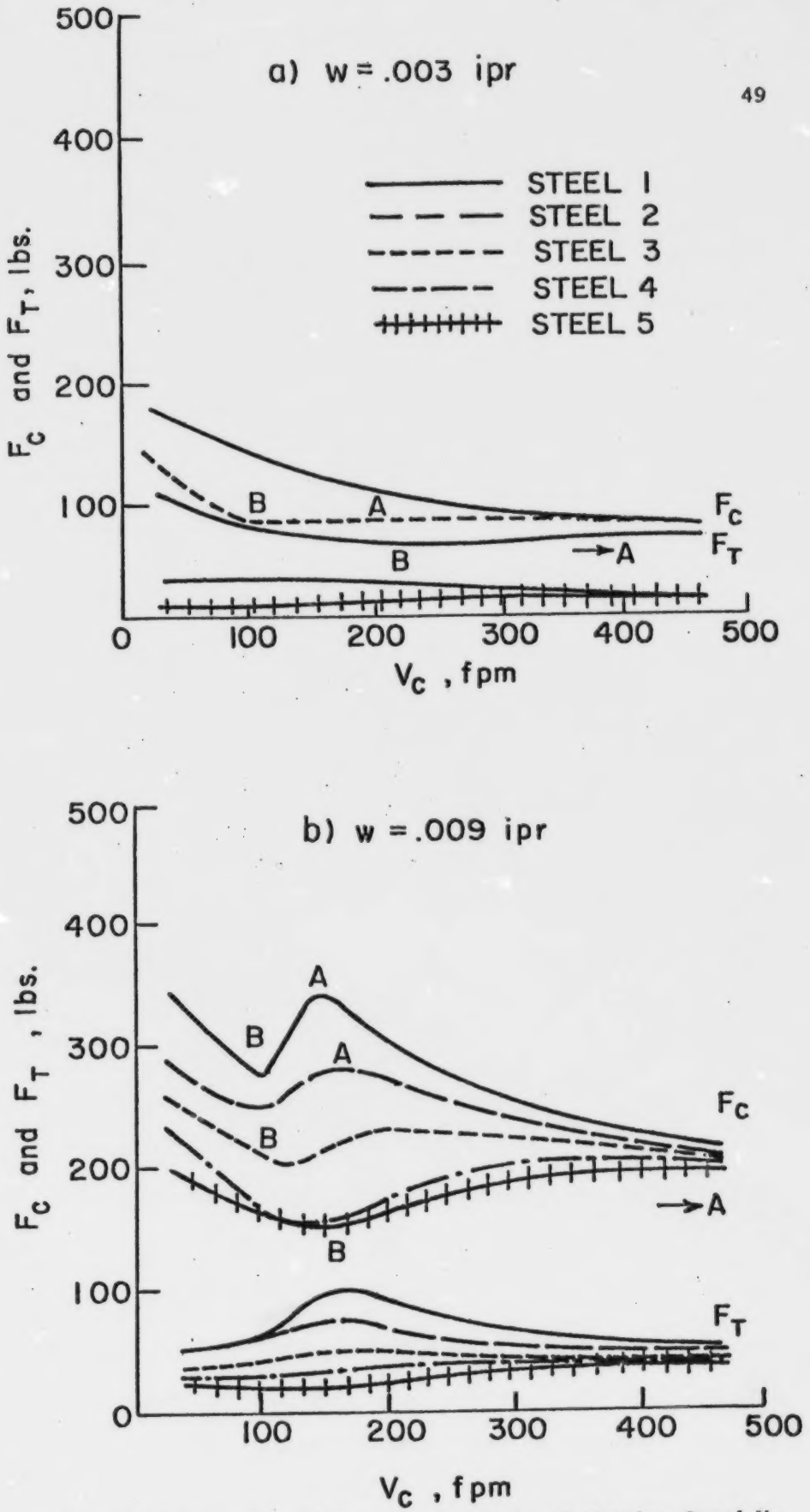


Fig.. AIV.2 - Cutting Forces $F_C$ and $F_T$ as a function of Cutting Speed $V_C$ for Resulphurised Steels (22,23).

sulphur additions on chip formation:

a) at all speeds, chip thickness decreases with increasing sulphur content, i.e., the strain in the chip decreases with increasing sulphur content.

b) chip curvature increases, and the contact area decreases, with sulphur content.

c) a BUE is present in all tightly curled chips, the smaller and more stable the BUE the greater the curl.

The effect of cutting direction, with respect to the orientation of second phase particles, on chip formation, has been elegantly illustrated by Iwata et al. (25), who studied the effect of perpendicular, transverse and parallel cutting, as defined in the diagram below, in a banded Cr-Mo steel at extremely low speeds.

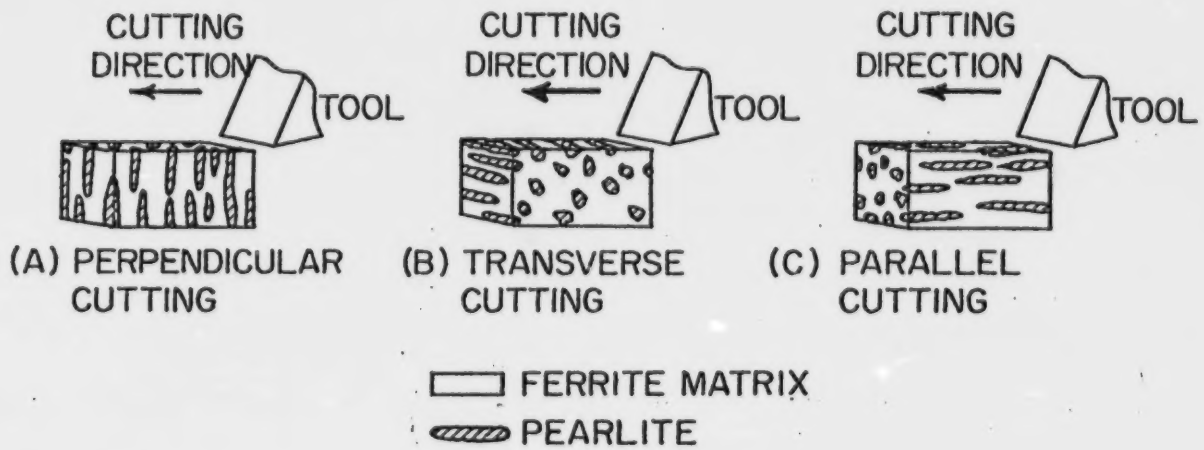


In the case of the normalised steel, a quasi-continuous type of chip is produced in perpendicular and transverse cutting and a 'tear-type' chip in parallel cutting. In each case crack nucleation occurred in the severely strained ferrite matrix, below the tool tip, but crack growth

was in the same direction as that of the maximum shear strain rate in perpendicular cutting, i.e. along the shear band and nearly perpendicular to the maximum principle strain rate direction in parallel cutting, i.e., in the cutting direction. Tear-type chip formation gives rise to a relatively damaged surface. One might expect inclusion fibre to have a similar effect on chip formation, a lameller tearing process occurring in parallel cutting through tensile forces generated by the insertion of the tool tip into a void created by decohesion.

## AIV.6 THE EFFECT OF LEAD

Shaw et al. (23) have studied the effect of lead on machinability using steels of the following composition:

| Designation | C | Mn | P | S | Si | Pb |
|---|---|---|---|---|---|---|
| Non-leaded (NL) | 0.14 | 0.48 | 0.064 | 0.027 | 0.07 | - |
| Leaded (L) | 0.14 | 0.49 | 0.060 | 0.025 | 0.08 | 0.22 |

The variation in cutting forces with speed and feed rate for hot-rolled steels is reproduced in Fig. AIV.3. As in the case of resulphurised grades, the overall thermal softening effect results in a decrease in cutting forces with increasing cutting speeds, but the addition of lead decreases BUE effects. Lead can either eliminate or reduce the size of a BUE by preventing microweld adhesion.

Shaw et al. (26) found that lead was very effective in reducing chip thickness at all cutting speeds, tool face friction and temperature, and cutting energy per unit volume. Leaded chips had greater curl and a smaller apparent area of contact between chip and

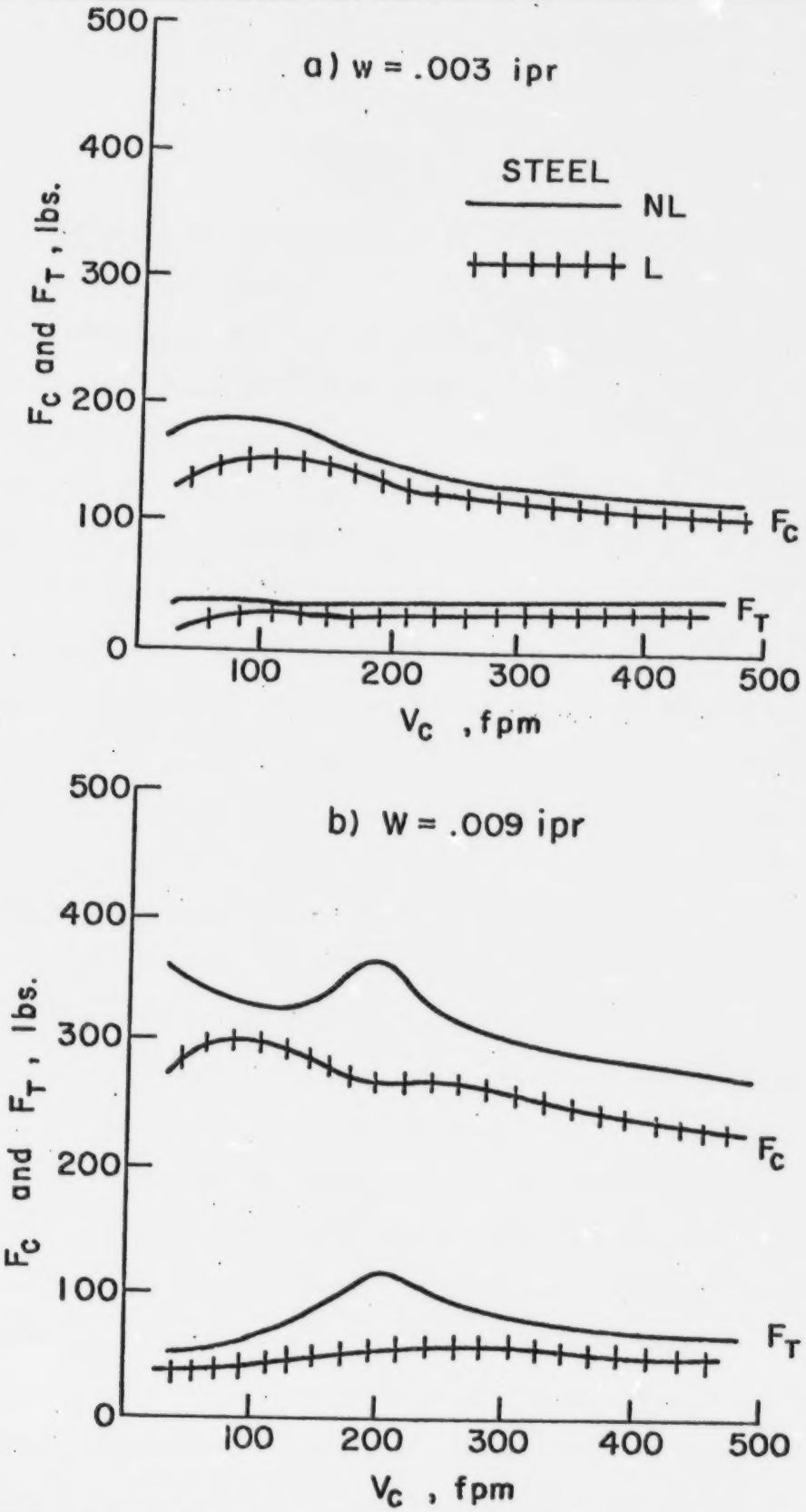


Fig. AIV.3 - Cutting Forces $F_C$ and $F_T$ as a function of Cutting Speed, $V_C$ for Non-leaded (NL) and Leaded (L) Steels (13).

tool. The mean shearing stress along the tool face tends to decrease with the decrease in tool friction and tends to increase with the decrease in the apparent area of contact.

Lead can therefore promote matrix decohesion, reduce microweld adhesion through the formation of a diffusion barrier film, act as an internal lubricant and provide a superior surface finish. These functional roles of lead can be very well fulfilled by other low melting point/high boiling point additives which form a soft phase of low shear strength and of negligible solubility in solid steel, e.g., bismuth.

Lead is reported (26) to have only a slight effect on mechanical properties, both yield and tensile strength being reduced by < 5%. Conflicting evidence is reported on the effect of lead on inpact properties and ductility. Shaw et al. (26) claim that the toughness and ductility of leaded steel is ~20% greater than those of the corresponding non-leaded steels, in contrast to Workman and Jacques (24) who reported decreases in toughness and ductility. More recently Bäcker (27) reports a 5% decrease in ductility for leaded SAE 4140 steels, and a four-fold increase in tool life for leaded quench and tempered SAE 4135 steel. Ito et al. (28) report a good correlation between tool life and 'Pb + S' contents in SAE 1050 steels and have achieved satisfactory tool life performance with lead contents as low as 0.03 - 0.08%, compared to the normal 0.2% contents.

## APPENDIX V

## EMPIRICAL STRUCTURE-DUCTILITY RELATIONSHIPS IN STEEL

The technological data base for steels, relating to:

a) the flow stress for a given strain,

b) the work-hardening rate,

c) the maximum uniform ductility prior to plastic instability

and d) the total available ductility,

has been ably summarised by Pickering (46).

The reduction of total strain to fracture is an important factor with respect to ease of chip formation. The effect of second phase MnS inclusions in decreasing total ductility is illustrated in Fig. AV.1 which also shows the effect of other second phase particles. The total ductility for a given volume fraction of sulphides is also much less when measured transverse to the sulphide stringers than when measured parallel to them, see Fig. AV.2.

The role of zirconium appears to be complex. When added in minimum amounts, equivalent to [6(%N)+(%S)], it combines with both nitrogen and sulphur. It can dissolve in MnS, reducing its plasticity or, more often, replaces MnS by ZrS which is virtually non-deformable. In addition, there is evidence which suggests that, by the elimination of inclusion fibres, inclusion shape control by zirconium can raise the ductile-brittle impact transition temperature by $\sim 50^{o}C$ through a decrease in crack-arresting characteristics. When zirconium additions greater than [6(%N)+(%S)] are used, the excess zirconium forms ZrC and $Zr_4C_2S_2$ which embrittle the steel and decrease the shelf energy.

The effect of various metallurgical variables on the measured

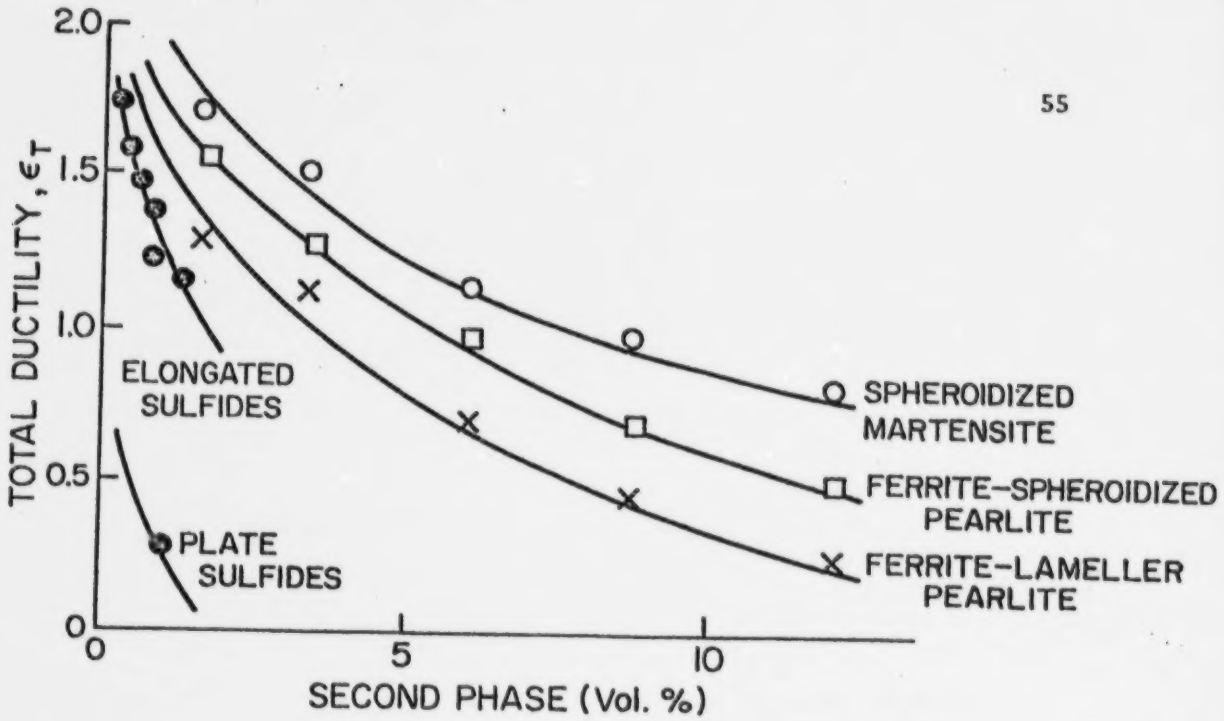


Fig. AV.1 - a) The Effect of Volume Fraction of Second Phase Particles in Total Ductility, $\epsilon_T$ (46).

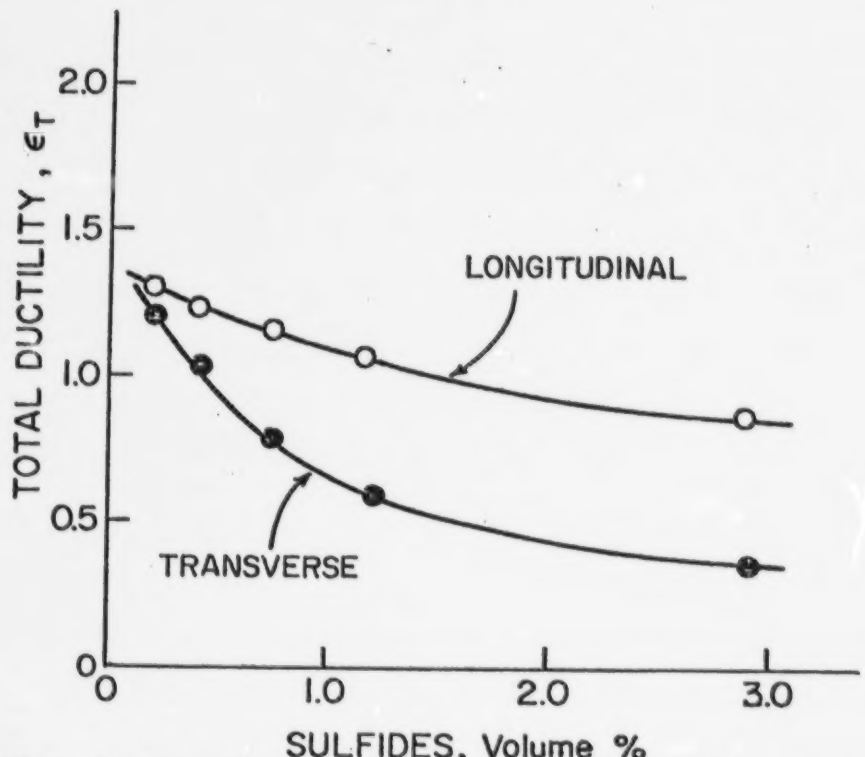


Fig. AV.1 - b) The Effect of Volume Fraction of Sulphides on Longitudinal and Transverse Total Ductility, $\epsilon_T$, (46).

work-hardening rate at a constant low strain is given by the following empirical relationship:

$$\left(\frac{d\sigma}{d\varepsilon}\right)_{\varepsilon=0.2} (MN/m^2) = 15.4\,[24 + 7.8\%C + 1.5\%Mn + 7.5\%Si + 36\%P + 9.3\%Sn + 98\%N_f + 1.0d^{-1/2}] \quad \text{AV.1}$$

where $N_f$ is the free nitrogen content and d is the grain diameter (mm). The total strain to fracture, $\varepsilon_T$, is given by the empirical relationship:

$$\varepsilon_T = 1.4 - 2.9\%C + 0.2\%Mn + 0.16\%Si - 2.2\%S - 3.9\%P - 0.25\%Sn + 0.017d^{-1/2} \quad \text{AV.2}$$

The effect of sulphur reflects the effect of second phase inclusions of MnS in the microstructure which follows an hyperbolic relationship, Fig. AV.1, rather than the linear relationship given above.

The addition of phosphorus increases $(d\sigma/d\varepsilon)_{\varepsilon=0.2}$ but decreases $\varepsilon_T$.

# APPENDIX VI

# CUTTING TEMPERATURES

## AVI.1 TEMPERATURE DISTRIBUTIONS

The mechanical energy of cutting is converted into heat, the three main sources being:

a) the shear zone where the shearing process generates heat,

b) the tool/chip interface where the friction force generates heat, and

c) the lower portion of the tool flank which rubs against the machined surface.

The interaction of these sources combined with the geometry of the cutting area and the physical properties of the tool and workpiece results in complex temperature distributions. The temperature distribution in the cutting zone for HSS machining (47) is reproduced in Fig. AVI.1 and the temperature distributions on the tool flank and tool-chip interface in carbide machining (48) are reproduced in Figs. AVI.2 and AVI.3, respectively. The temperature generated in the shear plane is a function of the shear work and the specific heat of the material. The temperature increase on the tool face depends on the friction at the tool-chip interface, a low coefficient of friction being desirable. The rise in temperature during machining results in thermal softening which is the basis for the decrease in cutting forces with cutting speed.

The temperature distribution is a function of many variables which include the thermal conductivity and specific heat of the workpiece and tool materials, depth of cut, cutting speed and the use of a cutting

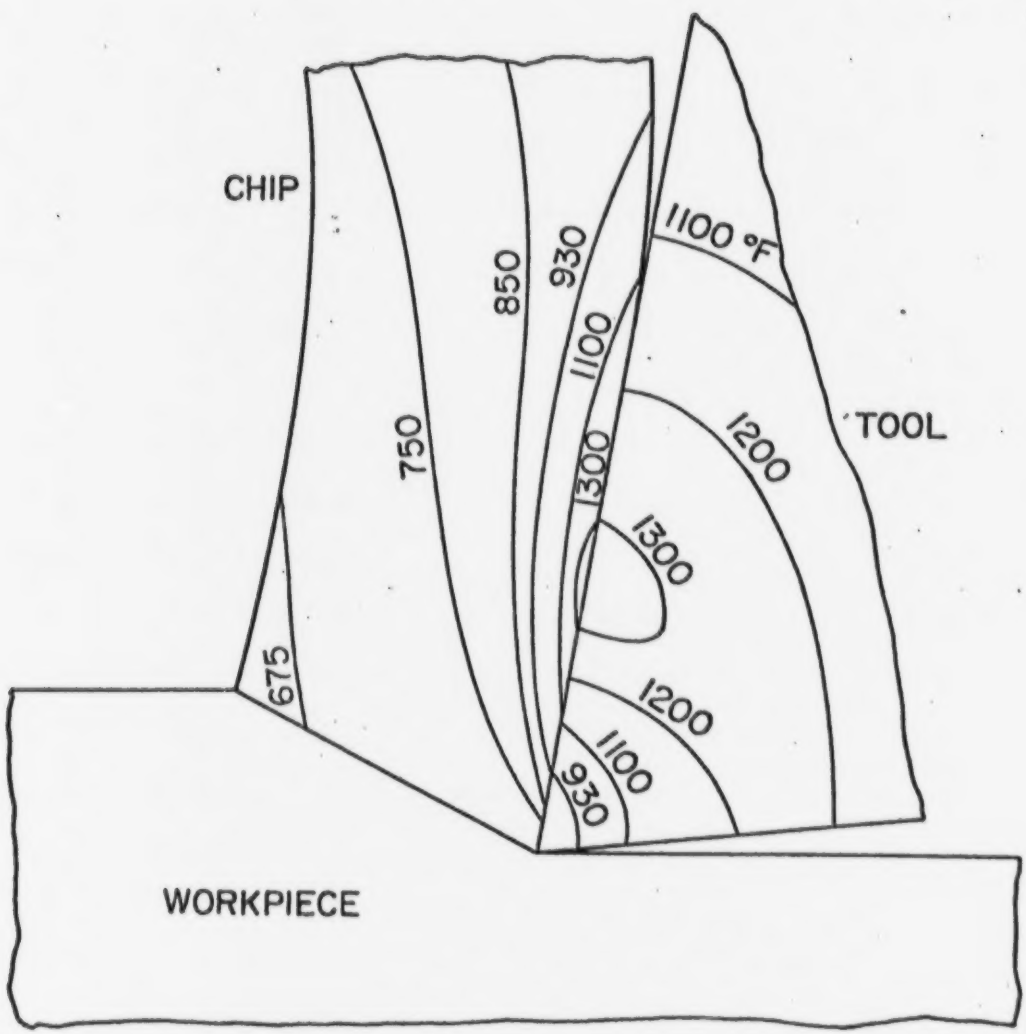


Fig. AVI.1 - Temperature Distribution in the Cutting Zone for HSS Machining (47).

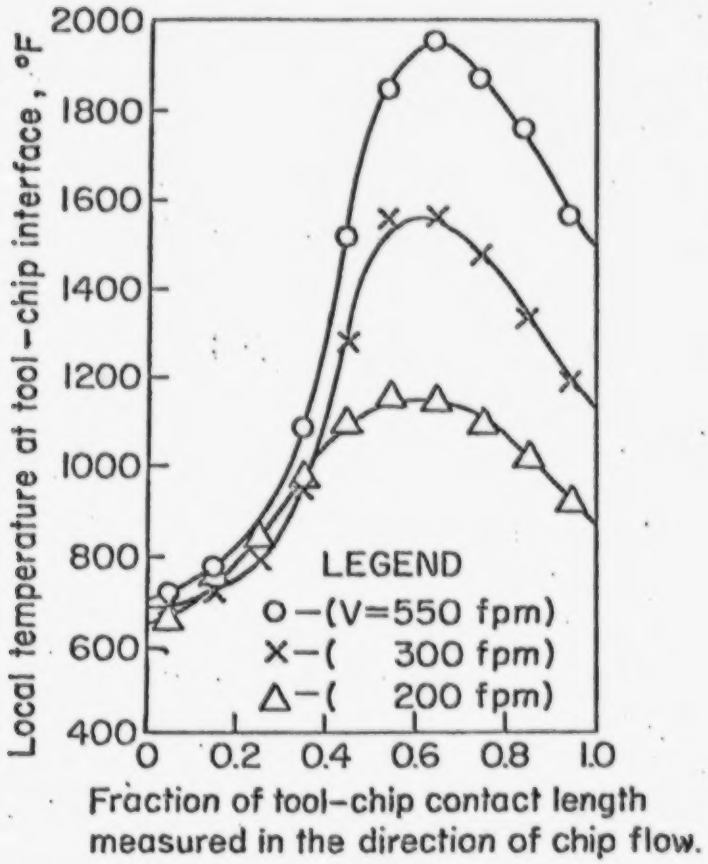


Fig. AVI.2 - Tool-Chip Interface Temperature Distribution in Carbide Cutting (48).

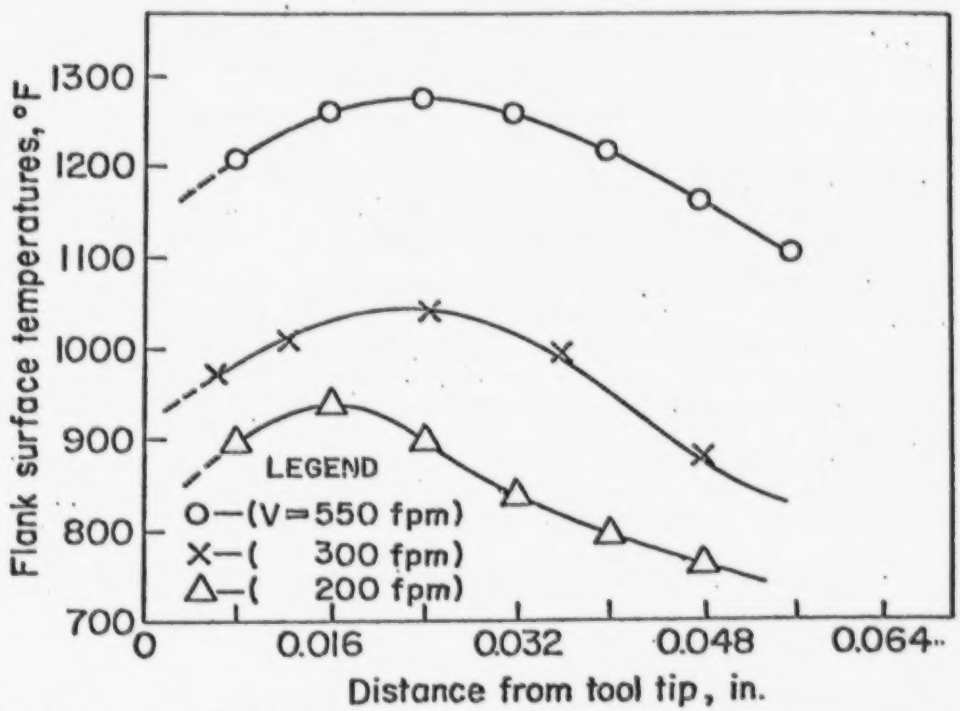


Fig. AVI.3 - Tool Flank Temperature Distribution in Carbide Cutting (48).

fluid. As the cutting speed increases, there is little time for the heat to dissipate away from the cutting area and hence the heat carried away by the chip increases. In the absence of a BUE there is an excellent correlation between tool wear and the tool-chip interface temperature.

## AVI.2 TEMPERATURE AND THE ROLE OF INCLUSIONS

The magnitude of the temperatures generated during the different machining processes determines the specific roles played by the various types of inclusions present in machining grades of steel. Alumina inclusions, while aiding the fracture process through crack nucleation and propagation are particularly harmful with respect to tool wear in both HSS and carbide machining. $CaO-Al_2O_3-SiO_2$ inclusions, with compositions close to the low melting ternary eutectics, can provide lubricating films and diffusion barriers, particularly in the case of Ti bearing carbide tools. This type of inclusion is still detrimental to tool wear at the low temperatures of HSS machining. In this case it is Pb, Bi and other low melting metallics which form the basis of internal lubricants and diffusion barriers.

## APPENDIX VII

## THE BUILT UP EDGE (BUE)

The formation of a built up edge is associated with high friction at the tool-chip interface. The BUE appears to be most stable (19) at low cutting speeds (low temperatures), large feeds, low rake angles and for conditions of workpiece, tool and environment which promote adhesion between the tool and the workpiece. Conversely, reversal of the above conditions leads to the reduction or elimination of the BUE, as will the use of cutting fluids at low speeds and free machining additives like Pb, which reduce adhesion.

The beneficial effects of a stable BUE are associated with an increase in the effective tool rake angle, thereby reducing the cutting forces, and protection of the cutting edge of the tool, thereby increasing tool life. It has a detrimental effect on surface finish, particularly when it becomes unstable, when some fragments are carried up the face of the tool with the chip and others are deposited on the machined surface, adversely affecting surface finish and tool wear.

The exact mechanism of BUE formation is unclear and the following explanation due to Shaw et al. (23) is based on the variation of the cutting force, $F_C$, with cutting speed, $V_C$, as represented in Fig. AIV.2. The BUE starts with a layer of material adhering to the surface of the tool, successive layers being added to it. The BUE will then become stable if its rupture strength is greater than that of the adjacent workpiece. Shaw et al. proposed that, at low speeds, it is possible for the BUE to have a higher rupture strength than the adjacent workpiece, even though it is at a higher temperature. The minima in the

$F_C$ vs. $V_C$ plots occur when these conditions are met, a stable BUE minimising the effective rake angle and reducing the cutting forces. At higher cutting speeds, when temperatures are in excess of the range in which the steel is susceptible to aging or "blue-brittleness", the BUE decreases in size or is eliminated and the cutting forces increase first and then decrease as the normal decrease in rupture strength with temperature takes effect.

The results of Stevenson and Duncan (49) are consistent with this hypothesis and Quinto et al. (50) have indicated that dynamic strain aging is possible at the strain rates of machining ($\sim 10^4$ $sec^{-1}$), since there is an 8 order of magnitude change in the diffusion coefficients of carbon and nitrogen with a temperature increase of 400°C.

The effect of sulphur in shifting the minima and maxima in Fig. AIV.2 to higher cutting speeds, is due to the decrease in magnitude of the cutting forces (temperature), a higher speed being necessary to achieve the critical temperature range. Cutting fluids and free-machining additives like Pb, can eliminate BUE formation by preventing the onset of adhesion.

## APPENDIX VIII

## TOOL WEAR, FRICTION AND SURFACE FINISH

### AVIII.1 TYPES OF TOOL WEAR

Tool wear can be generally classified as follows:

a) a uniform abrasive wear, which gives rise to a straight wear land on the flank face of the tool, called flank wear,

b) crater wear on the rake face of the tool,

c) localised wear, such as the rounding of the cutting edge,

and d) chipping of the cutting edge.

All of these phenomena, which are strongly influenced by the magnitude of cutting forces and temperature, alter the geometry of the cutting tool and affect cutting performance.

Flank wear is usually attributed to the shearing of microwelds between tool and workpiece, abrasion by hard particles and inclusions in the workpiece (31,33,16,19), and fragments of strain hardened BUE ploughing up the clearance face of the tool (22,26,51). Alumina inclusions, in particular, promote flank wear, as do cementite and precipitation-strengthening alloy carbides.

Crater wear is enhanced by the same factors which promote flank wear. It becomes intensified in the high temperature regions of the tool-chip interface, which occur some distance from the tool tip, see Appendix VI, and good correlations have been obtained between crater wear and measured tool-chip interface temperatures in the absence of a BUE (26). The interdiffusion of elements between chip and tool is an important factor influencing crater wear. The formation of an MnS diffusion barrier layer is reported to be one of the benefits in the

machining of resulphurised grades with high speed tool steels (42,52) and one of the more recent advances has been the development of steel grades containing $CaO-Al_2O_3-SiO_2$ inclusions of controlled composition which form silicate diffusion barriers on carbide tools (16,18,20,53). One of the beneficial effects of lead is attributed to a decrease in the tool-chip contact area (22).

## AVIII.2 THE TAYLOR RELATIONSHIP

The Taylor relationship (54):

$$V_C T^n = \text{constant} \qquad \text{AVIII.1}$$

where $V_C$ is the cutting speed, T is the time taken to reach a flank wear land of given dimensions, and n is an exponent which depends on the cutting conditions, is widely used in the assessment of tool wear. The relationship is usually used in the form:

$$\log T = \text{constant} - \frac{1}{n} \log V_C \qquad \text{AVIII.2}$$

in Taylor plots of log T vs log $V_C$, examples of which are reproduced in Fig. AVIII.1 (22).

A $V_{60}$ tool life parameter, for example, is the cutting speed at which a flank wear land of 0.03 in. develops in 60 minutes. Taylor tool life relationships obtained in the work of Shaw et al. (22), Fig. AVIII.1, in their study of the machinability of re-sulphurised hot rolled steels* using carbide tools, are summarised in Table AVIII.1.

For comparison purposes, the Taylor tool life relationships for the non-leaded (NL) and leaded (L) hot rolled steels obtained by Shaw et

---

* The composition of these steels is given in this review p. .

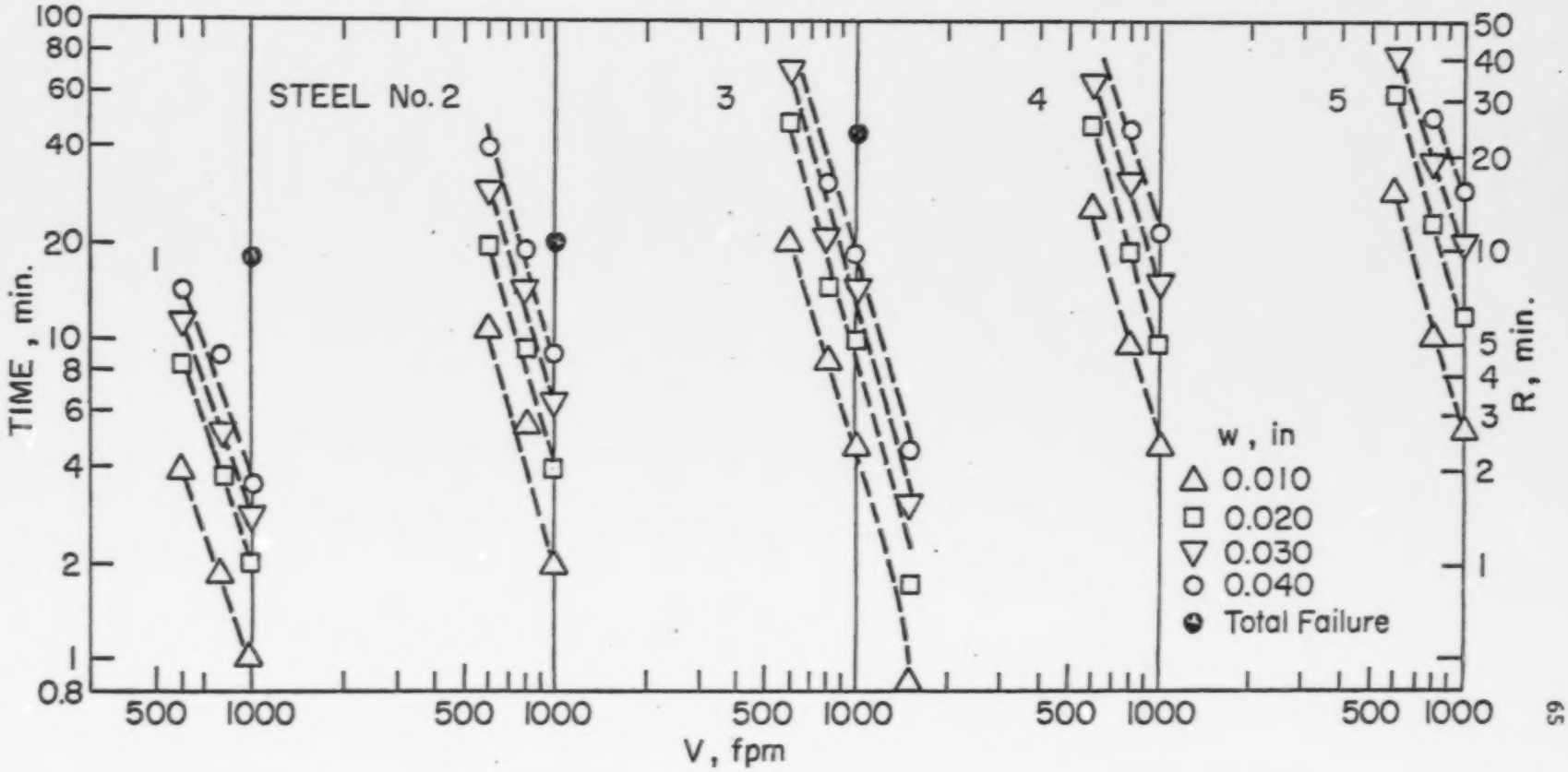


Fig. AVIII.1 - Taylor Tool Life Relationships for Resulphurised Hot-Rolled Steels (22).

al.* (14) are given in Table AVIII.2.

Table AVIII.1 Taylor Tool Life Equations (0.03 in wear land)
Feed: 0.0046 ipr. Depth of cut 0.10 in.

| Steel | % S | Equation | $V_{60}$ (fpm) |
|---|---|---|---|
| 1 | 0.033 | $VT^{0.33} = 1400$ | 330 |
| 2 | 0.110 | $VT^{0.33} = 1800$ | 490 |
| 3 | 0.180 | $VT^{0.33} = 2300$ | 630 |
| 4 | 0.260 | $VT^{0.33} = 2400$ | 640 |
| 5 | 0.370 | $VT^{0.33} = 2700$ | 680 |

Table AVIII.2 Taylor Tool Life Equations (0.03 in wear land)
Feed: 0.0046 ipr. Depth of cut 0.10 in.

| Steel | Equation | $V_{60}$ fpm |
|---|---|---|
| NL | $VT^{0.03} = 265$ | 235 |
| L | $VT^{0.03} = 350$ | 310 |

The marked decrease in the values of the exponent n and the 'constant' in the above relationships in Table AVIII.2 compared with those in Table AVIII.1, illustrates the effect of deoxidation practice. The NL and L steels were produced from a grade killed with silicon and aluminum and containing higher carbon and nitrogen contents than the resulphurised steels which were not deoxidised.

In his study on the effect of non-metallic inclusions on the machinability of low carbon free-cutting steels, Fröhlke (31) developed the relationship:

* The composition of these steels is given in this review, p. .

$$\log V_{60} = A + B.m + C \log N_o - D \log F_{ox} \qquad \text{A.VIII.3}$$

between the wear index, $V_{60}$, and the sulphide and oxide inclusion content, where $N_o$ and m are the ordinate intersection and the slope, respectively, of the residual class distribution of sulfides described by the relationship:

$$\log N_i = \log N_o - md_i \qquad \text{A.VIII.4}$$

$F_{ox}$ is the oxide area, and A, B, C, and D are constants. Eq. AVIII.3 emphasizes the role of MnS inclusion distribution and oxide inclusion area in the determination of tool wear.

A modified form of the Taylor equation involving the feed rate, f, and the depth of cut, d, is often used successfully:

$$V.T^n . f^\alpha . d^\beta = C \qquad \text{AVIII.5}$$

where n, $\alpha$, $\beta$ and C are constants. However, attempts to use a more generalised tool life equation involving the hardness and tensile strength of the work material (55) has only had limited success since the model is not applicable to material containing machinability sensitive second phase particles.

## AVIII.3 FRICTION (56)

The actual area of contact between two surfaces gliding over each other is considerably smaller than the area of overlap of the two surfaces. Two surfaces contact each other at small irregularities or hills which exist on every surface even though it may appear to be very smooth. The sum of the contact areas is very small compared with the area of overlap.

The normal force, N, that can be supported by plastic deformation of the asperities depends on the actual area of contact, $A_r$, and the

hardness of the asperities, H.

$$N = A_r \cdot H \qquad \text{AVIII.6}$$

Holm and Bowden (56) came to the conclusion that friction is caused not so much by the interlocking of the asperities - as commonly assumed - but by their momentary welding. In addition, they introduced the concept of a "raking action" of the surface asperities of a harder metal through those of a softer metal. The total frictional force, F, depends on the resistance of the asperities to shear, $\rho$, and on the raking force $F_R$:

$$F = FR + \rho.A_r = F_R + \rho N/H \qquad \text{AVIII.7}$$

i.e.

$$F/N = \mu = \tan\tau = (F_R/N) + (\rho/H) \qquad \text{AVIII.8}$$

The significance of these formulae lies in the value of the ratio $\rho/H$. In order to have a low coefficient of friction it is necessary to combine a material of great hardness with a material of low shear strength, c.f., bearing alloys.

In free-machining steels, where one of the dispersed phases can absorb the heat of friction by melting, the dual purpose of coolant and lubricant can be fulfilled.

The functional role of free-machining additives is the dispersion of a phase of relatively low shear strength in a relatively hard matrix with the objectives of:

a) facilitating crack initiation and propagation during chip formation,

b) providing a lubricating film of low shear strength, and

c) decreasing local heat generation through heat of fusion adsorption. Pb, Bi and other low melting metallics are particularly suited for

these purposes.

AVIII.4 WEAR

According to the theory of Holm and Bowden (56) a high frictional force and a large coefficient of friction are not necessarily indicators of heavy wear. In his model of surface movement at contact points on gliding surfaces, represented by the diagram below:

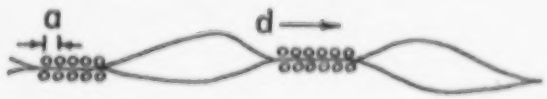


assuming that the upper surface is moved through a distance d relative to the lower surface and that the interatomic spacing is a, each atom of the upper surface will encounter d/a atoms of the lower surface. Since the total number of atoms in the actual area of contact is $A_r/a^2$, the total number of atomic encounters will be $A_r \cdot d/a^3$. The number of atoms worn away and contained in a volume of metal, V, removed by wear will be $V/a^3$. The number of atoms, Z, worn away by atomic encounter is then:

$$Z = \frac{V}{a^3} \cdot \frac{a^3}{A_r \cdot d} = \frac{V}{A_r \cdot d} \qquad \text{A.VIII.9}$$

Substituting the real area of contact according to Eq. AVIII.6 gives:

$$Z = V \cdot H/N \cdot d \qquad \text{A.VIII.10}$$

The height h of the layer of metal removed during the displacement d of the apparent area of contact, A, is given by the relationship:

$$h = V/A = Z \cdot N \cdot d/HA \qquad \text{A.VIII.10}$$

From this simple theory of wear it is expected that wear in metal cutting is dependent on:

a) the normal force between two sliding surfaces and the apparent area of contact,

b) the hardness and temperature of the tool (since hardness is a function of temperature),

c) the chip/tool hardness ratio,

d) the micro-structure of the workpiece and the atmospheric conditions at the cutting edge, since both affect the quantity Z.

Kronenberg (57) has pointed out that the relationship between friction and wear is less direct then commonly assumed since it is the normal force, N, which is the significant variable and not the frictional force, F. Kronenberg also points out that the significance of the coefficient of friction, $\mu$, in metal cutting requires re-interpretation. An increase in the coefficient of friction is often due to the fact that the frictional force, F, decreases at a slower rate than the normal force, N, and leads to the erroneous conclusion that frictional wear has increased.

## AVIII.5 SURFACE FINISH

One of the important factors which contributes to surface roughness is the BUE, portions of an unstable BUE being broken off and deposited on the machined surface. The factors which influence the stability of the BUE have been considered in Appendix VII.

At very low cutting speeds, the type of chip encountered is often discontinuous, giving a poor surface finish because of the interupted cutting action. As the speed increases a BUE begins to form, again affecting surface finish even though the chip is continuous. At higher cutting speeds the BUE becomes reduced in size or even eliminated and a

good surface finish results.

The effects on surface finish of such variables as feed rate, depth of cut, tool gemoetry, are difficult to isolate since they alter the geometry of the chip and hence cutting forces and temperature, which in turn affect the formation of the BUE. With regard to tool materials, it has been noted that ceramic and diamond tools can produce superior surface finishes because they are not susceptible to BUE formation.

## APPENDIX IX

## CUTTING FLUIDS

At constant cutting speed, the most important method of reducing tool-chip friction is through the introduction of a low shear strength solid material between the asperities of sliding surfaces (26). Cutting fluids reduce friction either by reaction or chemisorption and a good cutting fluid must be compatible with tool and workpiece at ambient temperatures and pressures but active at the temperatures and pressures of machining.

For a fluid to be effective it must penetrate to the tool tip. This takes time and cutting fluids are much more effective at decreasing tool-chip friction at low cutting speeds. Internal lubricants are much more effective at high cutting speeds. At high speeds the cooling action of a cutting fluid is more important than lubrication.

Shaw et al. (26) report that cutting fluids can interfer with the action of free-machining additives such as Pb and S. Oil-based fluids tend to prevent lead from spreading, the effect being more pronounced at high cutting speeds.

## REFERENCES


1. Merchant, M.E., J. App. Phys., vol. 16, No. 5, 1945, pp. 267-75.

2. Piispanen, V., Teknillinen Aikakauslehti, vol. 27, 1937, pp. 315-22.

3. Merchant, M.E., J. App. Phys., vol. 16, 1945, pp. 318-324.

4. Bridgman, P.W., Phys. Rev., vol. 48, 1935, pp. 825-47: Proc. Am. Acad., vol. 71, 1937, pp. 386-460: J. App. Phys., vol. 8, 1937, pp. 328-36: J. App. Phys., vol. 14, 1943, pp. 273-83.

5. Ramalingam, S., Trans. ASME, J. of Eng. for Industry, Vol. 92, 1970, pp. 93-102.

6. Kobayash, S. and Thomsen, E.G., Trans. ASME, J. of Eng. for Industry, Vol. 81, 1959, pp. 251-262.

7. Spaans, C., 'The Fundamentals of 3-D Chip Curl, Chip Breaking and Chip Control', Ph.D. Thesis, University of Delft, March, 1971.

8. Muller, T., 'Deformation Behaviour of Iron and Nickel at High Rates of Deformation', Thesis. Delft University of Technology, 1970, Delft, Waltman, 1970.

9. Green, G. and Knott, J.F., J. Eng. & Mat. Tech., 1976, pp. 37-44.

10. Rice, J.R. and Johnson, M.A., 'Inelastic Behaviour & Solids', Ed. M.F. Kanninen et al., McGraw Hill, New York, 1970, p. 641.

11. Smith, R.F. and Knott, J.F., 'Crack Opening Displacement and Fibrous Fracture in Mild Steel'. Practical Applications of Fracture Mechanics to Pressure Vessel Technology., Inst. Mech. Eng., London, 1971, pp. 65-75.

12. Hahn, G.T. and Rosenfield, A.R., ASTM, STP 432, 1968, p. 5.

13. Garrett, G.G. and Knott, J.F., Acta Met., Vol. 23, 1975, p. 841.

14. Gladman, T., Dulien, D. and McIvor, I.D., 'Structure - Property Relationships in High-Strenth Microalloyed Steels', Proceedings, Microalloying 75, 1977, pp. 32-54, Publishers: Union Carbide Corp.

15. Muan, A. and Osborn, E.F., 'Phase Equilibria Among Oxides in Steelmaking', Addison Wesley Publishing Co. Inc., 1965.

16. Iodkovsky, S.A., Berman, L.I., Alshannikov, V.P., Isaev, A.I., Cherny, A.P., Batyrev, V.A. and Shatrinova, A.V., Proceedings, International Symposium on Influence of Metallurgy on Machinability of Steel, Japan, 1977, pp. 95-106, Publishers: JISI/ASM.

17. Randak, A., Known, W. and Vöge, H., Proceedings, International Symposium on Influence of Metallurgy on Machinability of Steel, Japan, 1977, pp. 107-128. Publishers: JISI/ASM.

18. Fujiwara, T., Abeyama, S., Kimura, A., Nakamura, S. and Itoh, T., Proceedings, International Symposium on Influence of Metallurgy on Machinability of Steel, Japan, 1977, pp. 129-138. Publishers: JISI/ASM.

19. Brunet, J.-C., Hugo, M., Torterat, P. and Bellot, J., Proceedings, International Symposium on Influence of Metallurgy on Machinability of Steel, Japan, 1977, pp. 151-166. Publishers: JISI/ASM.

20. Thivellier, D., Mostacchi, A., Rousseau, D. and Tricot, R., Proceedings on International Symposium on Influence of Metallurgy on Machinability of Steel, Japan, 1977, pp. 139-150. Publishers: JISI/ASM.

21. Yamaguchi, Y., Shimohata, T., Kameda, T. and Furusawa, S., Proceedings, International Symposium on Influence of Metallurgy on Machinability in Steel, Japan, 1977, pp. 289-300. Publishers: JISI/ASM.

22. Boulger, F.W., Harner, H.E., Lankford, W.T. and Garvey, T.M., Trans. ASME, Vol. 79, 1957, pp. 1155.

23. Shaw, M.C., Usui, E. and Smith, P.A., Trans. ASME J. of Eng. for Industry, Vol. 83, 1961, pp. 181-192.

24. Thomsen, E.G., Kobayashi, S. and Shaw, M.C., Trans. ASME, J. of Eng. for Industry, Vol. 83, 1961, pp. 513-522.

25. Iwata, K., Ueda, K. and Mimura, H., Proceedings International Symposium on Influence of Metallurgy on Machinability of Steel, Japan, 1977, pp. 449-460, Publishers: JISI/ASM.

26. Shaw, M.C., Smith, P.A., Loewen, E.G. and Cook, N.H., Trans. ASME., Vol. 45, 1957, pp. 1143-1153.

27. Bäcker, L., Proceedings, International Symposium on Influence of Metallurgy on Machinability of Steel, Japan, 1977, pp. 27-40. Publishers, JISI/ASM.

28. Ito, T., Abeyama, S., Kimura, A., Osawa, M., Akatsu, S. and Niwa, S., Proceedings International Symposium on Influence of Metallurgy on Machinability of Steel, Japan, 1977, pp. 179-188. Publishers: JISI/ASM.

29. Thomsen, E.G., Yang, C.T. and Kobayashi, S., 'Mechanics of Plastic Deformation in Metal Processing', The MacMillan Company, New York, 1965.

30. Vlack, L.H., Van, Trans. ASM, Vol. 45, 1955, pp. 641-657.

31. Fröklke, M., International Symposium on Influence of Metallurgy on Machinability of Steel, Japan, 1977, pp. 41-56. Publishers: JISI/ASM.

32. Itoh, T., Abeyama, S., Kimura, A. and Nakamura, S., Proceedings, International Symposium on Influence of Metallurgy on Machinability of Steel, Japan, 1977, pp. 313-322. Publishers: JISI/ASM.

33. Ramalingam, S. and Watson, J.D., Mat. Science and Eng., Vol. 43, 1980, pp. 101-108.

34. Tipnis, V.A., Proceedings, International Symposium on Sulfide Inclusions on Steel, Port Chester, N.Y., 1974, pp. 480-495. Publishers: American Society for Metals.

35. Tipnis, V.A., Joseph, R.A. and Dubrava, J.H., International Automative Engineering Conference, Detroit, 1973. SAE Paper No. 730115.

36. Hilty, D.C., Proceedings, International Symposium on Influence of Metallurgy on Machinability of Steel, Japan, 1977, pp. 199-230. Publishers, JISI/ASM.

37. Opitz, H. and König, W., Archiv. für das Eisenhüttenwesen, Vol. 12(33), 1962, pp. 831-839.

38. Opitz, H., Gappisch, M., König, W., Pape, R. and Wicker, W., Archiv. für das Eisenhüttenwesen, Vol. 12(33), 1962, pp. 841-851.

39. Kalish, S.H. and August, J.S., Metal Progress, Vol. 16(1), 1979, pp. 64-70.

40. Payne, D.A., Bird, J.M., Ham, I. and Biggers, J.V., Trans. ASME, Journal of Engineering for Industry, Vol. 97, 1975, pp. 1126-1130.

41. Loskutov, V.F. and Khiznyak, V.G., Isvestiya, VUZ Chernaya Metallurgiya, Vol. 8, 1978, pp. 116-117.

42. Okusa, K., Kitagawa, R., Akasawa, T., Yokowawa, T. and Tasaka, K., Proceedings, International Symposium on Influence of Metallurgy on Machinability of Steel, Japan, 1977, pp. 461-470. Publishers: JISI/ASM.

43. Williams, J.E., Smart, E.F. and Milner, D.R., Metallurgia, Vol. 81, No. 485, 1970, pp. 89-93.

44. Keissling, R. and Lange, N., 'Non-Metallic Inclusions in Steel', Parts II and III. ISI Publications 100 and 115.

45. 'Free Machining Steel', Bulletin No. 60, LaSalle Steel Co., 1980, pp. 1-12.

46. Pickering, F.B., 'Physical Metallurgy and the Design of Steels', Applied Science Publishers Ltd., London, 1978.

47. Vieregge, G., Werkstatt und Betrieb, No. 11, 1953, p. 696.

48. Chao, B.T. et al., Trans. ASME, J. of Engineering for Industry, Vol. 83, 1961, pp. 496-504.

49. Stevenson, M.G. and Duncan, K.R., JISI, Vol. 211(10), 1973, pp. 710-717.

50. Quinto, D.T., Bhattacharya, D. and Thompson, R.W., Proceedings, International Symposium on Influence of Metallurgy on Machinability of Steel, Japan, 1977, pp. 433-447. Publishers: JISI/ASM.

51. Nagai, C., Kaneda, T., Furesawa, S., Takeshita, S. and Yamamoto, Y., Proceedings, International Symposium on Influence of Metallurgy on Machinability of Steels, Japan, 1977, pp. 57-66. Publishers JISI/ASM.

52. Blank, J.R., Naylor, D.J. and Warnell, P.H., Proceedings, International Symposium on Influence of Metallurgy on Machinability of Steels, Japan, 1977, pp. 397-420. Publishers: JISI/ASM.

53. Narutaki, N., Proceedings, International Symposium on Influence of Metallurgy on Machinability of Steels, Japan, 1977, pp. 167-178. Publishers: JISI/ASM.

54. Taylor, F.W., Trans. ASME, Vol. 28, 1907.

55. Takeyama, H., Murata, R., Yoshikawa, T. and Takada, K., Proceedings, International Symposium on Influence of Metallurgy on Machinability of Steel, Japan, 1977, pp. 15-26. Publishers: JISI/ASM.

56. Kronenberg, M., Machining Science and Application, Pergamon Press, London, 1966, p. 22-25.

57. Kronenberg, M., Tool Engineer, 1953, pp. 49-50.

# Number/
# Numéro
# 2

REQ. NO. 9-9119

# DEVELOPMENT OF NON-LEADED FREE MACHINING STEELS - PHASE II

FINAL REPORT

August 1, 1981 - March 31, 1983

DSS Contract #OSU80-00111

S.V. Subramanian

and

D.A.R. Kay

37 pp

Department of Metallurgy and Materials Science

McMaster University

Hamilton, Ontario, L8S 4L7

(416) 525-9140, Ext. 4293

MICROMEDIA
AUG 29 1983

March 1983

CONTENTS


| | Page |
|---|---|
| INTRODUCTION | 1 |
| 1. STEELMAKING | 1 |
| 2. MATERIALS CHARACTERISATION | 2 |
| 2.1 Chemical Analysis | 2 |
| 2.2 Inclusion Characterisation | 4 |
| 2.2.1 Inclusion Analysis | 4 |
| 2.2.2 Q.T.M. Analysis | 15 |
| 3. MACHINABILITY | 18 |
| 3.1 Tool Wear Tests | 18 |
| 3.2 Cutting Forces, Shear Angle and Chip Temperatures | 19 |
| 3.3 Built-Up Edge (BUE) | 29 |
| 4. CONCLUSIONS | 32 |
| 5. FUTURE WORK | 33 |
| 6. ACKNOWLEDGEMENTS | 33 |
| REFERENCES | 34 |
| APPENDIX | 35 |

## INTRODUCTION

Following the completion of Phase I of the current contract (1), a meeting was held with the representatives of the steel industry, EMR (CANMET) and McMaster University to develop a research programme for Phase II of the contract, which would be consistent with the technological capabilities and the needs of the steel industry. The general consensus of the meeting (2) was that Phase II research should be concerned with the production of fine-grained free-machining grades which did not contain hard, abrasive $Al_2O_3$ inclusions and the determination of the effect of their removal on machinability.

Subsequent to this meeting and after further discussion with individual steel companies, Burlington Steel Ltd. (Mr. M. Reinberg) agreed to produce two commercial heats of fine-grained continuously cast AISI/SAE 1146 grade steel, one heat using their standard Al-deoxidation practice (1146-C) and the other a modified Ca-deoxidation practice using Nb for grain refinement (1146-M).

The following sections of this report deal with the steelmaking practice, materials characterisation, and the machinability assessment for these two grades of steel.

## 1. STEELMAKING (Burlington Steel Ltd.)

Two 40 ton heats of fine-grained, continuously cast AISI 1146 grade steel:

| C | Mn | S | P |
|---|---|---|---|
| 0.42/0.49 | 0.70/1.00 | 0.08/0.13 | 0.04 max. |

were produced by Burlington Steel Ltd. One heat, designated 1146-C, was made using a standard Al-killed deoxidation practice and the other, designated 1146-M, using a modified Ca-deoxidation practice with a Nb addition for grain refinement.

The 1146-C material was supplied in the form of normalized 1-7/8"D bar and the 1146-M material in normalized 2"D bar.

## 2. MATERIALS CHARACTERISATION (Dept. of Energy, Mines and Resources (CANMET)

### 2.1 Chemical Analysis

The results of spectrochemical analyses carried out by Burlington Steel Ltd. and PMRL (CANMET) on the two steels are summarized in Table I. There are minor differences between the two sets of analytical data for each steel, notably in the carbon and niobium contents. The PMRL carbon analysis is, on average, 0.03% and 0.05% lower than the corresponding Burlington Steel analysis for the 1146-C and 1146-M steels, respectively. The PMRL niobium analysis is about 0.008% lower than the Burlington Steel analysis for both the 1146-C and 1146-M grades.

The differences in the carbon contents of the 1146-C and 1146-M steels are of more significance, the 1146-M steel containing about 0.05% more carbon than the 1146-C grade. The 1146-M steel contains more pearlite than the 1146-C grade, 75% vs. 55% (see below), and is therefore harder, 245 vs. 220 VPN. These differences affect the relative machinability of the two steels in a manner not related to the differences in inclusion content, see Section 3. The high niobium content of the 1146-M grade, 0.040-0.049%, relative to the aim, 0.035%, resulted in Fe-Nb solid solution/NbC eutectic precipitation in the

TABLE I: SPECTROCHEMICAL ANALYSIS - wt%

AISI 1146-C, 1 7/8" Dbar: Standard Practice - Al killed

AISI 1146-M, 2" Dbar: Ca and Nb Practice - No Al deoxidation

| Analysis† | Steel | Location | C | S | P | Si | Mn | Al | Nb | Ca* |
|---|---|---|---|---|---|---|---|---|---|---|
| AISI Spec | 1146 | --- | 0.42 / 0.49 | 0.08 / 0.13 | 0.04 / max | --- | 0.70 / 1.00 | ---- | ---- | ---- |
| B. Steel | 1146-C | --- | 0.42 | 0.094 | 0.015 | 0.26 | 0.82 | 0.013 | 0.012 | N/A |
| PMRL | 1146-C | Centre | 0.39 | 0.090 | 0.015 | 0.27 | 0.87 | 0.019 | 0.005 | N/A |
| PMRL | 1146-C | Mid-Radius | 0.37 | 0.080 | 0.015 | 0.27 | 0.83 | 0.018 | 0.005 | N/A |
| PMRL | 1146-C | Perimeter | 0.40 | 0.095 | | | | | | |
| PMRL | 1146-C | Centre | 0.41 | 0.090 | | | | | | |
| | | | | | | | | | | |
| B. Steel | 1146-M | ------ | 0.49 | 0.105 | 0.017 | 0.36 | 0.92 | 0.003 | 0.049 | 0.0029 |
| PMRL | 1146-M | Centre | 0.44 | > 0.090 | 0.015 | 0.35 | 0.97 | < 0.005 | 0.042 | |
| PMRL | 1146-M | Mid-Radius | 0.43 | > 0.090 | 0.015 | 0.34 | 0.98 | < 0.005 | 0.040 | 0.0070 |
| PMRL | 1146-M | Perimeter | 0.43 | 0.105 | | | | | | |
| PMRL | 1146-M | Centre | 0.44 | 0.095 | | | | | | |

† B. Steel: Burlington Steel

PMRL: Process Metallurgy Research Labs (CANMET)

* Wet chemical analysis

N/A: Not analyzed

centre of the bar, see below.

However, the volume fraction of the niobium carbide eutectic phase was found to be small. A quantitative analysis of the micro-segregation of the niobium carbide eutectic was therefore carried out for the hyper-peritectic system, taking due account of the chemical interaction effects. The computation results showed that the niobium activity is remarkably lowered in the presence of carbon in the micro-segregated liquid; as a consequence, the niobium carbide solubility product is not exceeded until the very end of solidification, i.e., when the fraction solidified is large. It is therefore possible to program niobium additions judiciously, in order to prevent the niobium carbide eutectic phase altogether.

## 2.2 Inclusion Characterisation

### 2.2.1 Inclusion Analysis

Mid-radius longitudinal sections from each steel were examined metallographically, Figures 1-7, and different inclusion types identified for microprobe analysis, Figures 1-6. The microprobe elemental analyses for the 1146-C and the 1146-M grades are given in Tables II and III respectively together with the identified inclusion type. The elemental compositions of the 1146-M oxide inclusions given in Table III, expressed in terms of the wt. percent contents of their respective oxides CaO, $Al_2O_3$, $SiO_2$, MgO and FeO and normalized to 100%, are tabulated in Table IV. The percentage CaO, $Al_2O_3$ and $SiO_2$ contents of these inclusions, again normalised to 100% are also given in Table IV and plotted on the $CaO-Al_2O_3-SiO_2$ equilibrium phase diagram given in Figure 8. The inclusions are seen to be essentially gehlenitic (2CaO.

Figure 1: 1146-C(L). Inclusion type: (a) $Al_2O_3$ (b) $Al_2O_3$/MnS (c) Fe/MnS (d) FeS/MnS (e) FeS/MnS

Figure 2: 1146-C(L). Inclusion type: (a) $Al_2O_3$ (b) $Al_2O_3$ (c) $Al_2O_3$/MnS (d) $Al_2O_3$/MnS (e) $Al_2O_3$/MnS (f) $Al_2O_3$/Fe (g) $Al_2O_3$/Fe

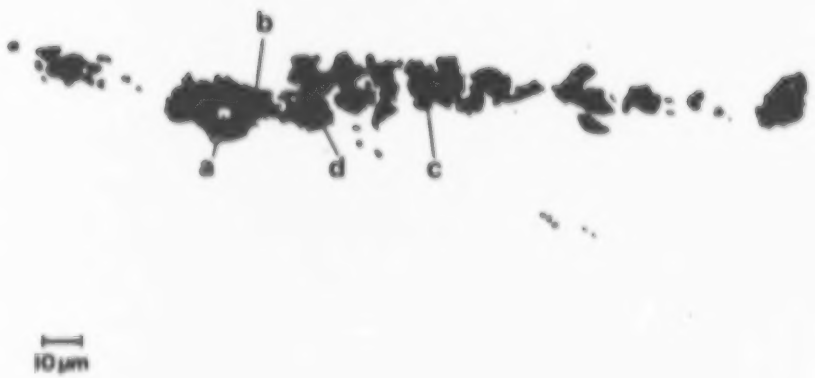


Figure 3: 1146-M(L). Inclusion type: (a) CaS (b) $C_2AS$ (c) $C_2AS$ (d) $C_2AS$

Figure 4: 1146-M(L). Inclusion type: (a) CaS (b) $C_2AS$

Figure 5: 1146-M(L). Inclusion type: (a), (b) and (c) Fe(Nb)-NbC eutectic

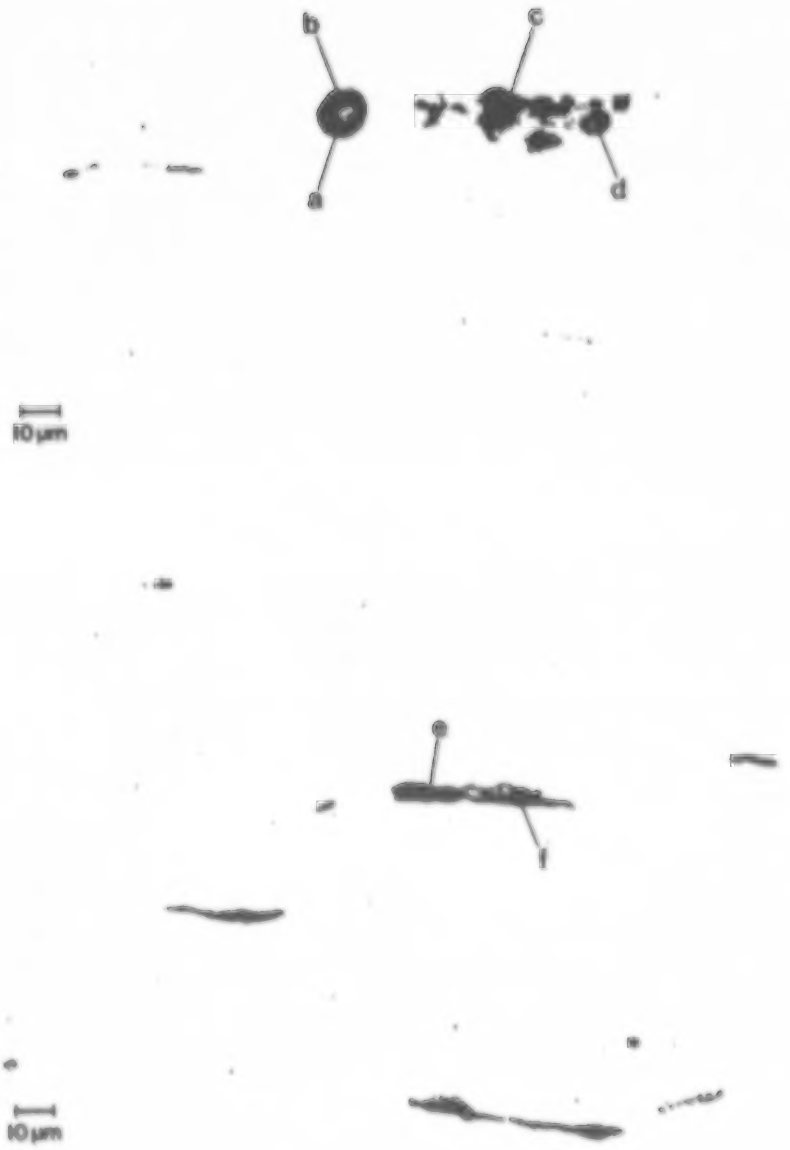


Figure 6: 1146-M(L). Inclusion type: (a) CaS (b) CaS/Fe (c) CaS (d) Mixed oxide (e) MnS (f) MnS

Figure 7: 1146-M(L) Micrograph showing Fe(Nb)-NbC eutectic and MnS inclusions at the centre of the bar.

TABLE II: MICROPROBE INCLUSION ANALYSIS - wt%

1146-C (See Micrographs in Figures 1 and 2)

| INCLUSION | Fe | Mn | Ti | Si | Al | Mg | Ca | S | O† | TYPE |
|---|---|---|---|---|---|---|---|---|---|---|
| 1.a | 1.38 | 0.78 | 0.90 | 2.18 | 41.32 | 0.66 | 5.35 | 0.17 | 47.06 | $Al_2O_3$ |
| 1.c | 82.62 | 8.70 | 0.10 | 0.31 | 0.60 | 0.04 | 0.14 | 6.59 | 0.91 | Fe/MnS |
| 1.d | 10.60 | 52.63 | ---- | ---- | ---- | ---- | 0.07 | 34.52 | 2.18 | FeS/MnS |
| 1.e | 11.90 | 52.17 | ---- | ---- | ---- | ---- | N/D | 33.77 | 2.15 | FeS/MnS |
| 2.a | 9.06 | 1.02 | 0.99 | 0.63 | 43.17 | 0.48 | 5.20 | 0.12 | 39.32 | $Al_2O_3$ |
| 2.b | 1.58 | 11.01 | N/D | 0.02 | 45.12 | 0.05 | 0.40 | 7.16 | 34.66 | $Al_2O_3$ |
| 2.c | 36.50 | 20.07 | N/D | 0.08 | 24.32 | 0.08 | 0.24 | 12.98 | 5.72 | $Al_2O_3$/MnS |
| 2.d | 17.69 | 17.99 | 0.01 | 0.08 | 29.47 | 0.16 | 1.40 | 11.49 | 21.71 | $Al_2O_3$/MnS |
| 2.e | 18.12 | 20.81 | 0.05 | 0.10 | 26.29 | 0.18 | 2.74 | 12.93 | 18.78 | $Al_2O_3$/MnS |
| 2.f | 14.75 | 0.61 | 0.39 | 0.25 | 39.64 | 0.41 | 3.92 | 0.34 | 39.69 | $Al_2O_3$/Fe |
| 2.g | 25.3 | 7.65 | 0.42 | 0.17 | 29.86 | 0.30 | 1.61 | 5.12 | 52.33 | $Al_2O_3$/Fe |
| 1.b | | | | | | | | | | $Al_2O_3$/MnS |

† Oxygen calculated by difference

N/D: Not detected

TABLE III: MICROPROBE INCLUSION ANALYSIS - wt%†

1146-M (See Micrographs in Figure 3 - 6)

| INCLUSION | Fe | Mn | Ti | Si | Al | Mg | Ca | S | Nb | TYPE |
|---|---|---|---|---|---|---|---|---|---|---|
| 3.a | 2.10 | 0.90 | N/D | 0.01 | 0.03 | N/D | 54.44 | 41.96 | 0.05 | CaS |
| 3.b | 3.49 | 0.37 | 0.17 | 10.61 | 15.14 | 8.54 | 22.21 | 0.68 | N/D | $C_2AS$* |
| 3.c | 1.51 | 0.42 | 0.26 | 11.80 | 12.55 | 1.68 | 28.33 | 0.33 | N/D | $C_2AS$ |
| 3.d | 1.44 | 0.54 | 0.48 | 10.66 | 14.20 | 1.29 | 29.04 | 1.44 | N/D | $C_2AS$ |
| 4.a | 1.72 | 0.90 | N/D | 0.02 | 0.06 | N/D | 54.54 | 41.59 | N/D | CaS |
| 4.b | 1.08 | 0.26 | 0.24 | 12.44 | 11.37 | 2.47 | 28.27 | 0.58 | N/D | $C_2AS$ |
| 5.a | 5.11 | 0.03 | --- | --- | --- | --- | 0.01 | N/D | 85.77 | Fe(Nb)-NbC |
| 5.b | 26.57 | 0.10 | --- | --- | --- | --- | N/D | N/D | 64.17 | Fe(Nb)-NbC |

† Oxygen calculated by difference

N/D: Not Detected

* $C_2AS \equiv 2CaO.Al_2O_3.SiO_2$ (gehlenite)

Fe(Nb)-NbC: Fe-Nb solid solution/NbC eutectic

TABLE III: MICROPROBE INCLUSION ANALYSIS - wt%† (cont'd)
1146-M (See Micrographs in Figures 3 - 6)

| INCLUSION | Fe | Mn | Ti | Si | Al | Mg | Ca | S | Nb | TYPE |
|---|---|---|---|---|---|---|---|---|---|---|
| 5.c | 10.28 | 0.05 | ---- | ---- | ---- | ---- | N/D | N/D | 74.77 | Fe(Nb)-NbC |
| 6.a | 2.47 | 1.02 | N/D | 0.01 | 0.04 | N/D | 53.73 | 41.03 | 0.01 | CaS |
| 6.b | 33.04 | 3.89 | N/D | 0.12 | 0.02 | N/D | 39.33 | 34.61 | 0.06 | CaS/Fe |
| 6.c | 6.83 | 3.17 | 0.03 | 0.15 | 0.63 | N/D | 47.67 | 37.90 | 0.02 | CaS |
| 6.d | 21.26 | 0.32 | 0.54 | 2.19 | 31.61 | 14.99 | 1.40 | 0.06 | 0.12 | Mixed oxide |
| 6.e | 3.11 | 57.60 | ---- | ---- | ---- | ---- | 0.09 | 36.20 | 0.09 | MnS |
| 6.f | 10.59 | 51.87 | ---- | ---- | ---- | ---- | 0.07 | 33.32 | 0.14 | MnS |

† Oxygen calculated by difference
N/D: Not Detected

Fe(Nb)-NbC: Fe-Nb solid solution/ NbC eutectic

TABLE IV: OXIDE INCLUSION COMPOSITION - wt.%: 1146-M

| INCLUSION | $(CaO + Al_2O_3 + SiO_2 + MgO + FeO) \equiv 100$ | | | | | $(CaO + Al_2O_3 + SiO_2) \equiv 100$ | | |
|---|---|---|---|---|---|---|---|---|
| | CaO | $Al_2O_3$ | $SiO_2$ | MgO | FeO | CaO | $Al_2O_3$ | $SiO_2$ |
| 3.b | 31.53 | 29.15 | 20.31 | 14.43 | 4.58 | 38.94 | 35.99 | 25.07 |
| 3.c | 43.94 | 26.26 | 24.56 | 3.09 | 2.15 | 46.37 | 27.72 | 25.91 |
| 3.d | 44.44 | 29.32 | 21.88 | 2.34 | 2.02 | 46.47 | 30.65 | 22.88 |
| 4.b | 39.40 | 25.30 | 22.60 | 10.81 | 1.89 | 45.13 | 28.98 | 25.89 |
| * | 40.68 | 19.37 | 29.42 | 8.30 | 2.23 | 45.47 | 21.65 | 32.88 |
| * | 43.16 | 28.00 | 24.30 | 2.71 | 1.83 | 45.22 | 29.33 | 25.45 |
| * | 44.02 | 23.89 | 25.99 | 4.56 | 1.55 | 46.88 | 25.44 | 27.68 |
| * | 45.16 | 23.01 | 26.83 | 3.09 | 1.92 | 47.54 | 24.22 | 28.24 |

* Inclusion analysis not reported in Table III

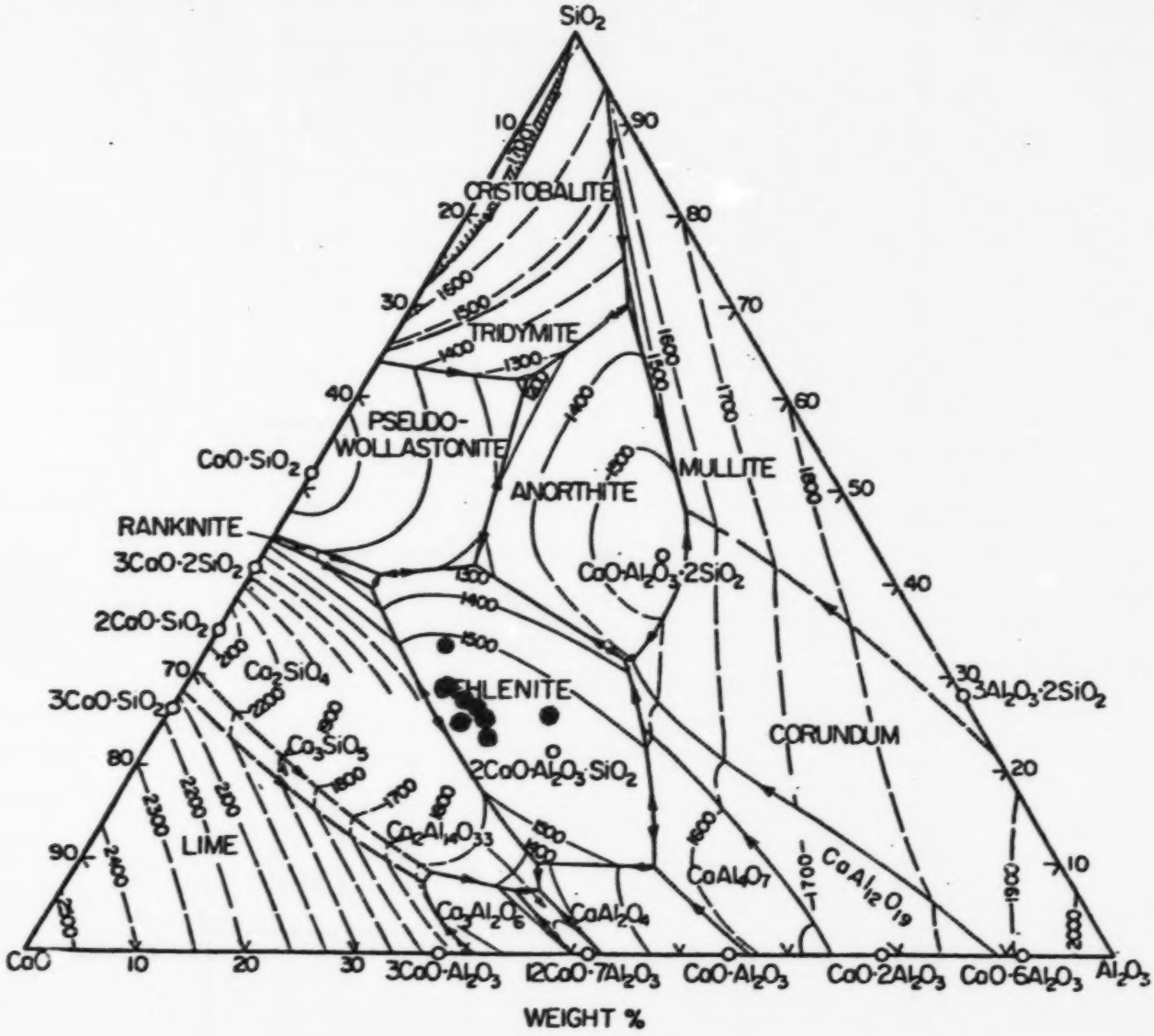


Figure 8 - The $CaO-Al_2O_3 - SiO_2$ Phase Diagram

● - Compositions of 1146-M Oxide Inclusions

$Al_2O_3.SiO_2$) in nature.

Two main inclusion types were identified in the 1146-C grade, one $Al_2O_3$-based and the other MnS-based. Four basic inclusion types were identified in the 1146-M grade: i) a CaS-based type, ii) a gehlenite-based type, iii) an MnS-based type and iv) a type formed by Fe-Nb solid solution/NbC carbide eutectic precipitation in the centre of the bar section.

The marked decrease in tool flank wear observed when machining the 1146-M grade, see Section 3, can be attributed, in part, to the absence of 'hard', abrasive $Al_2O_3$ inclusions.

### 2.2.2 QTM Analysis

The results of the QTM analysis of the oxide and sulphide inclusions in the two grades of steel, expressed in terms of their percentage by volume, V%, the number per $mm^2$, $\#/mm^2$, and their shape and size, are presented in Table V. It should be noted that the CaS inclusions in the 1146-M grade could not be distinguished from the oxide inclusions by the QTM and are therefore included with the oxides.

The values of V% and $\#/mm^2$ for the oxides in Table V, and the values of $\#/cm^2$ in the size distribution of Table VI indicate that there is about twice the number of oxide inclusions in the 1146-C grade compared to the 1146-M grade. This is the other major reason for the decreased tool flank wear associated with the 1146-M grade. As can be seen in Table V, the $\#/mm^2$ of manganese sulphide inclusions is smaller in the 1146-M grade but their length is greater.

The volume fractions of pearlite, as determined by the QTM, was greater in the 1146-M steel than in the 1146-C grade, 75 $\pm$ 5% and 55 $\pm$

TABLE V: QTM ANALYSIS

| STEEL | OXIDES | | | | SULPHIDES | | | |
|---|---|---|---|---|---|---|---|---|
| | V% | #/mm$^2$ | Average Size µm | Shape | V% | #/mm$^2$ | Average Size µm | Shape |
| 1146-C | 0.038 | 24.5 | 4.6(L)<br>3.6(T) | 1.28 | 0.81 | 324.4 | 10.6(L)<br>3.3(T) | 3.0 |
| 1146-M | 0.028* | 12.2 | 5.3(L)<br>4.5(T) | 1.23 | 0.77 | 231.5 | 12.3(L)<br>3.2(T) | 3.7 |

V%: volume % of inclusions ≡ area % of inclusions

#/mm$^2$: number of inclusions/mm$^2$

Size: two sizes are reported on longitudinal sections, one on the longitudinal direction (L) the other on the transverse(T)

Shape: the average aspect ratio of individual inclusions and not the ratio between average sizes (L) and (T)

*CaS inclusions cannot be distinguished from the oxides and are included in the oxide volume %.

Table VI: SIZE DISTRIBUTION OF OXIDES

(#/cm$^2$)

| Size Range μm | 1146-C | 1146-M |
|---|---|---|
| 0.7 - 2 | 612 | 244 |
| 2 - 4 | 710 | 244 |
| 4 - 6 | 564 | 301 |
| 6 - 8 | 270 | 207 |
| 8 - 10 | 125 | 114 |
| 10 - 12 | 54 | 53 |
| 12 - 14 | 37 | 17 |
| 14 - 16 | 20 | 13 |
| 16 - 18 | 15 | 12 |
| 18 - 20 | 5 | --- |
| > 20 | 40 | 17 |
| > 30 | 5 | 3 |

5%, respectively. This is consistent with the difference in carbon content and hardness between the two steels, see Section 2.1. In terms of 1146-M machinability, this difference in matrix properties resulted in higher values of the tangential cutting forces and increased crater wear, see Section 3.

## 3. MACHINABILITY (3)

Single point turning machinability tests were carried out on the MAZAK lathe of the Metal Cutting Laboratory at McMaster University (Professor J. Tlusty). The lathe is equipped with a cutting force dynamometer and a quick-stop device which enables the shear angle, $\phi$, at the junction of the 'frozen' chip and the workpiece, to be measured. Cutting tests were carried out using Balfour Ultra Capital 395 molybdenum-based high speed steel (HSS) tools and Kennametal K21 carbide tools.

The following cutting conditions and tool geometries were used with cutting speeds of 30-70 m/min for HSS cutting, and 100 and 150 m/min for carbide cutting:

| | |
|---|---|
| Rake angle ($\alpha$): | 10, 14 and 20$^{o}$ |
| Relief angle ($\gamma$): | 7$^{o}$ |
| Feed rate (f): | 0.1 mm/rev. |
| Depth of cut (b): | 2 and 3 mm. |

### 3.1 Tool Wear Tests

HSS tool flank wear tests were carried out by measuring the extent of flank wear as a function of cutting time for different cutting speeds. The result for cutting speeds of 30, 40, 50, 60 and 70 m/min.

are presented in Figures 9-13, respectively. Carbide tool flank wear was also determined after 30 minutes at 100 m/min. and 20 minutes at 150 m/min for comparison purposes. These results are summarised in Figure 14 where flank wear is expressed as a function of cutting speed. Flank wear typical of HSS and carbide tools is shown in Figures 15 and 16. It is clear from these results that the flank wear observed in cutting 1146-M steel is about one half of that observed in cutting 1146-C steel.

Typical HSS tool rake face crater wear is also shown in Figure 16. The enhanced crater wear observed when machining the 1146-M grade, is caused by higher tangential cutting forces, larger shear angles and higher rake face temperatures, see below, and arises from the higher carbon content and pearlite volume fraction in that steel.

## 3.2 Cutting Forces, Shear Angle and Chip Temperatures

The two components of the cutting force, the tangential force, $F_T$, and the normal force, $F_N$ for HSS machining are plotted versus cutting speed in Figure 17. The graph shows that the tangential cutting forces for the 1146-M steel are 8-10% higher than those of the 1146-C grade, whereas the normal or feed forces are approximately equal for both steels. The forces for both steels decreased with speed. The tool cutting the 1146-M grade failed thermally at 90 m/min., the higher cutting forces at 80 m/min. being indicative of impending failure. The higher tangential force for the 1146-M grade is due to the higher strength of this material.

Shear plane angles, $\phi$, were determined metallographically on samples of 'frozen' chips obtained in the quick-stop test, see Figure 18. Clearly defined shear plane angles were obtained for 1146-C at 50

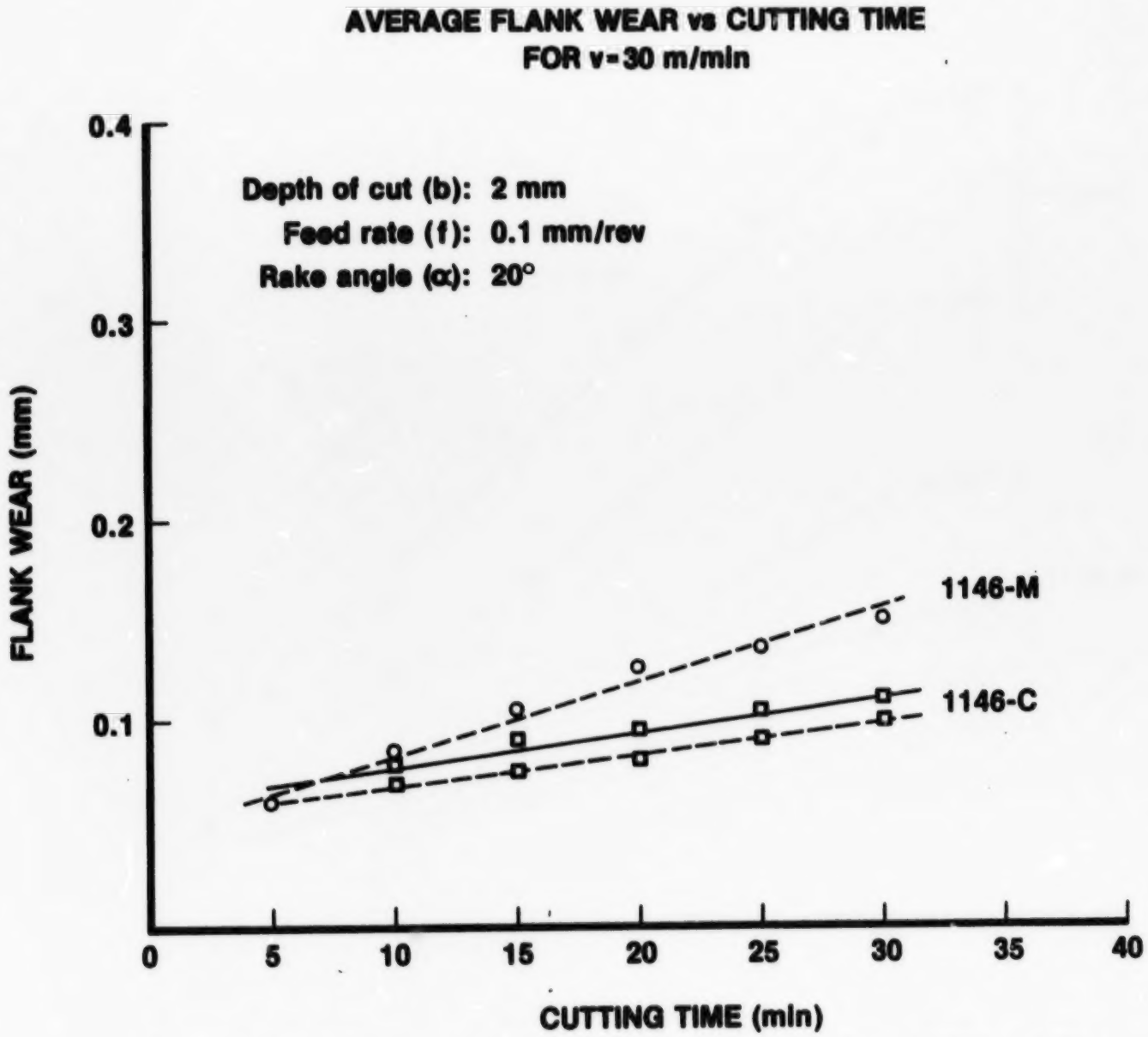


Figure 9: Flank Wear vs. Cutting Time for v = 30 m/min. Ultra Capital 395 HSS

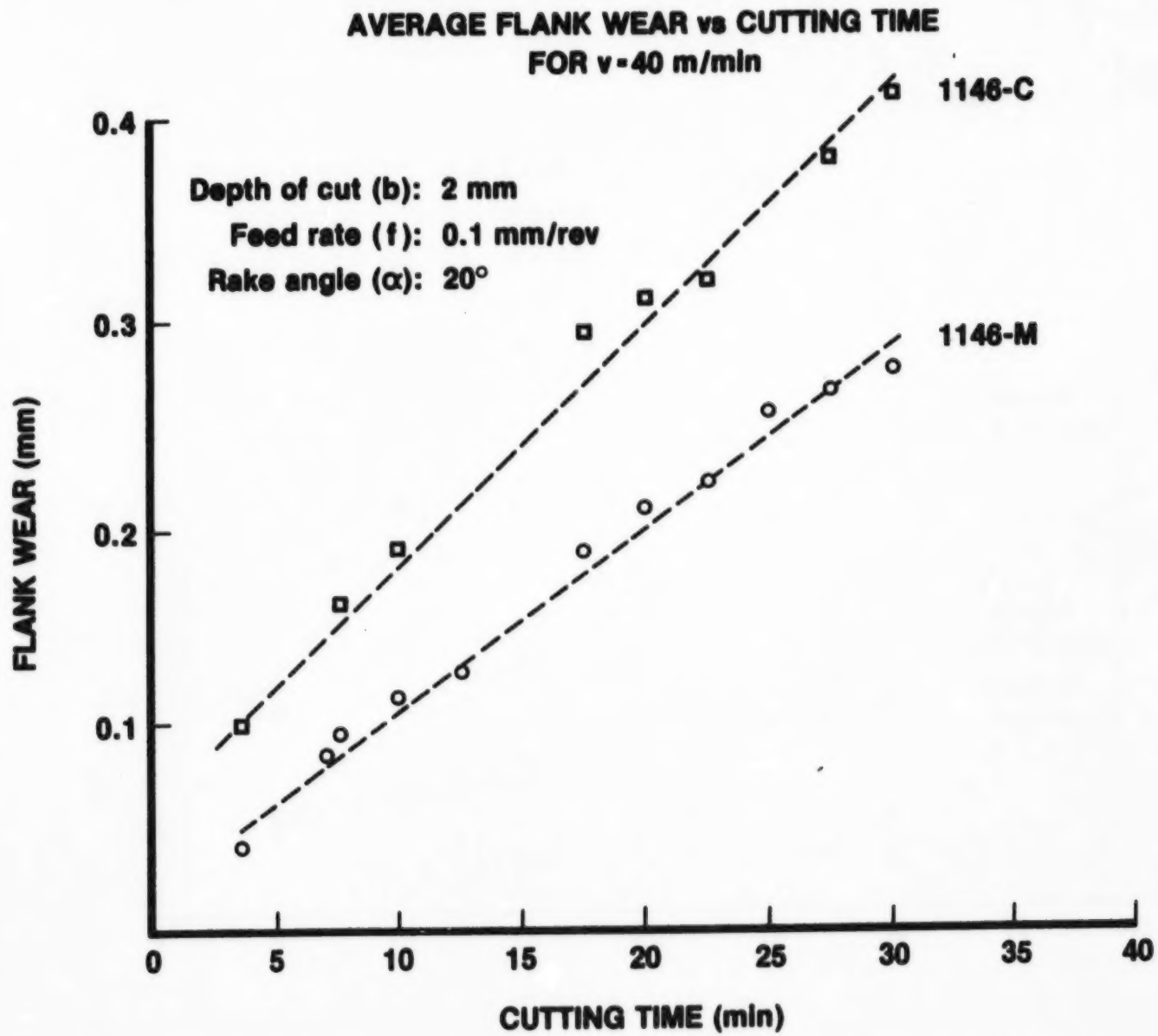


Figure 10: Flank Wear vs. Cutting Time for v = 40 m/min. Ultra Capital 395 HSS

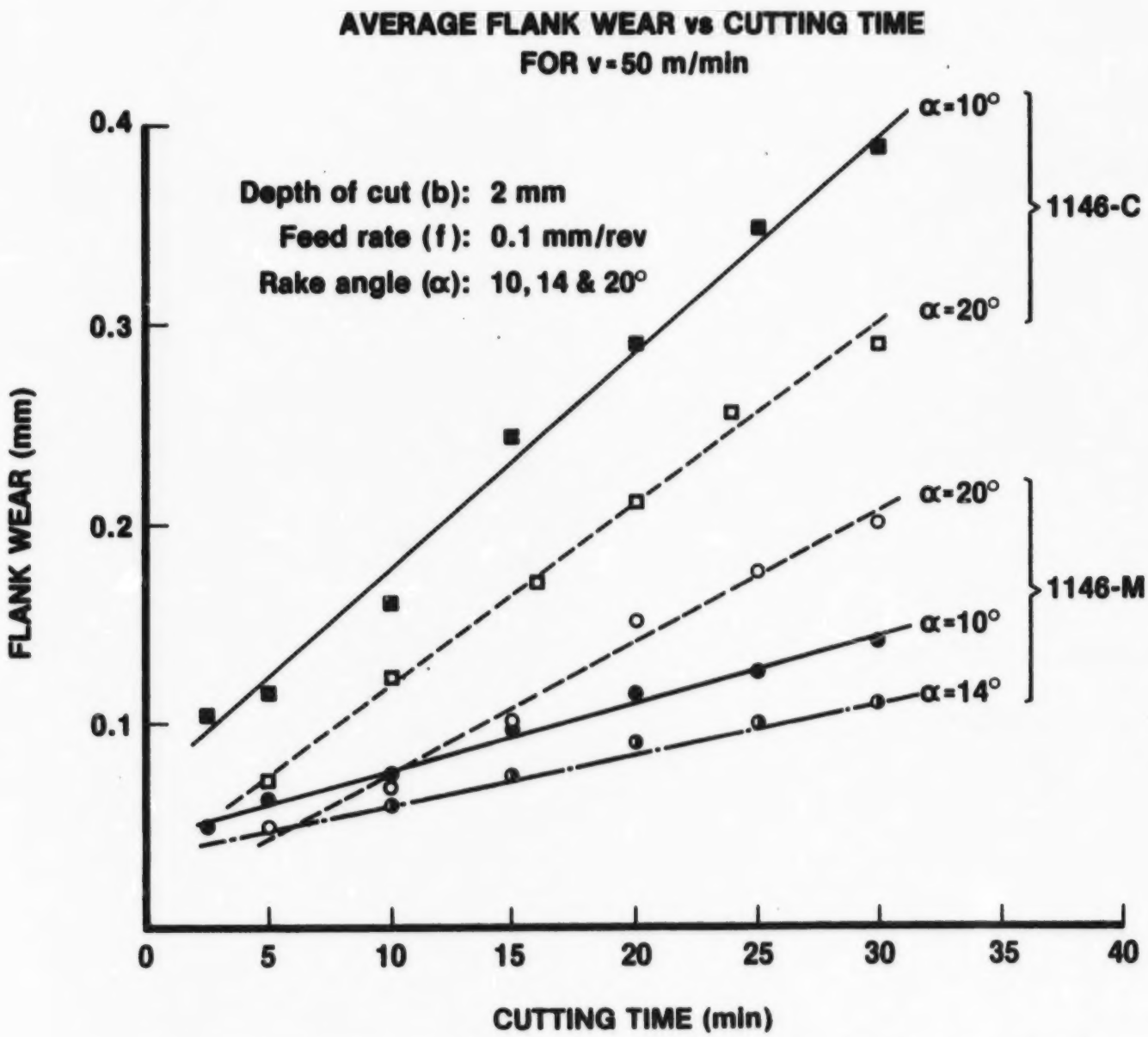


Figure 11: Flank Wear vs. Cutting Time for v = 50 m/min. Ultra Capital 395 HSS

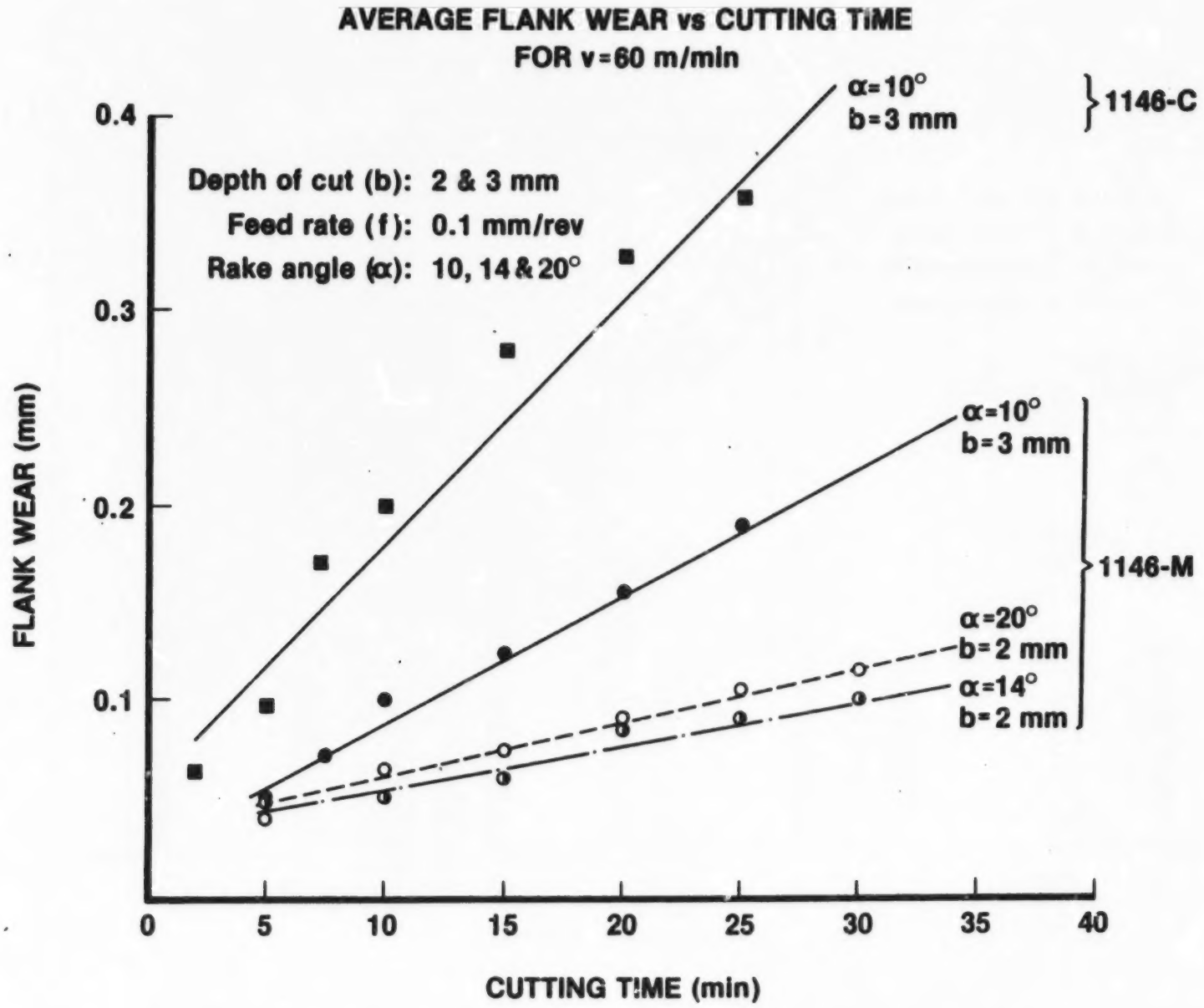


Figure 12: Flank Wear vs. Cutting Time for v = 60 m/min. Ultra Capital 395 HSS

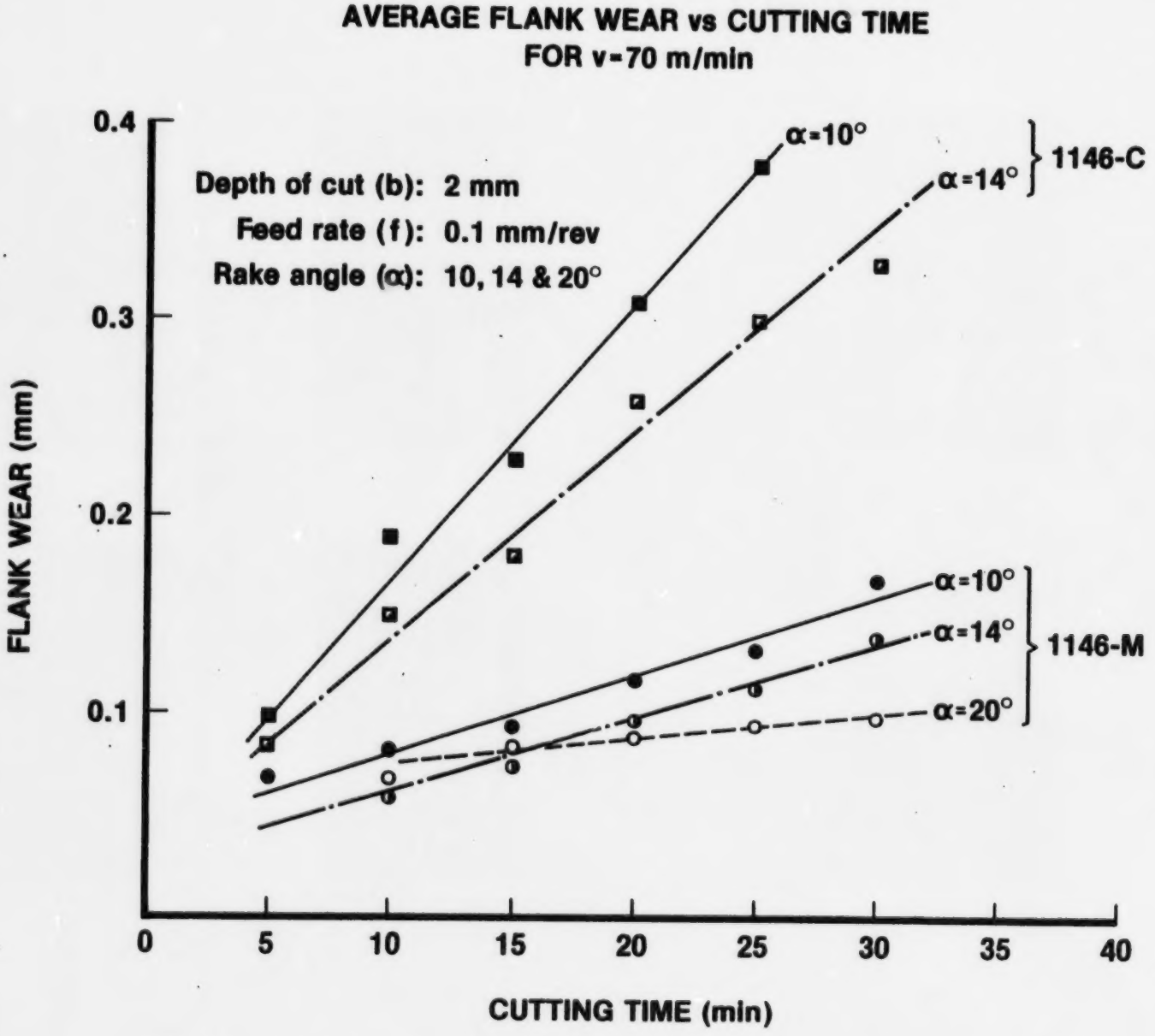


Figure 13: Flank Wear vs. Cutting Time for v = 70 m/min. Ultra Capital 395 HSS

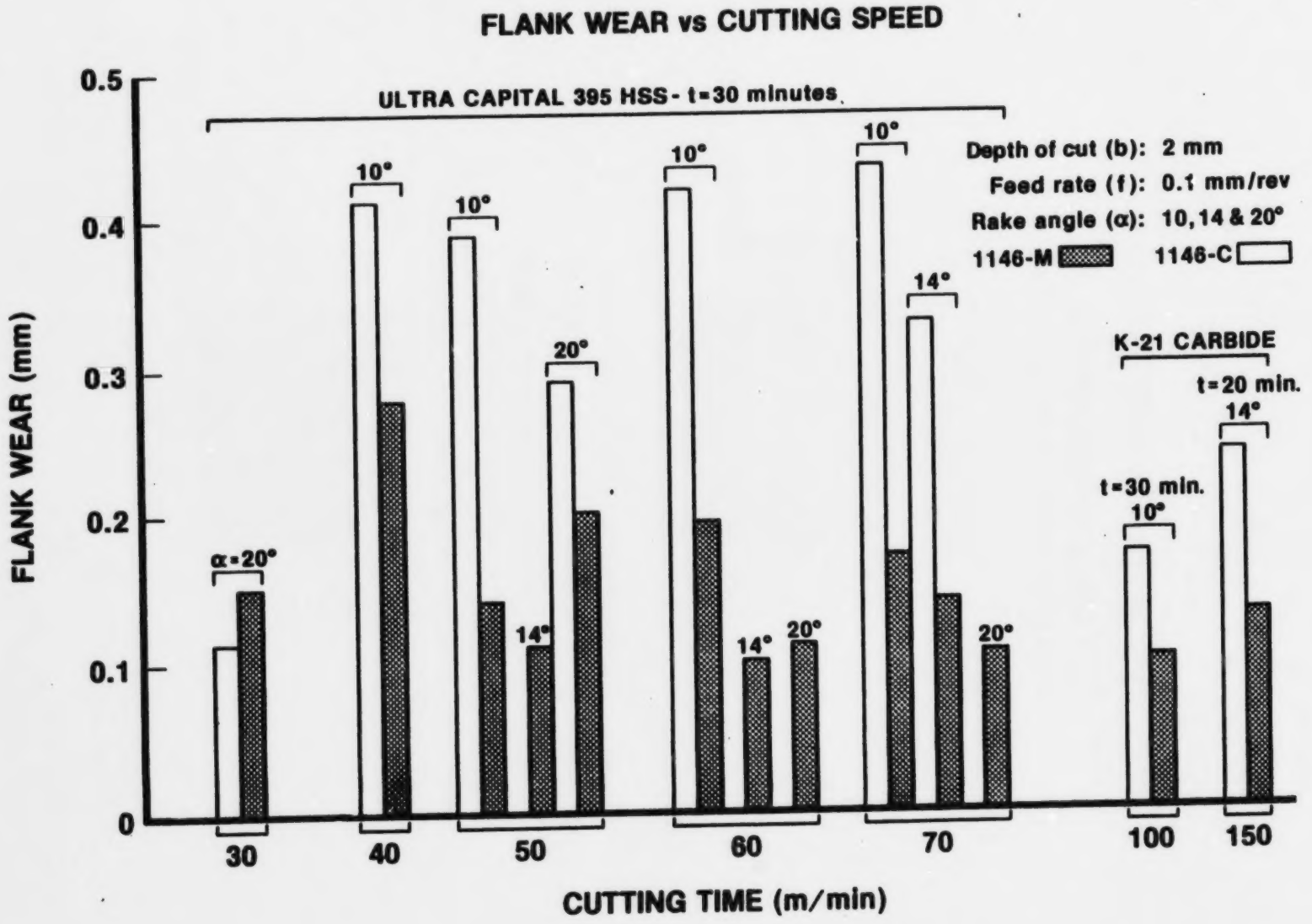


Figure 14: Flank Wear vs. Cutting Speed. Ultra Capital 395 HSS and K-21 Carbide

## HSS TOOL CRATER WEAR
## (Photographs x10)

**1146-C** **1146-M**

b=3 mm α=10° t=30 min
f=0.1 mm/rev v=40 m/min

## HSS TOOL FLANK WEAR
## (Photographs x10)

**1146-C** **1146-M**

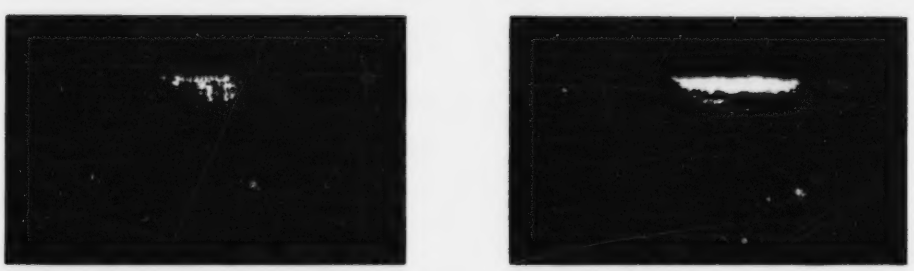

b=2 mm α=10° t=30 min
f=0.1 mm/rev v=40 m/min

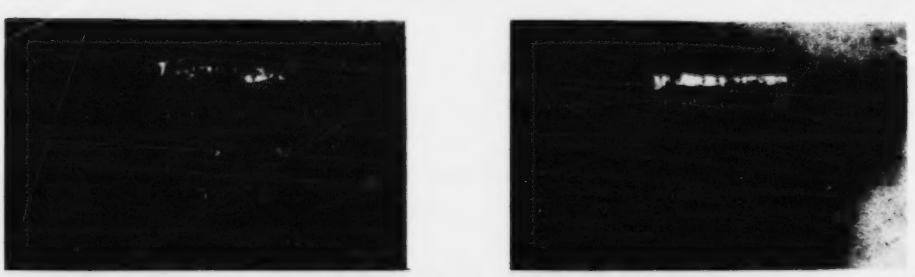

b=2 mm α=20° t=30 min
f=0.1 mm/rev v=50 m/min

Figure 15: Ultra Capital 395 HSS Tool Crater and Flank Wear.

## K-21 CARBIDE FLANK WEAR
## (Photographs x10)

**1146-C**

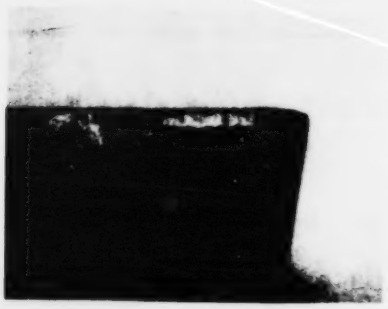

**b=2 mm  α=10°  t=20 min**

**f=0.1 mm/rev  v=150 m/min**

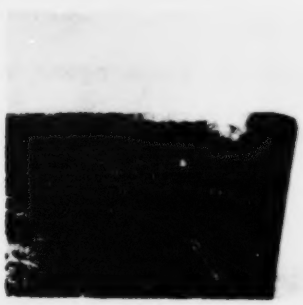

**1146-M**

Figure 16: K-21 Carbide Tool Flank Wear.

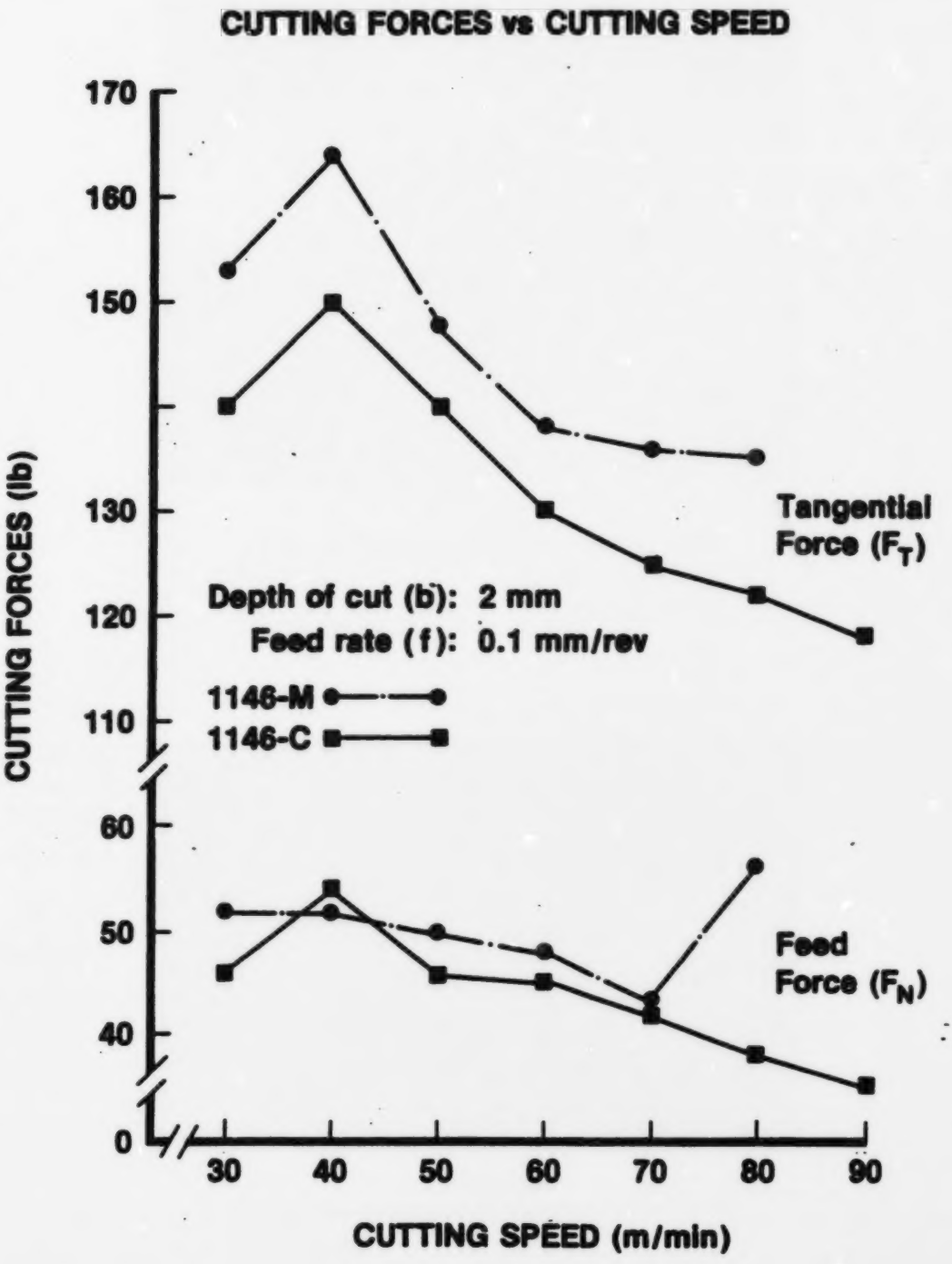


Figure 17: Tangential ($F_T$) and Feed ($F_N$) Forces vs. Cutting Speed for Ultra Capital 395 HSS

m/min. and 1146-M at 60 and 70 m/min., while other tests yielded samples with less clearly defined angles:

| STEEL | CUTTING SPEED - m/min | | |
|---|---|---|---|
| | 50 | 60 | 70 |
| ϕ (1146-C) | $34^{o}$ | -- | $40^{o}$ |
| ϕ (1146-M) | $41^{o}$ | $40^{o}$ | $42^{o}$ |

The slightly larger, shear angle for the 1146-M steel is indicative of a lower coefficient of friction.

The higher cutting forces required for the 1146-M steel are indicative of a higher cutting power and a higher cutting temperature. Temperature profiles in 1146-C and 1146-M chips, computed for the particular machining conditions indicated, are illustrated in Figure 19. Maximum temperatures of $670^{o}C$ were calculated for 1146-M chips compared with $630^{o}C$ for 1146-C chips. Crater wear is primarily caused by interdiffusion of material between the rake face of the tool and the chip, and is strongly temperature dependent. The enhanced crater wear observed for the 1146-M grade is therefore directly related to its higher carbon content and strength.

## 3.3 Built Up Edge (BUE) and Chip Form

BUE was deposited on the workpiece surface of both materials at the 30-50 m/min. lower speed range, indicating BUE instability. In fact, the BUE was easily removed from the tool with a fingernail. In general, the BUE height decreased with speed and rake angle and the

## QUICK STOP RESULTS
## (Photographs x5)

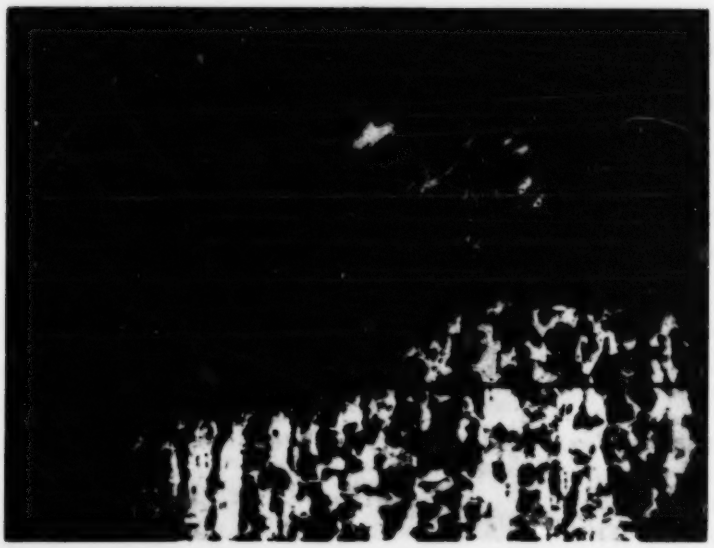

**1146-C**

| | |
|---|---|
| b = 2 mm | f = 0.1 mm/rev |
| v = 50 m/min | $\phi$ = 34° |

**1146-M**

| | |
|---|---|
| b = 2 mm | f = 0.1 mm/rev |
| v = 60 m/min | $\phi$ = 40° |

Figure 18: Quick Stop Results.

## TEMPERATURE PROFILE IN IDEAL CHIP: 1146-C

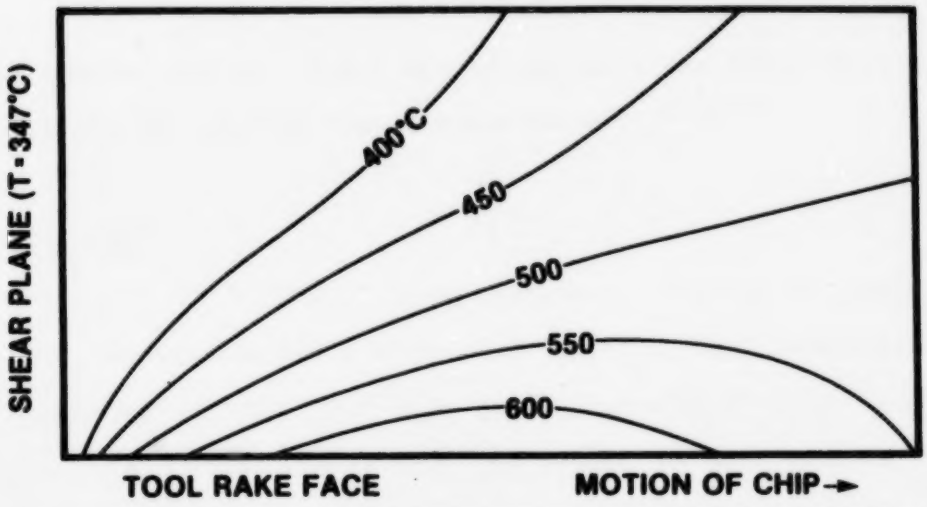


| | | | |
|---|---|---|---|
| Depth of cut ( b ): | 2 mm | Feed rate ( f ): | 0.1 mm/rev |
| Cutting speed ( v ): | 60 m/min | Rake angle ($\alpha$): | 10° |
| Tangential force ($F_T$): | 130 lb | Shear angle ($\phi$): | 40° |
| Normal force ($F_N$): | 45 lb | | |

## TEMPERATURE PROFILE IN IDEAL CHIP: 1146-M

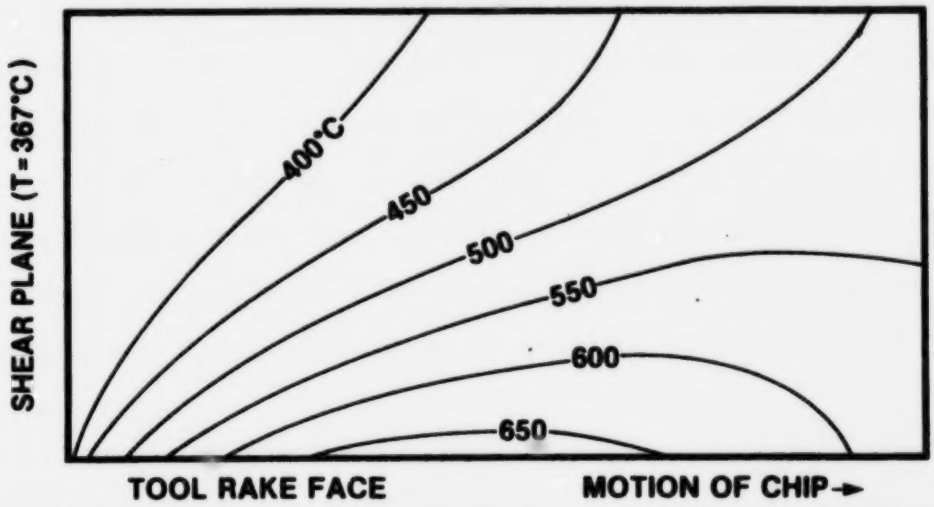


| | | | |
|---|---|---|---|
| Depth of cut ( b ): | 2 mm | Feed rate ( f ): | 0.1 mm/rev |
| Cutting speed ( v ): | 60 m/min | Rake angle ($\alpha$): | 10° |
| Tangential force ($F_T$): | 138 lb | Shear angle ($\phi$): | 40° |
| Normal force ($F_N$): | 48 lb | | |

Figure 19: Chip Temperature Profiles

shorter BUE was more difficult to remove at higher speeds. At 60 m/min. it could not be removed from the tool with a fingernail.

Chip form did not differ significantly for the two steels at speeds greater than 40 m/min. At the beginning of cutting with a sharp tool, the chips were long (~ 30 mm) with little curl, but after about 10-20 seconds the chips were very short and tightly curled (1-2 mm diameter). The chip length and diameter increased with rake angle. At 40 m/min. the 1146-C chip had a larger diameter curl (4-8 mm) than the 1146-M chip (1-2 mm). The above observations indicate that the crater forming on the rake face of the tool acts as a chip breaker, increasing the curl and decreasing the length of the chip.

Qualitative observations indicated that the surface finish of the 1146-M steel was superior to that of the 1146-C steel.

## 4. CONCLUSIONS

1. The 1146-C steel contained $Al_2O_3$-based and MnS inclusions.
2. The 1146-M steel contained 2 $CaO.Al_2O_3.SiO_2$ (gehlenite)-based, CaS and MnS inclusions.
3. Reduction of the Nb content to ~ 0.035% should prevent the precipitation of Fe-Nb solid solution/NbC eutectic precipitation in the centre of the as-cast billet.
4. The 1146-C steel contained about twice as many oxide-based inclusions as the 1146-M steel.
5. Flank wear with HSS and carbide tools was about one half of that for the 1146-C steel. This is attributed to the decreased number of oxide inclusions and the absence of $Al_2O_3$-based inclusions in the 1146-M steel.

6. The enhanced HSS tool crater wear on machining the 1146-M steel is attributed to the 0.05% higher carbon content.

## 5. FUTURE WORK

Future work at Burlington Steel Ltd. must develop deoxidation control for the reproducible production of $CaO.Al_2O_3.2SiO_2$ (anorthite)-based inclusions in AISI 1146 type steels containing Nb for grain refinement. A further significant improvement in machinability is anticipated.

The increased shear angle and the improved surface finish observed in the case of 1146-M are clearly associated with the matrix response to the machining process. Further work is required to identify microstructural mechanisms involved in chip formation. It is possible that normal crystallographic slip processes are precluded more readily in the machining of 1146-M - leading to plastic instabilities that originate shear bands at relatively lower overall shear strain - than in the case of 1146-C. It is essential to indentify the strains at which microband formation develop in each case, to characterise the work hardening behaviour once the shear bands develop, and to determine the total strain to fracture. Such a study will provide valuable information in the understanding of material matrix response to machining.

## 6. ACKNOWLEDGEMENTS

The authors should like to acknowledge the financial support of the Department of Energy, Mines and Resources (CANMET). Materials characterisation was carried out at CANMET and the work of Dr. J.D.

Boyd, Mr. D.A. Parsons, Dr. M. Shehata and Mrs. Vera Moore is gratefully acknowledged. Machinability tests were carried out in the Department of Mechanical Engineering of McMaster University and the work of Dr. J. Tlusty and Mr. S. Stasiw is gratefully acknowledged. The authors would also like to acknowledge the cooperation of Mr. M. Reinberg, Mr. J.A. Skarja and Mr. F. Atkinson of Burlington Steel Ltd. in the production of the steels which are the basis of this report.

## REFERENCES

1. S.V. Subramanian and D.A.R. Kay: "Development of Non-Leaded Free-Machining Steels - Phase I", Final Report, August 1981, DSS Contract #OSU80-001.

2. S.V. Subramanian and D.A.R. Kay: "Development of Non-Leaded Free-Machining Steels - Phase II", Interim Report, December 1981, DSS Contract #OSU80-001.

3. J. Tlusty and S. Stasiw: "Machinability Tests of Two Steels, 1146-C and 1146-M", Manufacturing Research and Design Group, McMaster University, Report #181, September 1982.

APPENDIX I

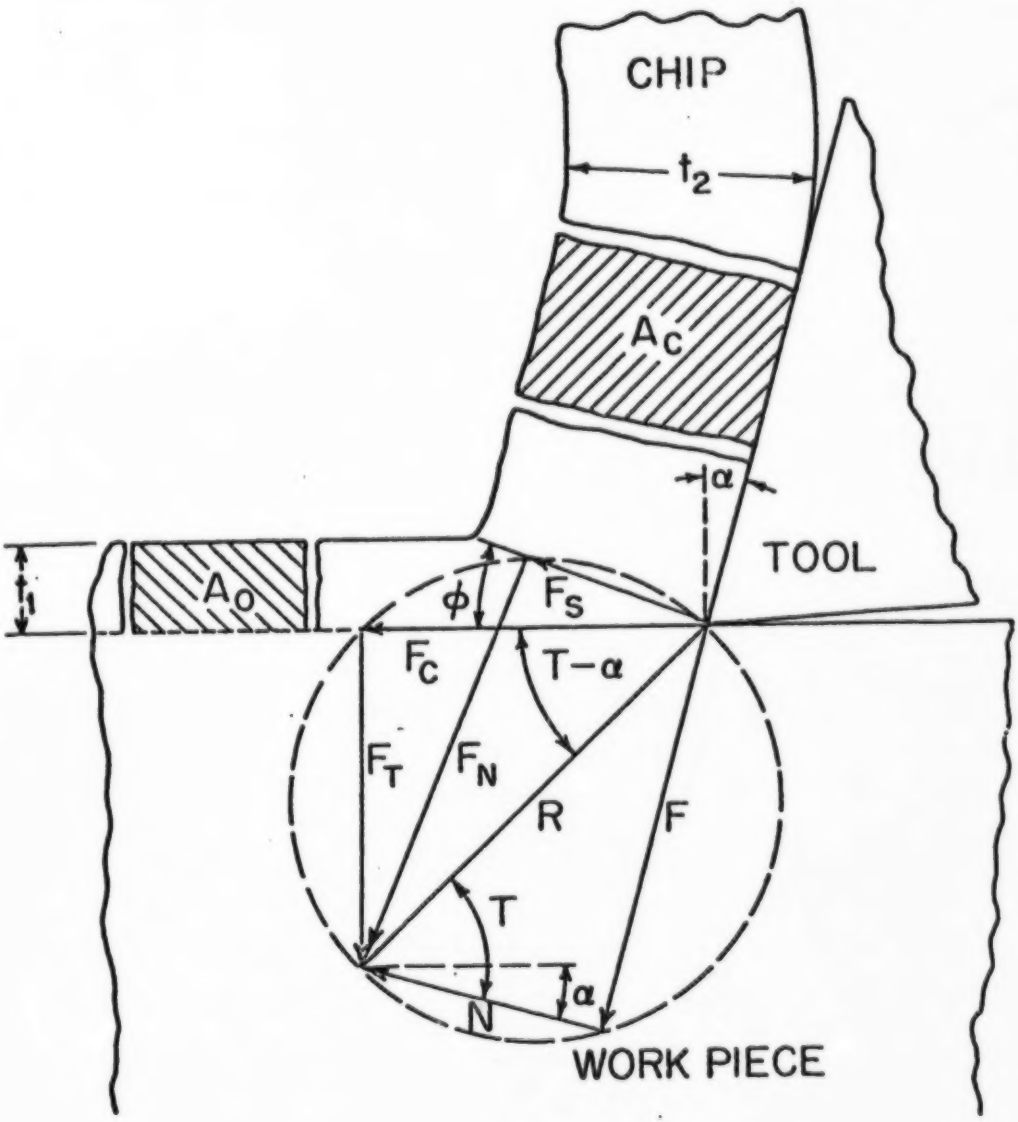


$F_T$ in the text — $F_C$ on this diagram

$F_N$ in the text — $F_T$ on this diagram

Figure A1: - The Composite Force Diagram of Merchant *

* Merchant, M.E., J. App. Phys., vol. 16, No. 5, 1945, pp. 267-75.